Analysis and control of elastic waves in phononic structures of poroelastic inclusions in a fluid

Athina Alevizaki

Normandie Université

THESE

Pour obtenir le diplôme de doctorat

Acoustique

Préparée au sein de l'Université Le Havre Normandie
En partenariat international avec l'Université Nationale et Kapodistrienne d'Athènes GRÈCE

Analysis and control of elastic waves in phononic structures of poroelastic inclusions in a fluid

Présentée et soutenue par
Athina ALEVIZAKI

Thèse soutenue publiquement le 28/09/2018 devant le jury composé de		
M. Jean-Marc CONOIR	Directeur de Recherche CNRS, IJLRA, Sorbonne Université Paris	Président
M. Jean-Philippe GROBY	Chargé de Recherche CNRS, HDR, LAUM, UMR CNRS 6613, Le Mans Université	Rapporteur
M. Bruno MORVAN	Professeur des Universités, LOMC, UMR CNRS 6294, Université Le Havre Normandie	Directeur de thèse
M. Olivier PONCELET	Chargé de Recherche CNRS, I2M, Université de Bordeaux	Examinateur
M. Pascal REMBERT	Maître de Conférences, LOMC, UMR CNRS 6294, Université Le Havre Normandie	Encadrant
Mme Rebecca SAINIDOU	Maître de Conférences, LOMC, UMR CNRS 6294, Université Le Havre Normandie	Encadrant
M. Nikolaos STEFANOU	Professeur des Universités, Section of Solid State Physics, Université Nationale et Kapodistrienne d'Athènes	Directeur de thèse
M. Jérôme VASSEUR	Professeur des Universités, IEMN	Rapporteur

Thèse dirigée par Bruno MORVAN, **laboratoire LOMC UMR CNRS 6294**
et co-dirigée par Nikolaos STEFANOU, **Section of Solid State Physics, Université Nationale et Kapodistrienne d'Athènes**

UNIVERSITÉ LE HAVRE NORMANDIE

ED PSIME

LABORATOIRE ONDES et MILIEUX COMPLEXES

What lies ahead us
and what lies behind us
is nothing compared to
what lies within us...

Preface

This dissertation was conducted under the collaboration of two universities: the University of Le Havre Normandy and the National and Kapodistrian University of Athens, and I was engaged in researching and writing it from September 2015 to July 2018. I would like to thank my supervisors, Professor Nikolaos Stefanou from the National and Kapodistrian University of Athens, Department of Physics, section of Solid State Physics and Professor Bruno Morvan, Maître de conférences Rebecca Sainidou and Maître de conférences Pascal Rembert from the university of Le Havre Normandy, Laboratoire Ondes et Milieux Complexes (LOMC) UMR CNRS 6294, for their excellent guidance and support during this process. They have been my mentors throughout all those years, with their patience and understanding they were able to shape my mind into that of a scientist, teaching me how to reason. Special thanks are owed to Dr. Sainidou and Dr. Rembert, not only for being my primary guides but also for their emotional support and friendly treatment.

PhD students are often motivated to pursue the PhD by scientific and humanistic curiosity, the desire to contribute to the academic community, service to others, or personal development. For me all these reasons are summed up to the original Greek meaning of the Doctor of Philosophy, which is "love of wisdom". The long days spent in the lab, battling shoulder to shoulder with my fellow scientists and friends, the joy for the synthesis, the hope for good results and the sadness and tiredness with each failed attempt, are all characteristics of this process. So, here I would like to thank my colleagues who shared this experience with me, PhD students Petros Pantazopoulos and Adamantia Kosma and Dr. Aristi Christofi.

The realization of this PhD would not have been possible without the financial support of the SUPERMEN project, through a postgraduate fellowship. This project is co-financed by the European Union through the European Regional Development Fund and by the Conseil Regional de Haute Normandie. A special thanks to Professor Pascal Pareige, deputy director of LOMC for his help and support in all administrative aspects during my PhD thesis.

This thesis is dedicated to my family. If I ever lost interest, they kept me motivated. My parents deserve a particular note of thanks: your wise counsel and kind words have, as always, served me well.

A.A.

Résumé

Dans le présent document de thèse, une extension de la méthode de calcul de la diffusion multiple stratifiée est développée en y incluant des structures phononiques à base de diffuseurs sphériques poroélastiques saturés immergés dans un fluide, en combinant la théorie de Biot avec le formalisme de diffusion multiple. La méthode est alors appliquée à une étude théorique, bien au-delà de l'approximation à grandes longueurs d'onde d'un milieu effectif, de la réponse acoustique d'un milieu granulaire à double porosité saturé, formé d'un réseau cristallin compact de sphères poreuses rigides ou molles. On montre que la variation de la taille des pores et/ou celle de la porosité dans une gamme allant du millimètre au micromètre pour le diamètre des sphères altère d'une façon significative les spectres de transmission, réflexion, et d'absorption d'une couche plane d'épaisseur finie de ces matériaux. Les spectres présentés sont analysés par référence aux modes acoustiques de sphères poreuses isolées d'une part, puis par rapport aux diagrammes de dispersion des cristaux infinis correspondants. Une interprétation cohérente de la physique sous-jacente est donnée. Ces résultats mettent en évidence l'occurrence de nouveaux modes, localisés dans la sphère, provenant des ondes longitudinales lentes propres aux milieux poroélastiques. Ces modes induisent quelques caractéristiques remarquables dans le comportement acoustique de ces matériaux à double porosité, comme des bandes d'absorption non-dispersive larges ou étroites en fréquence et/ou des bandes d'arrêt directionnel. Les propriétés acoustiques de ces structures phononiques à l'échelle sub-micrométrique, i.e. en régime hypersonique (GHz), peuvent être évaluées expérimentalement par diffusion Brillouin. Dans ce document, une approche théorique élasto-optique rigoureuse, basée sur les fonctions de Green, est proposée afin de décrire la diffusion inélastique de la lumière due aux variations spatiotemporelles de l'indice de réfraction du matériau induites par des phonons. Dans ce cadre des expressions analytiques de l'intensité d'un faisceau de lumière diffusé par une particule sphérique dans le vide sont dérivées, permettant ainsi d'améliorer la précision et rapidité des calculs précédents. Les grandes lignes de ce développement théorique jettent les bases pour une description rigoureuse de cet effet dans le cas de cristaux phononiques composés de particules sphériques colloïdales.

Περίληψη

Στη παρούσα διατριβή αναπτύσσεται μια επέκταση της υπολογιστικής μεθόδου στρωματικής πολλαπλής σκέδασης για φωνονικές δομές από ποροελαστικά σφαιρικά σώματα κορεσμένα με ρευστό, συνδυάζοντας τη θεωρία του Biot με τεχνικές πολλαπλής σκέδασης. Η μέθοδος εφαρμόζεται στη θεωρητική μελέτη, πέραν της προσέγγισης ενεργού μέσου σε μεγάλα μήκη κύματος, της ακουστικής απόκρισης κοκκωδών υλικών με πόρους σε διπλή κλίμακα, εμβαπτισμένων σε υγρό και σε κατάσταση κόρου, που αποτελούνται από σκληρές ή μαλακές πυκνά διατεταγμένες πορώδεις σφαίρες. Δείχνεται ότι μεταβολές του μεγέθους των πόρων και/ή του πορώδους σε σφαιρικούς κόκκους διαστάσεων της τάξης του χιλιοστού ή και λιγότερο τροποποιούν σημαντικά τα φάσματα διέλευσης, ανάκλασης και απορρόφησης πεπερασμένων πλακιδίων αυτών των υλικών. Τα φάσματα που υπολογίζονται αναλύονται αναφορικά τόσο με τις καταστάσεις του ακουστικού πεδίου στους πορώδεις σφαιρικούς κόκκους, όσο και με σχετικά διαγράμματα διασποράς αντίστοιχων άπειρων κρυστάλλων, παρουσιάζοντας μια συνεπή ερμηνεία των υπεύθυνων φυσικών μηχανισμών. Τα αποτελέσματα μας δείχνουν την ύπαρξη νέων καταστάσεων, εντοπισμένων στις σφαίρες, οι οποίες οφείλονται στα αργά διαμήκη κύματα που είναι ίδιο χαρακτηριστικό των ποροελαστικών μέσων. Στις καταστάσεις αυτές οφείλονται κάποια αξιοσημείωτα χαρακτηριστικά της ακουστικής συμπεριφοράς των υπό μελέτη υλικών με πόρους σε διπλή κλίμακα, όπως ευρείες ή στενές ζώνες απορρόφησης και/ή χάσματα διέλευσης σε συγκεκριμένες διευθύνσεις. Οι ακουστικές ιδιότητες φωνονικών (υπο)μικροδομών, στην περιοχή των άπω υπερήχων (GHz), μπορούν να διερευνηθούν, εν γένει, με πειράματα σκέδασης φωτός Brillouin. Στην παρούσα διατριβή ακολουθούμε μια αυστηρή πλήρως ελαστο-οπτική θεωρητική αντιμετώπιση της ανελαστικής σκέδασης φωτός λόγω χωρο-χρονικών μεταβολών του δείκτη διάθλασης του μέσου εξαιτίας των φωνονίων, βασισμένη σε συναρτήσεις Green, και καταλήγουμε σε αναλυτικές σχέσεις για τις εντάσεις των σκεδαζόμενων δεσμών φωτός από μεμονωμένα σφαιρικά σωματίδια στο κενό, βελτιώνοντας έτσι την αποτελεσματικότητα και την ακρίβεια προηγούμενων υπολογισμών. Το πλαίσιο αυτό αποτελεί επίσης τη βάση για μια αυστηρή περιγραφή του φαινομένου για φωνονικούς κρυστάλλους από κολλοειδή σφαιρικά σωματίδια.

Abstract

In the present thesis, an extension of the layer multiple scattering computational methodology to phononic structures of fluid-saturated poroelastic spherical bodies, combining Biot's theory with multiple scattering techniques, is developed. The method is applied to the theoretical study, beyond the long wavelength effective-medium approximation, of the acoustic response of double-porosity liquid-saturated granular materials consisting of close-packed hard or soft porous spheres. It is shown that variations of the pore size and/or the porosity within the millimeter and submillimeter-sized spherical grains significantly alters the transmission, reflection, and absorption spectra of finite slabs of these materials. The calculated spectra are analyzed by reference to the acoustic modes of the constituent porous spherical grains as well as to relevant dispersion diagrams of correspondingly infinite crystals, and a consistent interpretation of the underlying physics is presented. Our results provide evidence for the occurrence of novel, unprecedented modes, localized in the sphere, which arise from slow longitudinal waves that are peculiar to poroelastic media. These modes induce some remarkable features in the acoustic behavior of these double-porosity materials under study, such as broad or narrow dispersionless absorption bands and/or directional transmission gaps. The acoustic properties of phononic (sub)micro structures, in the hypersonic (GHz) regime, can be probed, in general, by Brillouin light scattering experiments. In the present thesis we undertake a rigorous full elasto-optic theoretical approach to inelastic light scattering due to phonon-induced spatiotemporal variations of the refractive index of a medium, based on Green's functions, and derive analytical expressions for the intensities of the scattered light beams by single spherical particles in vacuum, thus improving the computational efficiency and accuracy of previous calculations. The above framework provides, also, the basis for a rigorous description of the effect for phononic crystals of colloidal spherical particles.

CONTENTS

Introduction

Phononic crystals are composite materials with elastic coefficients (mass density and elastic moduli or, equivalently, mass density and elastic wave velocities) varying periodically in space [1,2]. In three dimensions they can be realized, e.g., by a periodic arrangement of solid or fluid inclusions in an otherwise homogeneous host material (solid or fluid) of different elastic coefficients while various other phononic architectures have been considered, also in one and two dimensions [3–6]. An interesting aspect of these materials arises from the possibility of frequency regions, known as absolute phononic band gaps, over which there can be no propagation of elastic waves in the crystal, whatever the direction of propagation [7–9], but appropriately designed periodic or aperiodic phononic structures can exhibit a plethora of other interesting physical phenomena, including filtering [10], waveguiding [11–13], sensing [14], negative refraction and focusing [15]. Most of these properties usually occur at wavelengths commensurate with the size of the unit cell. Nowadays, modern nanofabrication techniques allow for the realization of hypersonic phononic crystals operating in the GHz range, an example being colloidal crystals of silica nanospheres in a water-like liquid. At these frequencies, however, Brillouin light scattering experiments provide evidence that porosity in the silica particles cannot be neglected [16–18].

The acoustic properties of poroelastic materials, at different length scales, such as rocks, soil, polymer networks, colloidal particles, biological tissues, attract considerable interest in various scientific fields, e.g. geophysics, chemistry, materials physics, biomedical sciences [19–21]. Phononic crystals comprising poroelastic materials would offer the possibility of additional degrees of freedom, such as porosity, pore size, fluid viscosity, to control the propagation of elastic waves and could exhibit unprecedented, intriguing properties. However, to the best of our knowledge, apart from one-dimensional layered structures [22], phononic crystals of poroelastic inclusions in a fluid host medium have not been considered so far.

In the present thesis we develop an extension of the layer-multiple-scattering (LMS) method [23, 24] to phononic crystals of poroelastic spheres immersed in a fluid medium. Following Biot's theory [25–28] for poroelastic materials, we derive explicit expressions for the scattering transition T matrix of a submerged fluid-saturated poroelastic sphere, in the basis of vector spherical waves employed in our formalism. This matrix is a necessary

ingredient in the development of the LMS method for phononic crystals of poroelastic spheres. We demonstrate the applicability of the method on specific examples of close-packed *fcc* crystals of meso- and macroporous silica microspheres immersed in water, and present some novel results originating from the existence of the pores. Moreover, in the hope of uncovering new interesting properties, we explore other kinds of porous materials as well. For example, hierarchically porous materials, which contain a network of interconnected pores with sizes at different length scales, is a promising class of natural or synthetic structures offering a large spectrum of functionalities in various application domains [29], and also of interest for a fundamental theoretical understanding. In particular, hierarchically porous polymeric materials synthesized by various methods attract increasing interest in recent years [30–36] because of their potential applications in different fields, including catalysis, separation technology, gas storage, and bioengineering. However, the acoustic properties of such materials have not received considerable attention so far.

Biot's theory is perfectly appropriate for an effective description of poroelastic media with a more or less uniform pore distribution, i.e., a single-porosity structure. However, it fails to describe hierarchically porous materials with pore sizes at different length scales. Various homogenization methods, beyond Biot's theory, have been developed for a macroscopic description of such media and, in particular, of double-porosity deformable media characterized by two interconnected networks of fluid-saturated pores of very different sizes that exhibit very different permeabilities (see, e.g., Ref. [37] and references therein). The validity of these methods has been examined in a number of theoretical and experimental studies. Franklin *et al.* [38] studied acoustic wave propagation in a water-saturated double-porosity medium, consisting of a random array of parallel identical cylindrical holes of infinite length, perpendicular to the direction of propagation, in an otherwise single-porosity material described by Biot's theory. In this work, two-dimensional (2D) multiple-scattering calculations in the long-wavelength approximation were compared with the results of appropriate effective-medium descriptions. Acoustic wave propagation has also been investigated in periodic composites of two different porous media which occupy two disjoint subdomains at the mesoscopic scale, in one and two dimensions, through numerical simulations by the finite-element method in conjunction with relevant homogenization models in both high- and low-permeability-contrast regimes [39]. The predictions of analytical and semi-analytical effective-medium methods for the acoustic properties of double-porosity granular materials have been experimentally confirmed on expanded perlite and activated carbon, revealing stronger low-frequency sound absorption at reduced weight (porous grains) compared to a solid-grain granular material with similar mesoscopic characteristics [40]. Moreover, the observed macroscopic acoustic behavior of mineral double-porosity foams was also explained by relevant effective-medium modelling [41]. However, all local homogenization methods lose their validity if the size of the representative elementary volume, which defines the scale of heterogeneity, is not much smaller than the wavelength [37].

Focusing our study on the acoustic properties of water-saturated double-porosity materials with a specific morphology, formed by close-packed poroelastic spheres arranged in an *fcc* lattice, we will be restricted to wavelengths much longer than the radius of the sphere's pores and the distance between them, so that Biot's theory is applicable at this level, but not long enough compared to the interstitial void structure, thus requiring a rigorous description of acoustic multiple scattering between the spheres beyond a homogenization theory. We omit thermal losses since the saturating fluid is a liquid and thus, in contrast to the case of a gas, the characteristic thermal skin depth is much shorter than the corresponding viscous length, while viscosity is taken into account only in the fluid that fills the pores of the spheres [42]. It is worth noting that, though the open pores and the solid skeletal frame of the individual spheres, as well as the interstitial voids, have the percolating network topology, this is not the case for the solid material throughout the structure because neighboring spheres are touching but not consolidated. Therefore, while according to Biot's theory, transverse, fast and slow longitudinal waves subsist inside the spheres, only the common longitudinal waves in the fluid matrix (water) constitute propagating modes of the acoustic field in the double-porosity media under consideration [43].

As noted earlier in the introduction, our motivation to study phononic crystals of porous materials was triggered by Brillouin Light Scattering (BLS) experiments, i.e., inelastic light scattering due to the spatial and temporal variations of the refractive index of a material. These variations, in our case, are due to collective lattice vibrations (phonons) in the GHz frequency range, and this is why the development of lasers and the invention of the multi-pass tandem Fabry-Pérot interferometer were needed in order to use the effect as a spectroscopic technique. This technique has already been used for the characterization of the elastic properties of solids and liquids but with the advent of meso-scale periodic structures, in which the dominant frequencies are in the GHz range, it soon became apparent that the technique could be used, also, for the characterization of phononic microstructures. In the last decade, a lot of effort has been devoted in order to explain the Brillouin spectrum of such periodic microstructures of spherical particles [44–48]. The effort was focused, initially, on indirect explanations either by calculating the eigenmodes, the scattering cross section and the density of states of the individual particles or the frequency band structure of the phononic crystal, as well as using group theory. However, it became clear that only a detailed theoretical study, which takes into account the interaction of light with the elastic field, can give the correct relative intensities of the scattered light. Such a theoretical approach of the BLS by a spherical particle, based on Green's functions, is also attempted in the present thesis. We establish the theoretical foundations for a thorough description of the effect as well as the extension of BLS calculations to periodic structures.

The remainder of the thesis is structured as follows. In Chapter 1 we review the necessary elements of the theory of elasticity. In Chapter 2 we deal with elastic waves propagating in homogeneous elastic and poroelastic media. We review the theory of the

deformation of a poroelastic solid containing a compressible fluid that has been established by Biot, providing a brief summary of pertinent results from Biot's original analysis and present the corresponding theoretical basis for double-porosity media. In Chapter 3 we develop a formalism for acoustic wave scattering by isolated spherical elastic or poroelastic objects immersed in a fluid medium. The LMS method, for such scatterers, is developed in Chapter 4 and some original applications on phononic crystals of poroelastic spheres are presented in Chapter 5. Finally Chapter 6 is devoted to BLS by developing a unified analytical formalism, which can describe the observed BLS experimental spectra from isolated particles.

Chapter 1

Theory of elasticity

In this chapter we review the basic elements from the theory of elasticity and develop a formalism, based on tensor analysis, that will facilitate the further development of our method.

1.1 The strain tensor

Under the action of applied forces, a solid body of density ρ will exhibit deformation, which is translated into a change in its spacial coordinates, from x_i to x'_i, $i = 1, 2, 3$, where we assume $x_1 \equiv x$, $x_2 \equiv y$, $x_3 \equiv z$. The displacement of this point due to the deformation is, then, given by the vector $\mathbf{u} = \mathbf{r}' - \mathbf{r}$, which is known as the *displacement vector*. We can also write: $u_i = r'_i - r_i = x'_i - x_i$.

Let us consider two points very close together. If the position vector joining them before the deformation is $d\mathbf{r}$, the position vector joining the same two points in the deformed body is $d\mathbf{r}'$, so obviously $du_i = dx'_i - dx_i$. The distance between the points before the deformation is $dl = \sqrt{dx_i^2}$, and $dl' = \sqrt{dx_i'^2}$ after it [1], so we can write [2]

$$\begin{aligned} dl'^2 &= dx_i'^2 = (dx_i + du_i)^2 = \left(dx_i + u_{i,i'}dx_{i'}\right)^2 \\ &= dx_i^2 + \left(u_{i,i'}dx_{i'}\right)^2 + 2u_{i,i'}dx_i dx_{i'} \\ &= dx_i^2 + u_{i,i'}u_{i,i''}dx_{i'}dx_{i''} + 2u_{i,i'}dx_i dx_{i'} \\ &= dl^2 + u_{i,i'}u_{i,i''}dx_{i'}dx_{i''} + 2u_{i,i'}dx_i dx_{i'} \ . \end{aligned} \tag{1.1}$$

[1] We will use the Einstein notation or Einstein summation convention. According to this convention, when an index variable appears twice in a single term and is not otherwise defined, it implies summation of that term over all the values of the index.

[2] We will also use the comma derivative notation, which is common tensor notation for a derivative with respect to one of the coordinates. If several indices appear after the comma, they are all taken to be part of the differentiation.

Using

$$u_{i,i'}\ u_{i,i''}\ dx_{i'}dx_{i''} = u_{i'',i}\ u_{i'',i'}\ dx_i dx_{i'}$$
$$u_{i,i'}\ dx_i dx_{i'} = u_{i',i}\ dx_i dx_{i'} = \frac{1}{2}(u_{i,i'} + u_{i',i})dx_i dx_{i'}\ , \tag{1.2}$$

we finally obtain

$$dl'^2 = dl^2 + 2e_{ii'}dx_i dx_{i'}\ , \tag{1.3}$$

where the tensor $e_{ii'}$, known as the *strain tensor*, is defined as

$$\begin{aligned} e_{ii'} &\equiv \frac{1}{2}\left(u_{i,i'} + u_{i',i} + u_{i'',i}\ u_{i'',i'}\right) \\ &= \frac{1}{2}\left(\frac{\partial u_i}{\partial x_{i'}} + \frac{\partial u_{i'}}{\partial x_i} + \sum_{i''}\frac{\partial u_{i''}}{\partial x_i}\frac{\partial u_{i''}}{\partial x_{i'}}\right)\ . \end{aligned} \tag{1.4}$$

In almost all cases occurring in practice, the strains are small (meaning small displacements and small first derivatives of them), so the strain tensor will take the form

$$e_{ii'} = \frac{1}{2}\left(u_{i,i'} + u_{i',i}\right)\ . \tag{1.5}$$

A useful definition will be that of the volumetric strain, e,

$$e = e_{ii} = u_{i,i} = \sum_i \frac{\partial u_i}{\partial x_i} = \nabla\cdot\mathbf{u}\ . \tag{1.6}$$

The tensor $e_{ii'}$, as defined in Eqs. (1.4), (1.5), is dimensionless and symmetric, i.e.

$$e_{ii'} = e_{i'i}\ . \tag{1.7}$$

The above expressions apply for the Cartesian coordinate system, where the indices are running from 1 to 3. In spherical coordinates, the components of the strain tensor (always assuming small deformations) are

$$\begin{aligned} &e_{rr} = \frac{\partial u_r}{\partial r}, \quad e_{\theta\theta} = \frac{1}{r}\frac{\partial u_\theta}{\partial\theta} + \frac{u_r}{r}, \quad e_{\phi\phi} = \frac{1}{r\sin\theta}\frac{\partial u_\phi}{\partial\phi} + \frac{u_\theta}{r}\cot\theta + \frac{u_r}{r}, \\ &2e_{\theta\phi} = \frac{1}{r}\left(\frac{\partial u_\phi}{\partial\theta} - u_\phi\cot\theta\right) + \frac{1}{r\sin\theta}\frac{\partial u_\theta}{\partial\phi}, \quad 2e_{r\theta} = \frac{\partial u_\theta}{\partial r} - \frac{u_\theta}{r} + \frac{1}{r}\frac{\partial u_r}{\partial\theta}, \\ &2e_{\phi r} = \frac{1}{r\sin\theta}\frac{\partial u_r}{\partial\phi} + \frac{\partial u_\phi}{\partial r} - \frac{u_\phi}{r}\ . \end{aligned} \tag{1.8}$$

Like any symmetric tensor, $e_{ii'}$ can be *diagonalized* [3] at any given point, which means that we can choose coordinate axes (the *principal axes* of the tensor) in such a way that only the diagonal components are different from zero:

$$e_{ii'} = u^{(i)}\delta_{ii'} \ , \tag{1.9}$$

so Eq. (1.3) gives

$$dl'^2 \equiv dx_i'^2 = \left(1 + 2u^{(i)}\right) dx_i^2 \ , \tag{1.10}$$

from which

$$dx_i' = \left(1 + 2u^{(i)}\right)^{1/2} dx_i \cong \left(1 + u^{(i)}\right) dx_i \tag{1.11}$$

or

$$du_i = dx_i' - dx_i \cong u^{(i)} dx_i \ . \tag{1.12}$$

Thus, to first-order approximation,

$$dV' = \prod_i dx_i' \cong \prod_i \left(1 + u^{(i)}\right) dx_i = dV \prod_i \left(1 + u^{(i)}\right) \cong dV \left(1 + \sum_i u^{(i)}\right) \ . \tag{1.13}$$

The trace of a tensor is invariant under a similarity transformation, so

$$dV' = dV\,(1 + e_{ii}) = dV(1 + e) \ . \tag{1.14}$$

We emphasize that the Eqs. (1.11), (1.12), and (1.14) are valid for small deformations. It is obvious, from Eq. (1.14), that the relative volume change under the deformation is given by the sum of the diagonal components. If this sum is zero,

$$e = e_{ii} = 0 \ , \tag{1.15}$$

then the volume of the body is unchanged by the deformation, only its shape being altered. Such a deformation is called *pure shear*, and, indeed e measures the volumetric changes of the body.

Eq. (1.12) suggests that there exists a coordinate system where the strain in any volume element may be regarded as composed of independent strains in three mutually perpendicular directions, namely those of the principal axes of the strain tensor. Each of these strains is a simple extension (or compression) in the corresponding direction, and the quantity $u^{(i)}$ is consequently equal to the relative extension along the ith principal axis. Moreover, if $u^{(i)} = \text{constant} \equiv \mathcal{U}$, then the deformation will change the volume of

[3] A symmetric matrix can always be diagonalized using a unitary similarity transformation. In the general case of a complex matrix the condition is to be Hermitian [49].

the body, but not its shape, and such a deformation is called *hydrostatic compression*. The tensor is, in this case,

$$e_{ii'} = \mathcal{U}\delta_{ii'} \ , \ \mathcal{U} = \text{constant} \ . \tag{1.16}$$

It must be noted that if a deformation is pure shear in a specific coordinate system then it will remain the same in any other system, while if it is hydrostatic compression, this will hold true for only that particular system.

Any deformation can be represented as the sum of a pure shear one and a hydrostatic compression. To do so, we need only to use the identity

$$e_{ii'} = f_{ii'} + g_{ii'} \ , \tag{1.17}$$

with

$$f_{ii'} \equiv e_{ii'} - \frac{1}{3}\delta_{ii'}e \ , \quad g_{ii'} \equiv \frac{1}{3}\delta_{ii'}e \ . \tag{1.18}$$

The first term on the right-hand side of Eq. (1.17), $f_{ii'}$, corresponds evidently to a pure shear deformation, since the sum of its diagonal elements is zero, while the second term, $g_{ii'}$, corresponds to a hydrostatic compression, since it has the form (constant) $\times \delta_{ii'}$. To sum up:
a) In case of *pure shear deformation*

$$e = 0 \Rightarrow g_{ii'} = 0, \ f_{ii'} = e_{ii'} \text{ and } f_{ii} = e = 0 \ . \tag{1.19}$$

b) In case of *hydrostatic compression*

$$e_{ii'} = \mathcal{U}\delta_{ii'} \Rightarrow f_{ii'} = 0, \ g_{ii'} = e_{ii'}, \ \sum_{ii'} g_{ii'} = e = 3\mathcal{U} \text{ and } \sum_{ii'} f_{ii'} = 0 \ . \tag{1.20}$$

These deformations are linearly independent, since they rule each other out: if $e_{ii'} = \mathcal{U}\delta_{ii'}$, then $e_{ii} = 3\mathcal{U} \neq 0$ ($\mathcal{U} \neq 0$ in order to have a deformation) and if $e_{ii} = 0$, then the diagonal elements must have opposite signs, so there is no way that they all have the same value $\mathcal{U}$.

1.2 The stress tensor

When a deformation occurs, the arrangement of the molecules is changed, causing forces to arise within the body. These are called *internal forces* and have a very short range of action. Hence, it follows that the forces by surrounding parts, exerted on any part of a given volume δV of the body, act only on the surface of that part.

Let us consider the total force on some portion δV of the body. This total force is equal to the sum of all the forces on all the volume elements in that portion of the body, i.e. it can be written as the volume integral $\mathbf{F}_{\delta V} = \int_{\delta V} \boldsymbol{\mathcal{F}} \, dV$, where $\boldsymbol{\mathcal{F}}$ is the total force

per unit volume acting on an infinitesimal volume dV. However, the internal forces, with which various parts of the portion δV act on one another, do not contribute in the total resultant force, since they are canceled by Newton's third law. The remaining *external* forces are those exerted on δV by the portions of the body surrounding it, and as we noted before they are superficial. Thus, referring to the ith component of the force, we have $F_{\delta V;i} = \oint_S \sigma_{ii'}\, dS_{i'}$, where $\sigma_{ii'}$ is a second order tensor. It has dimensions of pressure and denotes the ith component of the force per unit area that acts on the surface element $dS_{i'}$, perpendicular to the i'th direction. So, $\sigma_{i'i'}$ is the force per unit area perpendicular to $dS_{i'}$, whereas $\sigma_{ii'}$, $i \neq i'$, are the tangential components of force per unit area on $dS_{i'}$. The tensor $\sigma_{ii'}$ is called the *stress tensor*.

Using *Gauss Theorem* we end up with

$$F_{\delta V;i} = \int_{\delta V} \mathcal{F}_i\, dV = \oint_S \sigma_{ii'}\, dS_{i'} = \int_{\delta V} \sigma_{ii',i'}\, dV\ , \tag{1.21}$$

and by comparing the two expressions for $\mathbf{F}_{\delta V}$ we have

$$\mathcal{F}_i = \sigma_{ii',i'} = \sum_{i'} \frac{\partial \sigma_{ii'}}{\partial x_{i'}}\ . \tag{1.22}$$

This expression connects the stress tensor to the force. It can be proven [50] that the stress tensor is symmetric

$$\sigma_{ii'} = \sigma_{i'i}\ . \tag{1.23}$$

If the stress tensor is both diagonal and isotropic, i.e.,

$$\sigma_{ii'} = -p\delta_{ii'}\ , \tag{1.24}$$

it corresponds to hydrostatic compression. It must be noted that the negative sign denotes an inward flow to the surface $dS_{i'}$.

1.3 Hooke's law

Since the tensor $e_{ii'}$ is linked to the displacement due to deformations, and the tensor $\sigma_{ii'}$ is linked to the forces, and given that deformations occur under the action of forces, we can assume that the two tensors must be connected. Indeed, the infinitesimal work done per unit volume is $\delta R = \mathcal{F}_i \delta u_i$, consequently the total work, using Eqs. (1.22), (1.23), will be

$$\begin{aligned} W &= \int \mathcal{F}_i \delta u_i dV = \int \sigma_{ii',i'} \delta u_i dV = \int \left[(\sigma_{ii'} \delta u_i)_{,i'} - \sigma_{ii'} (\delta u_i)_{,i'} \right] dV \\ &= \cancelto{0}{\oint_S \sigma_{ii'} \delta u_i dS_{i'}} - \int \sigma_{ii'} \delta u_{i,i'} dV \\ &= -\frac{1}{2} \int \sigma_{ii'} \delta \left(u_{i,i'} + u_{i',i} \right) dV = -\int \sigma_{ii'} \delta e_{ii'} dV\ , \end{aligned} \tag{1.25}$$

where we assume that, at the limits of the body, the stress is zero. Then, the infinitesimal work per unit volume is

$$\delta R = -\sigma_{ii'}\delta e_{ii'} \text{ or } dR = -\sigma_{ii'}de_{ii'} \ . \tag{1.26}$$

For the simple case of hydrostatic compression Eq. (1.24) holds true and with the help of Eq. (1.14) we obtain: $dR = -\sigma_{ii'}de_{ii'} = p\ de_{ii} = p\ dv$, where dv is the relative volume change during the deformation $de_{ii'} \equiv e'_{ii'} - e_{ii'}$ and equals to $dv = \frac{dV''-dV'}{dV}$, where dV'' and dV' are the volumes caused by the deformations $e'_{ii'}$ and $e_{ii'}$ respectively. So, we end up with the expected result for the work: *infinitesimal work per unit volume*= (*pressure*)×(*relative volume change*).

Using Eq. (1.26), and known thermodynamic expressions, we calculate the Helmholtz free energy per unit volume F [4]

$$dF = -dR - SdT = \sigma_{ii'}de_{ii'} - SdT \ , \tag{1.27}$$

thus leading to

$$\sigma_{ii'} = \left.\frac{\partial F}{\partial e_{ii'}}\right|_T \ . \tag{1.28}$$

Our goal is to link the two tensors $\sigma_{ii'}$ and $e_{ii'}$ using the Helmholtz free energy. We know that when the stress on a body is zero, then we expect the strain to be zero too, meaning:

$$\sigma_{ii'} = 0 \Rightarrow e_{ii'} = 0 \ . \tag{1.29}$$

In order to satisfy this condition and since Eq. (1.28) is true, it follows that there is no linear term in the expansion of F in powers of $e_{ii'}$. Also, considering as reference level the state where the strain of the body is zero and remembering that we always assume small strains, then we can say that F will be the sum of the squares of all the components $e_{ii'}$. So for an isotropic body at some temperature (constant throughout the body), F is

$$F = \frac{1}{2}\lambda e_{ii}^2 + \mu e_{ii'}^2 \ , \tag{1.30}$$

where λ, μ are called *Lamé* coefficients and so far they are nothing more than coefficients of proportionality with dimensions of energy density (energy per unit volume). Rewriting $e_{ii'}$ using Eqs. (1.17), (1.18), (1.19), we obtain

$$\begin{aligned} e_{ii'}^2 &= f_{ii'}^2 + g_{ii'}^2 + 2f_{ii'}g_{ii'} \\ &= f_{ii'}^2 + \frac{1}{9}\delta_{ii'}^2 e^2 + \frac{2}{3}\delta_{ii'}f_{ii'}e \\ &= f_{ii'}^2 + \frac{1}{3}e^2 + \frac{2}{3}f_{ii}e \\ &= f_{ii'}^2 + \frac{1}{3}e^2 \ , \end{aligned} \tag{1.31}$$

[4] There is no confusion with the ith component of the force F_i, because the component i is missing.

therefore Eq. (1.30) becomes

$$F = \frac{K}{2} e^2 + \mu f_{ii'}^2 \ , \tag{1.32}$$

with

$$K \equiv \lambda + \frac{2\mu}{3} \ . \tag{1.33}$$

Based on Eqs. (1.32) and (1.19), (1.20) we make a useful observation: a) in case of pure shear deformation, i.e. $e_{ii} = 0$, then $F = \mu (f_{ii'})^2 = \mu (e_{ii'})^2$, and b) in case of hydrostatic compression, i.e. $e_{ii'} = \mathcal{U} \delta_{ii'}$, then $F = \frac{9K}{2} \mathcal{U}^2$. Namely:

$$F = \begin{cases} \mu f_{ii'}^2 = \mu e_{ii'}^2 \ , & \text{pure shear deformation} \\ 9K\mathcal{U}^2/2 = Ke^2/2 \ , & \text{hydrostatic compression} \end{cases} \ . \tag{1.34}$$

In a state of thermodynamic equilibrium, the free energy is a minimum. If no external forces act on the body, then F as a function of $u_{ii'}$ must have a minimum for $u_{ii'} = 0$. Minimizing Eq. (1.34) leads to $\mu > 0$ and $K > 0$ respectively. The quantities K and μ are called respectively the *bulk modulus* or *modulus of hydrostatic compression* and the *shear modulus* or *modulus of rigidity*. Equations (1.30) and (1.32) are equivalent, but the second one has the advantage, when used in combination with Eq. (1.34) to give a more clear meaning to K, μ: they are moduli of the Helmholtz free energy in the cases of hydrostatic compression and pure shear deformation respectively. Moreover, μ is zero for fluids because they do not support pure shear deformations. K relates to the *coefficient of hydrostatic compression*, κ_T, as we will see here below.

Starting from Eq. (1.28) and differentiating F from Eq. (1.30) we have

$$\sigma_{ii'} = \lambda e \frac{\partial e_{i''i''}}{\partial e_{ii'}} + 2\mu e_{i''i'''} \frac{\partial e_{i''i'''}}{\partial e_{ii'}} \tag{1.35}$$

and

$$\frac{\partial e_{i''i''}}{\partial e_{ii'}} = \delta_{ii''} \delta_{i'i''} = \delta_{ii'} \ , \quad \frac{\partial e_{i''i'''}}{\partial e_{ii'}} = \delta_{ii''} \delta_{i'i'''} \ , \tag{1.36}$$

so

$$\sigma_{ii'} = \lambda e \delta_{ii'} + 2\mu e_{ii'} \ , \tag{1.37}$$

and using K from Eq. (1.33)

$$\sigma_{ii'} = Ke + 2\mu \left(e_{ii'} - \frac{1}{3} e \delta_{ii'} \right) \ , \tag{1.38}$$

or from Eq. (1.18)

$$\sigma_{ii'} = 3K g_{ii'} + 2\mu f_{ii'} \ . \tag{1.39}$$

Finally, Eqs. (1.37), (1.38), (1.39) are the requested expressions and confirm that the stress is a linear function of the strain, which is the well known *Hooke's law*, valid only for

small strains. We can also write the stress tensor as a sum of two parts, one that is due to pure shear deformation and one due to hydrostatic compression, based on Eq. (1.39).

a) In case of *pure shear deformation*

$$\sigma_{ii'} = 2\mu f_{ii'} \Rightarrow \sigma_{ii} = 0 \; . \tag{1.40}$$

b) In case of *hydrostatic compression*

$$\sigma_{ii'} = 3Kg_{ii'} = Ke\delta_{ii'} = 3K\mathcal{U}\delta_{ii'} \; , \tag{1.41}$$

which, compared to Eq. (1.24), gives $p = -Ke = -3K\mathcal{U}$. We can now relate the bulk modulus K to the coefficient of hydrostatic compression

$$\kappa_T \equiv -\frac{1}{V}\left.\frac{\partial V}{\partial p}\right|_T \; . \tag{1.42}$$

Since the deformations are small, $\mathcal{U}$ and p are small quantities, and we can write the ratio of the relative volume change to the pressure, $3\mathcal{U}/p$, in the differential form $V^{-1}(\partial V/\partial p)_T$, with the help of Eqs. (1.24), (1.41), (1.42), we have

$$\kappa_T = -\frac{e}{p} = \frac{1}{K} \; . \tag{1.43}$$

From Eqs. (1.40), (1.41) it is clear that the properties of $e_{ii'}$, depending on the kind of deformation, are depicted in $\sigma_{ii'}$.

The components $i, i' = 1, 2, 3$ in the expressions (1.37), (1.38), (1.39) refer to the cartesian coordinates x, y, z, but the same expressions apply for the spherical coordinates as well, if we match the coordinates r, θ, ϕ to the components $i, i' = 1, 2, 3$.

We will complete this section by introducing a new quantity, called the *surface traction* $\boldsymbol{\tau}(\mathbf{r})$, which is especially useful when dealing with inhomogeneous media, where a discontinuity exists. The components of the surface traction $\boldsymbol{\tau}(\mathbf{r})$ at a given point $\mathbf{r}$ of an interface are defined [51] as

$$\tau_i(\mathbf{r}) = \sigma_{ii'}(\mathbf{r})n_{i'}(\mathbf{r}) = \sigma_{i'i}(\mathbf{r})n_{i'}(\mathbf{r}) \; , \tag{1.44}$$

where $n_{i'}(\mathbf{r})$ is the ith Cartesian component of the unitary vector $\hat{\mathbf{n}}(\mathbf{r})$ that is perpendicular to the interface at the point $\mathbf{r}$. So, for example, if the interface is parallel to the xy plane, then $\hat{\mathbf{n}}(\mathbf{r}) = \hat{\mathbf{e}}_z$ and from Eqs. (1.37), (1.44) we have

$$\begin{aligned}
\tau_x &= \sigma_{xz} = \mu\left[\frac{\partial u_x}{\partial z} + \frac{\partial u_z}{\partial x}\right] \\
\tau_y &= \sigma_{yz} = \mu\left[\frac{\partial u_y}{\partial z} + \frac{\partial u_z}{\partial y}\right] \\
\tau_z &= \sigma_{zz} = \lambda\nabla\cdot\mathbf{u} + 2\mu\frac{\partial u_z}{\partial z} \; .
\end{aligned} \tag{1.45}$$

Correspondingly, if the interface is spherical with its center at the origin, then $\hat{\mathbf{n}}(\mathbf{r}) = \hat{\mathbf{r}}$ and we have

$$\begin{aligned}
\tau_r &= \sigma_{rr} = \lambda \nabla \cdot \mathbf{u} + 2\mu \frac{\partial u_r}{\partial r} \\
\tau_\theta &= \sigma_{r\theta} = \mu \left[\frac{1}{r} \frac{\partial u_r}{\partial \theta} + \frac{\partial u_\theta}{\partial r} - \frac{u_\theta}{r} \right] \\
\tau_\phi &= \sigma_{r\phi} = \mu \left[\frac{1}{r \sin\theta} \frac{\partial u_r}{\partial \phi} + \frac{\partial u_\phi}{\partial r} - \frac{u_\phi}{r} \right] .
\end{aligned} \tag{1.46}$$

1.4 The wave equation

We have already related the stress to the force through Eq. (1.22) and the stress $\sigma_{ii'}$ to the deformation $e_{ii'}$ through Eqs. (1.37), (1.38), (1.39). Therefore, it comes natural to relate the force to the displacement vector, through $e_{ii'}$. Indeed, based on Eqs. (1.5), (1.22) and (1.37) we have

$$\begin{aligned}
\mathcal{F}_i &= \sigma_{ii'',i''} = \delta_{ii''} \left(\lambda e_{i'i'}\right)_{,i''} + 2 \left(\mu e_{ii''}\right)_{,i''} \\
&= \delta_{ii''} \left(\lambda u_{i',i'}\right)_{,i''} + \left(\mu u_{i,i''} + \mu u_{i'',i}\right)_{,i''}
\end{aligned} \tag{1.47}$$

and in vector form

$$\begin{aligned}
\boldsymbol{\mathcal{F}} &= (\lambda + 2\mu) \nabla(\nabla \cdot \mathbf{u}) - \mu \nabla \times \nabla \times \mathbf{u} + (\nabla \cdot \mathbf{u}) \nabla \lambda \\
&+ (\nabla \mu \cdot \nabla)\mathbf{u} + \nabla(\mathbf{u} \cdot \nabla \mu) - \mathbf{u} \cdot \nabla(\nabla \mu) .
\end{aligned} \tag{1.48}$$

This is the expression of the force per unit volume that causes the deformations versus the displacement vector. In case of equilibrium, the condition is $\boldsymbol{\mathcal{F}}_{tot} = \mathbf{0}$, where $\boldsymbol{\mathcal{F}}$ is included in $\boldsymbol{\mathcal{F}}_{tot}$, along with the rest of the forces applied to the body.

If the body is not in the state of equilibrium, then the equation of motion becomes $\boldsymbol{\mathcal{F}}_{tot} = \rho \boldsymbol{\alpha}$, where $\boldsymbol{\alpha}$ is the acceleration and ρ is the mass density. In order to obtain the equation of motion for an isotropic elastic medium we will neglect the effect of the rest of the forces and, based on the above, we have

$$\boldsymbol{\mathcal{F}} = \rho \boldsymbol{\alpha} = \rho \frac{\partial^2 \mathbf{u}}{\partial t^2} . \tag{1.49}$$

From Eqs. (1.47), (1.49) we finally obtain

$$\rho \frac{\partial^2 u_i}{\partial t^2} = \left[\lambda \delta_{ii''} u_{i',i'} + \mu (u_{i,i''} + u_{i'',i}) \right]_{,i''} . \tag{1.50}$$

It is noted that, in the general case of an inhomogeneous medium, the mass density ρ and the Lamé coefficients λ, μ are functions of the position and one should use the form of Eq. (1.48). In the present work we assume that the Lamé coefficients are real (which is true for media without absorption) and positive quantities, independent of the frequency.

Chapter 2

Acoustic waves in homogeneous elastic and poroelastic media

In this chapter we deal with elastic wave propagation in homogeneous elastic and poroelastic media. We review the theory of the deformation of a poroelastic solid containing a compressible fluid that has been established by Biot [25–28], summarizing pertinent results from Biot's original analysis, and present the corresponding theoretical basis for double-porosity media.

2.1 Elastic homogeneous medium

Let us examine the propagation of elastic waves, of given frequency Ω, in a homogeneous and isotropic elastic medium of mass density ρ and Lamé coefficients λ, μ [52]. In such a medium, the elastic parameters ρ, λ and μ do not depend on the position and, assuming harmonic time dependence $\mathbf{u}(\mathbf{r},t) = \mathrm{Re}[\mathbf{u}(\mathbf{r})\exp(-\mathrm{i}\Omega t)]$, the wave equation (1.49) yields

$$-c_l^2\nabla[\nabla\cdot\mathbf{u}(\mathbf{r})] + c_t^2\nabla\times[\nabla\times\mathbf{u}(\mathbf{r})] = \Omega^2\mathbf{u}(\mathbf{r})\ , \tag{2.1}$$

where $c_l = \sqrt{(\lambda+2\mu)/\rho}$ and $c_t = \sqrt{\mu/\rho}$ are the propagation velocities of longitudinal and transverse waves, respectively. We note again that the Lamé coefficients are real numbers in a non-absorbing medium but, in the case where dissipation losses are present, they become complex [53]. It can be proven [1] that the elastic field can be expressed as a sum of two independent terms, one longitudinal (irrotational, $\nabla\times\mathbf{u}(\mathbf{r}) = \mathbf{0}$) and one transverse (solenoidal, $\nabla\cdot\mathbf{u}(\mathbf{r}) = \mathbf{0}$), so Eq. (2.1) splits in two independent Helmholtz equations

$$\nabla^2\mathbf{u}(\mathbf{r}) + Q_l^2\mathbf{u}(\mathbf{r}) = 0,\ \nabla\times\mathbf{u}(\mathbf{r}) = 0, \tag{2.2}$$

[1] Following Helmholtz theorem, under the condition that the curl and the divergence of the vector $\mathbf{u}$ become zero at infinity, which is true in our case.

and

$$\nabla^2\mathbf{u}(\mathbf{r}) + Q_t^2\mathbf{u}(\mathbf{r}) = 0, \;\; \nabla\cdot\mathbf{u} = 0\,, \tag{2.3}$$

with $Q_\nu = \Omega/c_\nu$, $\nu = l, t$. We note that in a non-viscous fluid ($\mu = 0$ or equivalently $c_t = 0$), only longitudinal waves can propagate. Equations (2.2), (2.3) accept plane wave solutions

$$\mathbf{u}(\mathbf{r}) = \mathbf{u}_0(\mathbf{Q}_\nu)\exp(\mathrm{i}\mathbf{Q}_\nu\cdot\mathbf{r}), \tag{2.4}$$

with $\mathbf{u}_0(\mathbf{Q}_\nu) = u_0(\mathbf{Q}_\nu)\hat{\mathbf{e}}$, $\mathbf{Q}_\nu = Q_\nu\hat{\mathbf{e}}_1(\mathbf{Q}_\nu)$, where u_0 denotes the magnitude and the unit vector $\hat{\mathbf{e}}$ the polarization of the elastic wave.

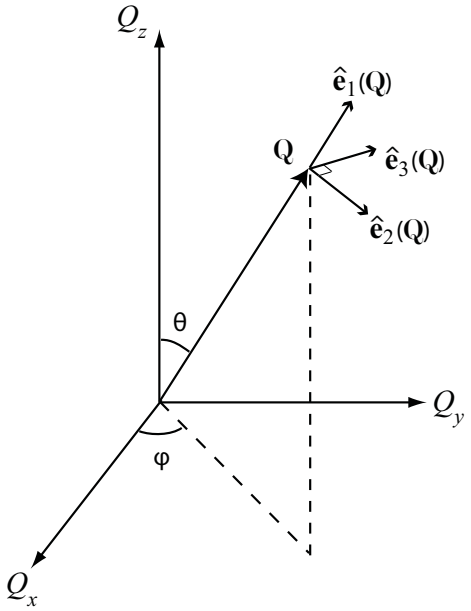

Figure 2.1: Local coordinate system.

For longitudinal waves $\hat{\mathbf{e}} = \hat{\mathbf{e}}_1(\mathbf{Q}_l)$, while for transverse waves $\hat{\mathbf{e}}\perp\hat{\mathbf{e}}_1(\mathbf{Q}_t)$. There are two independent transverse waves, which correspond to two independent polarizations, i.e., $\hat{\mathbf{e}} = \hat{\mathbf{e}}_2(\mathbf{Q}_t)$, $\hat{\mathbf{e}} = \hat{\mathbf{e}}_3(\mathbf{Q}_t)$. With $\hat{\mathbf{e}}_\mathrm{p}(\mathbf{Q})$, p $= 1, 2, 3$, we denote the radial, polar and azimuthal unit vectors for a specific vector $\mathbf{Q}$ (see Fig. 2.1). Therefore, the index p also denotes the polarization ν of the elastic field.

2.2 Poroelastic homogeneous medium

In the framework of Biot's theory, a fluid-saturated poroelastic material is considered as a macroscopically homogeneous and isotropic two-component (solid-fluid) system, which

can be described in terms of average parameters. Its skeletal frame is made of a solid material, characterized by mass density ρ_s, bulk modulus K_s, and shear modulus μ_s in its consolidated compact form, while the bare skeletal frame has different elastic moduli, K_b and μ_b. The term bare skeletal frame, or else lattice, refers to a drained medium such that the pores are assumed to be evacuated. The fluid, of mass density ρ_f and bulk modulus K_f, fills the whole volume of interconnected pores. The fluid may possess a nonzero viscosity, and energy absorption by the lattice is introduced by replacing certain real-valued lattice parameters (K_b and μ_b) by complex-valued quantities. It should be noted that sealed pore space is considered as part of the solid frame and the (effective) porosity f is defined as the volume fraction occupied by the fluid.

Consider a volume of the solid-fluid system represented by a cube of unit size. The stress tensor is separated into two parts. The force component acting on the solid parts of each face of the cube is one part. This is denoted as the symmetric tensor, according to Eq. (1.23), $\tau_{ii'} \equiv \sigma^{(s)}_{ii'} = \sigma^{(s)}_{i'i}$. The forces acting on the fluid part of each face of the cube are represented by the tensor $s_{ii'} \equiv \sigma^{(f)}_{ii'} = -fp\delta_{ii'}$, according to Eq. (1.24) for the case of hydrostatic compression. In the present analysis we assume that we are dealing with a statistically isotropic porous material in such a way that for all cross sections we always observe the same ratio of fluid to solid area, explaining why the porosity appears in the definition of the stress tensor of the fluid. Following the same steps as in Chapter 1 to determine the stress-strain relations, we retain the same Eqs. (1.27), (1.28), with the only difference that now the stress tensor is composed by two parts that are coupled to each other. Denoting the average macroscopic displacement fields of the solid frame and the saturating fluid in space-time $(\mathbf{r}, t)$ by $\mathbf{u}$ and $\mathbf{U}$, respectively, and the corresponding strain tensors by $e_{ii'}$ and $E_{ii'}$, we generalize Eqs. (1.37) and (1.41) to obtain the relevant effective stress tensors

$$\tau_{ii'} = \lambda_b e\delta_{ii'} + 2\mu_b e_{ii'} + \mathcal{Q}E\delta_{ii'} \ , \tag{2.5}$$

$$s_{ii'} = \mathcal{Q}'e\delta_{ii'} + \mathcal{R}E\delta_{ii'} \ , \tag{2.6}$$

where we recall that $e = e_{ii} = \boldsymbol{\nabla}\cdot\mathbf{u}$, $E = E_{ii} = \boldsymbol{\nabla}\cdot\mathbf{U}$ are the volumetric strains [Eqs. (1.6)]. Because of the existence of a potential energy the coupling coefficients $\mathcal{Q}, \mathcal{Q}'$ must be the same $\mathcal{Q} = \mathcal{Q}'$. Using compact tensor/vector notation, Eqs. (2.5), (2.6) can be written as

$$\begin{aligned} \overleftrightarrow{\boldsymbol{\tau}} &= \mu_b \overleftrightarrow{\mathbf{I}} \times \boldsymbol{\nabla} \times \mathbf{u} + 2\mu_b \boldsymbol{\nabla}\mathbf{u} + \overleftrightarrow{\mathbf{I}}(\mathcal{P} - 2\mu_b)\boldsymbol{\nabla}\cdot\mathbf{u} + \overleftrightarrow{\mathbf{I}}\mathcal{Q}\boldsymbol{\nabla}\cdot\mathbf{U} \\ \overleftrightarrow{\mathbf{s}} &= \overleftrightarrow{\mathbf{I}}\mathcal{Q}\boldsymbol{\nabla}\cdot\mathbf{u} + \overleftrightarrow{\mathbf{I}}\mathcal{R}\boldsymbol{\nabla}\cdot\mathbf{U} \ , \end{aligned} \tag{2.7}$$

where it is tacitly assumed that the strains associated with these stresses are small and

the quantities $\mathcal{P}$, $\mathcal{Q}$, $\mathcal{R}$ are given by [54]

$$\begin{aligned}\mathcal{P} &= K_s\frac{(1-f)(1-f-K_b/K_s)+fK_b/K_f}{1-f-K_b/K_s+fK_s/K_f}+\frac{4\mu_b}{3}\\ \mathcal{Q} &= \frac{fK_s(1-f-K_b/K_s)}{1-f-K_b/K_s+fK_s/K_f}\\ \mathcal{R} &= \frac{f^2K_s}{1-f-K_b/K_s+fK_s/K_f}\,.\end{aligned} \tag{2.8}$$

In order to clarify the significance of these constants, while writing the stress-strain relations in order to find the form of the effective stress tensors for the solid-fluid system, Biot noticed that $\mathcal{P}=K_b+4\mu_b/3$, and is a positive quantity. The coefficient $\mathcal{R}$ measures the pressure required on the fluid to force a certain volume of the fluid into the aggregate, while the total volume remains constant. It is also a positive quantity. The coefficient $\mathcal{Q}$ describes the coupling between the volume change of the solid and of the fluid and it is also of positive sign. The macroscopic stress tensor, $\overleftrightarrow{\boldsymbol{\sigma}}$, and the mean pore fluid pressure, p, are given by

$$\overleftrightarrow{\boldsymbol{\sigma}}=\overleftrightarrow{\boldsymbol{\tau}}+\overleftrightarrow{\mathbf{s}} \tag{2.9}$$

and

$$\overleftrightarrow{\mathbf{s}}=-\overleftrightarrow{\mathbf{I}}\,fp\,, \tag{2.10}$$

respectively. Although the fluid may have a nonzero viscosity, Eq. (2.10) retains the form of a stress tensor within the small strain limit of nonviscous hydrodynamics.

Biot derived a phenomenological Lagrangian density for a fluid-lattice system, assumed to be homogeneous for low-frequency wave propagation, firstly in the absence of dissipation. A unit cube of the aggregate is considered as an element. The element is assumed to be small relative to the wavelength of the elastic waves and in turn the size of the pores is assumed small compared to the size of the element. The limitation of frequencies which is hereby introduced will turn out to be academic for most practical problems. In general, the kinetic energy of a system can always be written as the sum of three homogeneous functions of the generalized velocities: a term independent of the velocities, a term linear in the velocities and a term quadratic in the velocities. If the transformation equations do not contain the time explicitly, as may occur when the constraints are independent of time (scleronomous) −which is our case here− then only the last term is nonvanishing and the kinetic energy T of the system per unit volume always has a homogeneous quadratic form in the generalized velocities and may be expressed as [55]

$$2T=\rho_{11}\dot{\mathbf{u}}\cdot\dot{\mathbf{u}}+\rho_{22}\dot{\mathbf{U}}\cdot\dot{\mathbf{U}}+2\rho_{12}\dot{\mathbf{u}}\cdot\dot{\mathbf{U}}\,, \tag{2.11}$$

where overdot denotes partial time derivative. This expression is based on the assumption that the material is statistically isotropic, hence the directions x, y, z are equivalent and

uncoupled dynamically. Let us discuss the significance of the expression for the kinetic energy. The coefficients $\rho_{11}, \rho_{22}, \rho_{12}$ are mass coefficients which take into account the fact that the relative fluid flow through the pores is not uniform. Lagrange's equations will be

$$\frac{\partial}{\partial t}\left(\frac{\partial T}{\partial \dot{u}_i}\right) = \tau_{ij,j}, \tag{2.12}$$

$$\frac{\partial}{\partial t}\left(\frac{\partial T}{\partial \dot{U}_i}\right) = s_{ij,j}, \tag{2.13}$$

for $i = 1, 2, 3$, where the force components on the right-hand side are expressed as stress gradients. Eqs. (2.12) and (2.13) together with Eq. (2.11) can be combined into

$$\begin{pmatrix} \rho_{11} & \rho_{12} \\ \rho_{12} & \rho_{22} \end{pmatrix} \begin{pmatrix} \ddot{u}_i \\ \ddot{U}_i \end{pmatrix} = \begin{pmatrix} \tau_{ij,j} \\ s_{ij,j} \end{pmatrix} , \tag{2.14}$$

showing the coupling between the solid and the fluid. It is interesting to note that, because of the coupling coefficient, an acceleration of the solid without average motion of the fluid produces a pressure gradient in the fluid. This is physically caused by an apparent mass effect of the fluid on the solid.

We will now discuss what happens in the case of dissipation due to viscous drag. Biot supplemented the Lagrangian density with a dissipation term, which accounts for viscous drag forces associated with the relative motion within the system, and then Eq. (2.14) can be generalized in the following form

$$\begin{aligned} \rho_{11}\ddot{\mathbf{u}} + \rho_{12}\ddot{\mathbf{U}} + b(\dot{\mathbf{u}} - \dot{\mathbf{U}}) &= \boldsymbol{\nabla} \cdot \overleftrightarrow{\boldsymbol{\tau}} \\ \rho_{12}\ddot{\mathbf{u}} + \rho_{22}\ddot{\mathbf{U}} - b(\dot{\mathbf{u}} - \dot{\mathbf{U}}) &= \boldsymbol{\nabla} \cdot \overleftrightarrow{\mathbf{s}} , \end{aligned} \tag{2.15}$$

where b is a damping coefficient and the last term on the left-hand sides of Eqs. (2.15) accounts for frictional dissipation associated with relative motion between the fluid and solid components of the medium. The quantities ρ_{11}, ρ_{12}, ρ_{22}, are related to the fluid's density ρ_f and the solid's density ρ_s through

$$\begin{aligned} \rho_{11} &= (1-f)\rho_s + (\xi - 1)f\rho_f \\ \rho_{12} &= -(\xi - 1)f\rho_f \\ \rho_{22} &= \xi f \rho_f \end{aligned} \tag{2.16}$$

where $\rho_{11} + 2\rho_{12} + \rho_{22} = \rho_{tot} = (1-f)\rho_s + f\rho_f$ is the total mass of the system and with ξ ($\xi > 1$), the so-called *tortuosity*[2] of the medium, being an intrinsic geometrical property related to variations in pore shapes and orientations [56–61]. The best value of ξ should be determined, of course, by the experimental data themselves, i.e., it should furnish the

[2]Biot refers to the factor ξ as a *structural* factor.

best fit for dispersion and attenuation data. In fact, by arguing that the value of ξ is independent of the saturating fluid, Johnson and Sen determined ξ from fourth-sound measurements using super-fluid ^{4}He as a pore fluid in various substrates [62]. It is worth noting here that the term ρ_{12} describes the *inertial* (as opposed to viscous) drag that the fluid exerts on the solid as the latter is accelerated relative to the former and vice-versa. That is why, instead of tortuosity, ξ is also called the inertial drag parameter. We will see in the following that two distinct limits exist in this problem. One where the solid and the fluid are locked due to viscous drag and another where they are locked due to inertial drag. Intrinsic absorption of the solid frame and the infiltrated fluid can be taken into account by considering complex elastic constants, as we have already noted.

At low frequencies, assuming that the flow of the fluid relative to the solid through the pores is of the Poiseuille type, the coefficient b is related to Darcy's coefficient of permeability, κ_D, through the relation $b = f^2\eta/\kappa_D$, where η is the fluid viscosity [25]. The assumption of Poiseuille flow breaks down at high frequencies and b can be written in a general form, which encompasses both the low and high frequency ranges, as follows [26]

$$b = \frac{f^2\eta}{\kappa_D}\frac{\mathrm{i}\zeta^2 J_0'(\sqrt{\mathrm{i}}\zeta)}{4\sqrt{\mathrm{i}}\zeta J_0(\sqrt{\mathrm{i}}\zeta) + 8J_0'(\sqrt{\mathrm{i}}\zeta)}\ , \tag{2.17}$$

where J_0 is the zero-order Bessel function of the first kind [63], and the prime denotes first derivative with respect to the argument of the function. In the simple case of cylindrical pores parallel to the direction of the flow, $\zeta = R_p\sqrt{\Omega\rho_f/\eta}$, where R_p is a characteristic pore size parameter that takes into account the geometry of the pores. The expression that multiplies the factor $f^2\eta/\kappa_D$ in the right-hand side of Eq. (2.17), considered as a function of the real dimensionless variable ζ over the entire range $0 \le \zeta < \infty$, $\left[F_1(\zeta) = \frac{\mathrm{i}\zeta^2 J_0'(\sqrt{\mathrm{i}}\zeta)}{4\sqrt{\mathrm{i}}\zeta J_0(\sqrt{\mathrm{i}}\zeta)+8J_0'(\sqrt{\mathrm{i}}\zeta)}\right]$, behaves similarly to the simple function $F_2(\zeta) = \sqrt{1-\mathrm{i}(\zeta/4)^2}$, their absolute relative difference $\Delta = \left|\frac{F_1(\zeta)-F_2(\zeta)}{[F_1(\zeta)+F_2(\zeta)]/2}\right|$ being always less than 10%, as is shown in Fig. 2.2.

Moreover, the geometrical parameters f, ξ, κ_D, R_p, which characterize the pores and are in general unrelated, for a set of non-intersecting canted cylindrical pores are related to each other by the equation $fR_p^2 = 8\xi\kappa_D$, which leads to the following simple yet effective form for b [64]

$$b = \frac{f^2\eta}{\kappa_D}\left(1 - \mathrm{i}\frac{\xi\kappa_D\rho_f\Omega}{2f\eta}\right)^{1/2}\ . \tag{2.18}$$

In the case of a poroelastic medium we assume monochromatic time-harmonic solutions of Eqs. (2.15), of angular frequency Ω, in the form $\mathbf{u}(\mathbf{r},t) = \mathrm{Re}[\mathbf{u}(\mathbf{r})\exp(-\mathrm{i}\Omega t)]$ and $\mathbf{U}(\mathbf{r},t) = \mathrm{Re}[\mathbf{U}(\mathbf{r})\exp(-\mathrm{i}\Omega t)]$. Decomposing the general displacement fields into longitudinal and transverse vector components, denoted by a subscript l and t, respectively,

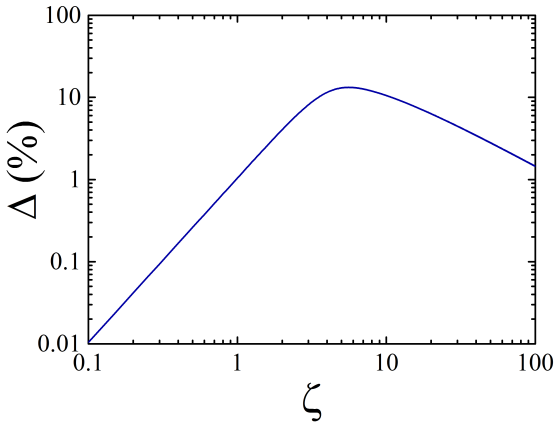

Figure 2.2: Δ versus ζ.

Eqs. (2.7) and (2.15) lead to two separate systems of linear equations. For the longitudinal modes we obtain

$$\mathcal{P}\boldsymbol{\nabla}[\boldsymbol{\nabla}\cdot\mathbf{u}_l(\mathbf{r})]+\mathcal{Q}\boldsymbol{\nabla}[\boldsymbol{\nabla}\cdot\mathbf{U}_l(\mathbf{r})]+\widetilde{\rho}_{11}\Omega^2\mathbf{u}_l(\mathbf{r})+\widetilde{\rho}_{12}\Omega^2\mathbf{U}_l(\mathbf{r})=0 \tag{2.19a}$$

$$\mathcal{Q}\boldsymbol{\nabla}[\boldsymbol{\nabla}\cdot\mathbf{u}_l(\mathbf{r})]+\mathcal{R}\boldsymbol{\nabla}[\boldsymbol{\nabla}\cdot\mathbf{U}_l(\mathbf{r})]+\widetilde{\rho}_{12}\Omega^2\mathbf{u}_l(\mathbf{r})+\widetilde{\rho}_{22}\Omega^2\mathbf{U}_l(\mathbf{r})=0\,, \tag{2.19b}$$

where $\widetilde{\rho}_{11}=\rho_{11}+\mathrm{i}b/\Omega$, $\widetilde{\rho}_{12}=\rho_{12}-\mathrm{i}b/\Omega$, and $\widetilde{\rho}_{22}=\rho_{22}+\mathrm{i}b/\Omega$. Equations (2.19) accept plane-wave solutions [see Eq. (2.4)] of the form $\mathbf{u}_l(\mathbf{r})=\mathbf{u}_{l0}\exp(\mathrm{i}\mathbf{Q}\cdot\mathbf{r})$ and $\mathbf{U}_l(\mathbf{r})=\mathbf{U}_{l0}\exp(\mathrm{i}\mathbf{Q}\cdot\mathbf{r})$, where the wavenumber Q satisfies the biquadratic equation

$$(\mathcal{P}\mathcal{R}-\mathcal{Q}^2)Q^4-(\widetilde{\rho}_{11}\mathcal{R}+\widetilde{\rho}_{22}\mathcal{P}-2\widetilde{\rho}_{12}\mathcal{Q})\Omega^2Q^2+(\widetilde{\rho}_{11}\widetilde{\rho}_{22}-\widetilde{\rho}_{12}^2)\Omega^4=0\,. \tag{2.20}$$

The two positive roots of Eq. (2.20), Q_1 and Q_2, which are physically acceptable, correspond to the so-called fast and slow longitudinal waves, respectively, with $Q_\nu=\Omega/c_\nu, \nu=1,2$. The corresponding displacement fields are related through $\mathbf{U}_\nu=A_\nu\mathbf{u}_\nu$, where

$$A_\nu=-\frac{\widetilde{\rho}_{11}\Omega^2-\mathcal{P}Q_\nu^2}{\widetilde{\rho}_{12}\Omega^2-\mathcal{Q}Q_\nu^2}=-\frac{\widetilde{\rho}_{12}\Omega^2-\mathcal{Q}Q_\nu^2}{\widetilde{\rho}_{22}\Omega^2-\mathcal{R}Q_\nu^2}\,,\quad \nu=1,2\,. \tag{2.21}$$

On the other hand, the transverse modes satisfy the equations

$$\begin{aligned}\mu_b\boldsymbol{\nabla}\times\boldsymbol{\nabla}\times\mathbf{u}_t(\mathbf{r})-\widetilde{\rho}_{11}\Omega^2\mathbf{u}_t(\mathbf{r})-\widetilde{\rho}_{12}\Omega^2\mathbf{U}_t(\mathbf{r}) &= 0\\ \widetilde{\rho}_{12}\mathbf{u}_t(\mathbf{r})+\widetilde{\rho}_{22}\mathbf{U}_t(\mathbf{r}) &= 0\,,\end{aligned} \tag{2.22}$$

which accept plane wave solutions of the form $\mathbf{u}_t(\mathbf{r})=\mathbf{u}_{t0}\exp(\mathrm{i}\mathbf{Q}_3\cdot\mathbf{r})$ and $\mathbf{U}_t(\mathbf{r})=\mathbf{U}_{t0}\exp(\mathrm{i}\mathbf{Q}_3\cdot\mathbf{r})$ with wavenumber

$$Q_3=\Omega\left[\frac{\widetilde{\rho}_{11}}{\mu_b}\left(1-\frac{\widetilde{\rho}_{12}^2}{\widetilde{\rho}_{11}\widetilde{\rho}_{22}}\right)\right]^{1/2}\,. \tag{2.23}$$

As follows directly from the second of Eqs. (2.22),

$$\mathbf{U}_t = -(\widetilde{\rho}_{12}/\widetilde{\rho}_{22})\mathbf{u}_t \equiv A_3\mathbf{u}_t \ . \tag{2.24}$$

An intuitive explanation of the appearance of two longitudinal waves in a poroelastic medium can be provided by analogy to the formation of bonding and antibonding molecular orbitals from the individual atomic states. In a similar manner, the longitudinal modes of the solid and fluid components of the poroelastic medium interact and form two hybrid longitudinal modes with two different propagation velocities. We will attempt to further clarify this point, following D. L. Johnson and T. J. Plona's study on the acoustic properties of water-saturated samples of both fused (i.e., consolidated) and unconsolidated spherical glass beads [43]. Their experimental results confirm the presence of two longitudinal waves, fast and slow, in the consolidated case, whereas only one longitudinal wave exist in the unconsolidated sample. The fact that a minor change in microgeometry resulted to such a radical change in acoustic behavior led them to suspect the bare skeletal frame moduli K_b and μ_b. Hence they considered two limits in the Biot theory[3]:

a) *stiff-frame* limit, where the pore fluid is much more compressible than the frame $K_f \ll K_b$, $\mu_b < K_s$ and, in this limit, Eq. (2.20) provides the two longitudinal velocities

$$c_1^{stiff} = \left(\frac{\mathcal{P}\rho_{22}}{\rho_{11}\rho_{22}-\rho_{12}^2}\right)^{1/2} , \tag{2.25}$$

$$c_2^{stiff} = \left(\frac{K_f}{\rho_f\xi}\right)^{1/2} . \tag{2.26}$$

In this stiff-frame limit the fluid and solid motions are largely decoupled. The fast wave is essentially motion of the solid only, dragging along some of the fluid, whereas the slow wave is essentially motion of the fluid only. This means that some, but not all, of the fluid is dragged along by the oscillations of the stiff frame.

b) *weak-frame* limit, namely that of weak frame moduli $K_b, \mu_b \ll K_f, K_s$. If we idealize the unconsolidated grains as a suspension, we may take the extreme limit that $K_b = \mu_b = 0$[4]. In this case the slow wave speed is identically zero and the fast wave speed is

$$c_1^{weak} = \left[\bar{\kappa}_T^{-1}\frac{f^2\rho_{11}+(1-f)^2\rho_{22}-2f(1-f)\rho_{12}}{\rho_{11}\rho_{22}-\rho_{12}^2}\right]^{1/2} , \tag{2.27}$$

$$c_2^{weak} = 0 \ , \tag{2.28}$$

where $\bar{\kappa}_T = \overline{\frac{1}{K}} = \frac{1-f}{K_s} + \frac{f}{K_f}$ is the average isothermal compressibility of the system. In the case where the inertial drag parameter ξ is very large, which corresponds to a perfect

[3] Assuming we are in the high-frequency limit, $\lim_{\Omega\to\infty}\tilde{\rho}_{ij}(\Omega) = \rho_{ij}$, the velocities become nondispersive.

[4] In this case the quantities $\mathcal{P}, \mathcal{Q}, \mathcal{R}$ satisfy the following equation: $\mathcal{P}\mathcal{R} - \mathcal{Q}^2 = 0$.

locking of fluid and solid motion together, the fast wave speed formula simplifies greatly and reduces to Wood's formula [65]

$$\lim_{\xi\to\infty} c_1 = \sqrt{\frac{\bar{\kappa}_T^{-1}}{\rho_{tot}}}\,. \tag{2.29}$$

We note that, because the fluid and the solid are locked together by viscous forces, this asymptotic value also applies to the low-frequency limit, which is characterized by viscous losses, regardless of ξ.

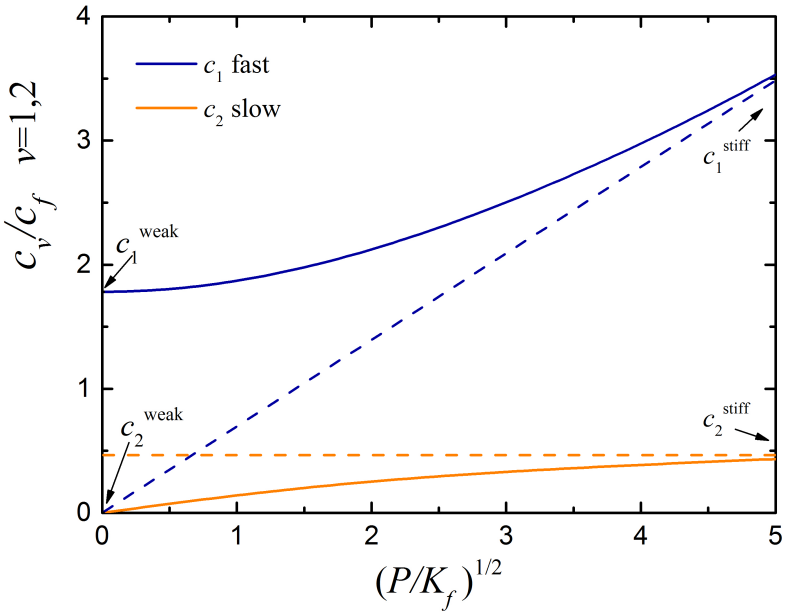

Figure 2.3: Fast and slow longitudinal wave velocities calculated as a function of frame modulus for water-saturated porous silica spherical particles. The solid lines refer to Eq. (2.20), while the dashed lines represent the fully consolidated stiff frame values given by Eqs. (2.25), (2.26). In the limit $K_b = \mu_b = 0$ the wave speed values are given from Eqs. (2.27), (2.28).

We consider water-saturated porous silica spherical particles with mass density $\rho_s = 2200$ kg m^{-3} and bulk modulus $K_s = 36.9397$ GPa for silica; and mass density $\rho_f = 1000$ kg m^{-3} and bulk modulus $K_f = 2.1904$ GPa for water. For porosity $f = 10\%$ the tortuosity is given by $\xi = f^{-2/3}$, for a random array of needles [59]. Now we will consider c_1, c_2 as continuously varied functions of K_b and μ_b, while keeping f, ξ fixed, in order to focus more clearly on the effects of the frame moduli. We have assumed the proportionality $K_b = 1.21\mu_b$ to be constant (corresponding to a constant Poisson's ratio)

and have calculated the fast a slow velocities as a function of $(\mathcal{P}/K_f)^{1/2}$. The results are shown in Fig. 2.3. It can be easily seen that starting from the unconsolidated values given by Eqs. (2.27), (2.28) both of the wave speeds change continuously to the fully consolidated stiff frame values given by Eqs. (2.25), (2.26), indicated by the dashed lines. A heuristic interpretation of the dashed lines in Fig. 2.3 is to view the poroelastic medium as a bimodal system under the influence of some coupling perturbation. This means that the dashed lines represent the bare speeds of two uncoupled (unhybridized) modes, a fluid mode and a frame mode, and in the parameter region where the two speeds are comparable, the modes become mixed (we will have hybridization) and thus the speeds are renormalized by the mutual interactions.

2.3 Double-porosity homogeneous medium

J. G. Berryman and H. F. Wang formulated a phenomenological theory for the poroelastic behavior of a double-porosity medium by extending Biot's theory, and identified the coefficients in these linear equations [66, 67]. The generalization from the single porosity model increases the number of independent coefficients from three to six for an isotropic applied stress.

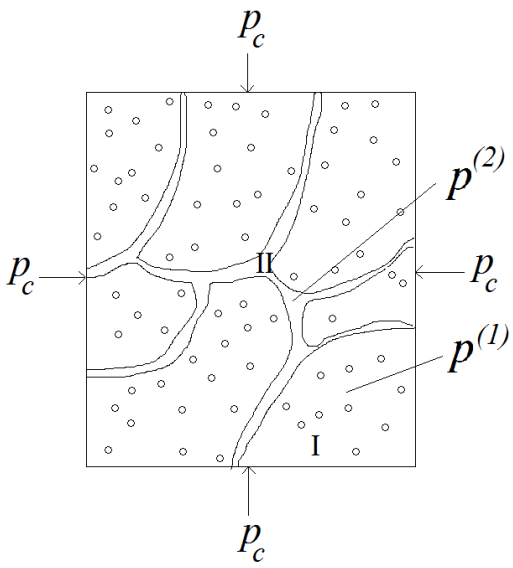

Figure 2.4: Schematic representation of a double-porosity medium.

As originally formulated, Biot's theory applies to a homogeneous porous medium. However, porosity and permeability often occur on several distinct spatial cases. Thus, the need arises for more general models incorporating qualitatively different types of porosity.

Berryman and Wang considered the elements of a double-porosity model to be: porous matrix intersected by fractures. In such a structure, though, the same fluid is assumed to fill the pores and the fractures, there are two different types of porosity, characterized by different scales and environments. First, the system of small porous within the solid frame (region I in Fig. 2.4), with porosity $f^{(1)}$ and volume fraction of the porous matrix $v^{(1)}$, saturated by the fluid; the displacement of the fluid in that scale is denoted by $\mathbf{U}^{(1)}$. Second the system of the fractures (region II in Fig. 2.4) saturated by the fluid which is now in contact with the porous matrix I, and its displacement is denoted by $\mathbf{U}^{(2)}$. The fracture porosity is denoted by $f^{(2)}$ and the volume fraction of the fractures by $v^{(2)}$. Of course $v^{(1)} + v^{(2)} = 1$. In this description, we put $f^{(2)} = 1$ in order to account correctly for the void space.

In each of these two distinct systems an internal fluid pore pressure is present, $p^{(k)}$, $k = 1, 2$, generating in an analogous to the simple poroelasticity [Eq. (2.10)] manner a macroscopic fluid pressure across interfaces:

$$s_{ij}^{(k)} = -v^{(k)} f^{(k)} p^{(k)} \delta_{ij} \ . \tag{2.30}$$

The solid is characterized by its displacement $\mathbf{u}$, as usually, related to the corresponding stress tensor τ_{ij}. The presence of these two distinct pore fluid systems introduces a new set of equations in order to account correctly for the interaction between these components. Instead of two, we have three equations describing

- the elastic behavior of the solid
- the elastic and fluid flow behavior of the pore matrix fluid (region I) interacting with the fractures and the solid
- the elastic and fluid flow behavior of the fracture fluid (region II) interacting with the pore matrix fluid and the solid.

In all the above equations coupling terms are considered to account correctly for all possible interactions. For the purpose of our subsequent analysis, we will neglect the dissipation due to viscous loss mechanisms. Then, Lagrange's equations read

$$\frac{\partial}{\partial t}\left(\frac{\partial T}{\partial \dot{u}_i}\right) = \tau_{ij,j}, \text{ for } i = 1, 2, 3, \tag{2.31}$$

$$\frac{\partial}{\partial t}\left(\frac{\partial T}{\partial \dot{U}_i^{(k)}}\right) = s_{ij,j}^{(k)}, \text{ for } i = 1, 2, 3 \text{ and } k = 1, 2 \ , \tag{2.32}$$

where T is the kinetic energy for the systems of two fluids. We generalize Biot's approach [Eq. (2.11)] by including coupling terms describing the interactions between the different

constituents

$$\begin{aligned} 2T &= \rho_{11}\dot{\mathbf{u}}\cdot\dot{\mathbf{u}} + \rho_{22}\dot{\mathbf{U}}^{(1)}\cdot\dot{\mathbf{U}}^{(1)} + \rho_{33}\dot{\mathbf{U}}^{(2)}\cdot\dot{\mathbf{U}}^{(2)} \\ &+ 2\rho_{12}\dot{\mathbf{u}}\cdot\dot{\mathbf{U}}^{(1)} + 2\rho_{13}\dot{\mathbf{u}}\cdot\dot{\mathbf{U}}^{(2)} + 2\rho_{23}\dot{\mathbf{U}}^{(1)}\cdot\dot{\mathbf{U}}^{(2)} , \end{aligned} \tag{2.33}$$

with ρ_{ij} being mass density coefficients that take into account the fact that the relative flow of fluid through the pores is not uniform, and that oscillations of solid mass in the presence of fluid leads to induced mass effects.

In summary, Eqs. (2.31), (2.32) and (2.33) can be combined into

$$\begin{pmatrix} \rho_{11} & \rho_{12} & \rho_{13} \\ \rho_{12} & \rho_{22} & \rho_{23} \\ \rho_{13} & \rho_{23} & \rho_{33} \end{pmatrix} \begin{pmatrix} \ddot{u}_i \\ \ddot{U}_i^{(1)} \\ \ddot{U}_i^{(2)} \end{pmatrix} = \begin{pmatrix} \tau_{ij,j} \\ s_{ij,j}^{(1)} \\ s_{ij,j}^{(2)} \end{pmatrix} , \tag{2.34}$$

showing the coupling between the solid and both types of fluid components. The mass density coefficients ρ_{ij} are given by the following relations

$$\rho_{11} = (1-f)\rho_s + (\xi-1)f\rho_f , \tag{2.35}$$

$$\rho_{22} = \xi^{(1)}v^{(1)}f^{(1)}\rho_f , \tag{2.36}$$

$$\rho_{33} = \xi^{(2)}v^{(2)}f^{(2)}\rho_f , \tag{2.37}$$

$$2\rho_{12}/\rho_f = (\xi^{(2)}-1)v^{(2)}f^{(2)} - (\xi^{(1)}-1)v^{(1)}f^{(1)} - (\xi-1)f , \tag{2.38}$$

$$2\rho_{13}/\rho_f = (\xi^{(1)}-1)v^{(1)}f^{(1)} - (\xi^{(2)}-1)v^{(2)}f^{(2)} - (\xi-1)f , \tag{2.39}$$

$$2\rho_{23}/\rho_f = (\xi-1)f - (\xi^{(1)}-1)v^{(1)}f^{(1)} - (\xi^{(2)}-1)v^{(2)}f^{(2)} , \tag{2.40}$$

where $f = v^{(1)}f^{(1)} + v^{(2)}f^{(2)} = v^{(1)}f^{(1)} + v^{(2)}$ is the total porosity and ξ, $\xi^{(1)}$, $\xi^{(2)}$ are the total, pore matrix, and fracture tortuosity, respectively. Berryman [57] has shown that

$$\xi^{(i)} = 1 + r\left(\frac{1}{f^{(i)}} - 1\right) , \tag{2.41}$$

where the factor r depends on micro-geometry and is expected to lie in the range $0 \le r \le 1$, with $r = \dfrac{1}{2}$ for spherical grains. Because $f^{(2)} = 1$ by assumption, note that $\xi^{(2)} = 1$, for the fracture porosity. Though it is more difficult to estimate the overall tortuosity ξ, it can be shown [68, 69] that it will lie between the values $\xi^{\pm}$ given by the formula

$$\frac{1}{f/\xi^{\pm} + 2/F_m} = \frac{v^{(1)}}{f^{(1)}/\xi^{(1)} + 2/F_m} + \frac{v^{(2)}}{1 + 2/F_m} , \tag{2.42}$$

where $1/F_m = f^{(2)}/\xi^{(2)} = 1$ for ξ^- and $1/F_m = f^{(1)}/\xi^{(1)}$ for ξ^+. If we assume that the overall tortuosity of the fractured double-porosity medium is dominated by the fractures,

which is valid for situations in which $v^{(2)} \ll 1$, then we can use the lower limit for the overall tortuosity, meaning $\xi = \xi^-$. The bounds in (2.42) should generally be used for applications to media in which such assumption is not valid.

Since we have dealt with the left-hand side of Lagrange's equation, we must now find the expressions for the stress elements τ_{ij} and $s_{ij}^{(k)}$. Without any loss of generality, we can choose three independent variables to be the external confining pressure p_c, and the fluid pressures in the porous matrix $p^{(1)}$, and in the fractures $p^{(2)}$. The dependent variables are chosen to be the volumetric strain, e, and Biot's increment of fluid content (fluid volume accumulation per unit bulk volume) in the porous matrix, $\zeta^{(1)}$, and fractures, $\zeta^{(2)}$, separately. These quantities are related to the displacements by $\zeta^{(k)} = -v^{(k)} f^{(k)} \nabla \cdot (\mathbf{U}^{(k)} - \mathbf{u})$, $k = 1, 2$. Then the phenomenological approach relates each dependent variable linearly to the independent variables. The double-porosity theory with six independent coefficients, a_{ij}, is a straightforward generalization of Biot's original equations [66] (see Appendix D)

$$\begin{pmatrix} e \\ -\zeta^{(1)} \\ -\zeta^{(2)} \end{pmatrix} = \begin{pmatrix} a_{11} & a_{12} & a_{13} \\ a_{12} & a_{22} & a_{23} \\ a_{13} & a_{23} & a_{33} \end{pmatrix} \begin{pmatrix} -p_c \\ -p^{(1)} \\ -p^{(2)} \end{pmatrix} . \tag{2.43}$$

The six coefficients occur in three classes, corresponding to the original Biot coefficients. The coefficient $a_{11} = 1/K$ is an effective compressibility of the combined fracture-matrix system, the coefficients a_{12} and a_{13} are generalized poroelastic expansion coefficients, i.e., the ratio of bulk strain to porous matrix pressure and fracture pressure, respectively. The terms a_{22}, a_{23} and a_{33} are generalized storage coefficients, i.e., a_{ij} is the volume of fluid that flows into a control volume (normalized by the control volume) of phase $i-1$ due to a unit increase in fluid pressure in phase $j-1$.

Parameter (GPa^{-1})	Formula
a_{11}	$1/K$
a_{12}	$-\alpha^{(1)} K_s^{(1)} / K^{(1)} K_s$
a_{13}	$-\alpha/K - a_{12}$
a_{22}	$v^{(1)} \alpha^{(1)} / B^{(1)} K^{(1)}$
a_{23}	$v^{(1)} \alpha^{(1)} / K^{(1)} - a_{12}$
a_{33}	$v^{(2)}/K_f + v^{(1)}/K^{(1)} - (1-2\alpha)/K + 2a_{12}$
$\bar{a}_{33}$	$a_{33} - v^{(2)}/K_f$

Table 2.1: Stress-strain parameters in double-porosity modeling as derived by Berryman and Wang [67]

In Table 2.1 we summarize a list of formulas relating these parameters to properties

of the constituents. The input parameters are defined as: K and $K^{(1)}$ [5] are the (jacketed) frame bulk moduli of the whole and the porous matrix, respectively, K_s and $K_s^{(1)}$ are the unjacketed bulk moduli for the whole and the porous matrix, $\alpha = 1 - K/K_s$ and $\alpha^{(1)} = 1 - K^{(1)}/K_s^{(1)}$ are the corresponding Biot-Willis parameters [54], K_f is the pore fluid bulk modulus, $\nu^{(1)}$ is the Poisson's ratio of the porous matrix, and $B^{(1)}$ is Skempton's pore-pressure buildup coefficient [70] for the matrix. Note that the existence of a second pore pressure and increment of fluid content, in the case of double-porosity model, leads to the definition of several Skempton-like or Biot-Willis-like coefficients.

Using the constitutive relations in (2.43), plus the usual relations of linear elasticity, we express the vector on the right-hand side of (2.31) in terms of macroscopic variables and, assuming isotropic media, we derive the following relations[6]

$$\tau_{ij,j} = (\lambda+\mu)e_{,\,i} + \mu u_{i,jj} - 3K[\beta^{(1)}p^{(1)}_{,\,i} + \beta^{(2)}p^{(2)}_{,\,i}]\,, \quad (2.44)$$

$$-3K[\beta^{(1)}p^{(1)}_{,\,i} + \beta^{(2)}p^{(2)}_{,\,i}] = -p_{c,\,i} - Ke_{,\,i}\,, \quad (2.45)$$

$$p^{(1)}_{,\,i} = -\tilde{a}_{12}e_{,\,i} + \tilde{a}_{22}\zeta^{(1)}_{,\,i} + \tilde{a}_{23}\zeta^{(2)}_{,\,i}\,, \quad (2.46)$$

$$p^{(2)}_{,\,i} = -\tilde{a}_{13}e_{,\,i} + \tilde{a}_{23}\zeta^{(1)}_{,\,i} + \tilde{a}_{33}\zeta^{(2)}_{,\,i}\,, \quad (2.47)$$

where we denote with tilded elements $\tilde{a}_{ij}$ the elements of the inverse matrix of Eq. (2.43). From the condition of hydrostatic external stress, we identify the parameters $\beta^{(1)}$, $\beta^{(2)}$ and λ, μ. We have $-3\beta^{(1)} = a_{12}$, $-3\beta^{(2)} = a_{13}$, $a_{11} = 3(\bar{s}_{11} + 2\bar{s}_{12}) = \frac{1}{K}$ with $\bar{s}_{11} = \frac{1}{E}$ and $\bar{s}_{12} = -\frac{\nu}{E}$, where E, ν, K, λ, μ are all parameters for the drained medium, Young's modulus, Poisson's ratio, bulk modulus and Lamé coefficients, respectively [7]. Substituting Eqs. (2.46),(2.47) into (2.44) leads to

$$\tau_{ij,j} = (K_u + \tfrac{1}{3}\mu)e_{,\,i} + \mu u_{i,jj} - K_u[B^{(1)}\zeta^{(1)}_{,\,i} + B^{(2)}\zeta^{(2)}_{,\,i}]\,, \quad (2.48)$$

where $K_u = K(1 - a_{12}\tilde{a}_{12} - a_{13}\tilde{a}_{13})$, is the undrained bulk modulus for the double-porosity medium, and the Skempton's coefficient for the matrix and fractures respectively are given by: $B^{(1)} = -\frac{a_{12}a_{33}-a_{13}a_{23}}{a_{22}a_{33}-a_{23}^2}$, $B^{(2)} = -\frac{a_{13}a_{22}-a_{12}a_{23}}{a_{22}a_{33}-a_{23}^2}$.

It was observed by Berryman and Wang [66] that the fluid-fluid coupling term a_{23} was small or negligible for the examples considered, so we can extract and evaluate a somewhat simplified version of these formulas, from the more general analysis presented so far, we will therefore make the approximation $a_{23} \equiv 0$ in the remainder of this chapter.

[5] $K^{(1)}$ corresponds to K_b of the Biot theory for the single porosity.

[6] Analogous expressions for single-porosity with and without elastic anisotropy are given in Berryman [71].

[7] It is important to use the compliances $\bar{s}_{ij}$, rather than using the inverse relation in terms of the stiffnesses, because they are simply related to the drained constants. Also we used the overlined symbol to avoid confusion with the stress tensor elements s_{ij}.

Eqs. (2.44), (2.45) will remain unchanged, but (2.46) and (2.47) will both be replaced by a single equation

$$-3[\beta^{(1)}p^{(1)}_{,\,i}+\beta^{(2)}p^{(2)}_{,\,i}]=B^{(1)}[-\zeta^{(1)}_{,\,i}-3\beta^{(1)}p_{c,\,i}]+B^{(2)}[-\zeta^{(2)}_{,\,i}-3\beta^{(2)}p_{c,\,i}]\,, \tag{2.49}$$

also the main equation (2.48) will preserve the same form, but the new K_u will be given from the equation: $K_u=\frac{K}{1-3K[\beta^{(1)}B^{(1)}+\beta^{(2)}B^{(2)}]}$. To obtain the expression we need, we combine (2.48) with (2.43) and take the divergence,

$$\begin{pmatrix}\tau_{ij,\,ji}\\ -p^{(1)}_{,\,ii}\\ -p^{(2)}_{,\,ii}\end{pmatrix}=\begin{pmatrix}K_u+\frac{4}{3}\mu & B^{(1)}K_u & B^{(2)}K_u\\ \tilde{a}_{12} & \tilde{a}_{22} & \tilde{a}_{23}\\ \tilde{a}_{13} & \tilde{a}_{23} & \tilde{a}_{33}\end{pmatrix}\begin{pmatrix}e_{,\,ii}\\ -\zeta^{(1)}_{,\,ii}\\ -\zeta^{(2)}_{,\,ii}\end{pmatrix}\,. \tag{2.50}$$

Assuming a harmonic time dependence of the form $\exp(-\mathrm{i}\Omega t)$, Eq. (2.34) takes the form

$$-\Omega^2\begin{pmatrix}\rho_{11} & \rho_{12} & \rho_{13}\\ \rho_{12} & \rho_{22} & \rho_{23}\\ \rho_{13} & \rho_{23} & \rho_{33}\end{pmatrix}\begin{pmatrix}u_i\\ U^{(1)}_i\\ U^{(2)}_i\end{pmatrix}=\begin{pmatrix}\tau_{ij,j}\\ s^{(1)}_{ij,j}\\ s^{(2)}_{ij,j}\end{pmatrix}\,, \tag{2.51}$$

and it is also convenient to notice that

$$\frac{\partial}{\partial x_i}\begin{pmatrix}u_i\\ U^{(1)}_i\\ U^{(2)}_i\end{pmatrix}=\begin{pmatrix}e\\ U^{(1)}_{i,\,i}\\ U^{(2)}_{i,\,i}\end{pmatrix}=\begin{pmatrix}1 & 0 & 0\\ 1 & \frac{1}{v^{(1)}f^{(1)}} & 0\\ 1 & 0 & \frac{1}{v^{(2)}f^{(2)}}\end{pmatrix}\begin{pmatrix}e\\ -\zeta^{(1)}\\ -\zeta^{(2)}\end{pmatrix}\equiv\mathbf{V}\begin{pmatrix}e\\ -\zeta^{(1)}\\ -\zeta^{(2)}\end{pmatrix}\,, \tag{2.52}$$

which allows us to write the final equation in terms of the macroscopic strain and fluid contents e, $\zeta^{(1)}$ and $\zeta^{(2)}$. Note that the final equality in (2.52) defines the matrix $\mathbf{V}$, which we will need again later in the analysis.

Taking the divergence[8] of (2.51), then substituting (2.52) and (2.50), and finally taking the spatial Fourier transform (having wavenumber k), we obtain the eigenvalue problem associated with wave propagation:

$$\begin{aligned}\begin{pmatrix}K_u+\frac{4}{3}\mu & B^{(1)}K_u & B^{(2)}K_u\\ \tilde{a}_{12} & \tilde{a}_{22} & \tilde{a}_{23}\\ \tilde{a}_{13} & \tilde{a}_{23} & \tilde{a}_{33}\end{pmatrix}\begin{pmatrix}e\\ -\zeta^{(1)}\\ -\zeta^{(2)}\end{pmatrix} &= c^2\begin{pmatrix}1 & 0 & 0\\ 0 & \frac{1}{v^{(1)}f^{(1)}} & 0\\ 0 & 0 & \frac{1}{v^{(2)}f^{(2)}}\end{pmatrix}\begin{pmatrix}\rho_{11} & \rho_{12} & \rho_{13}\\ \rho_{12} & \rho_{22} & \rho_{23}\\ \rho_{13} & \rho_{23} & \rho_{33}\end{pmatrix}\\ &\times\begin{pmatrix}1 & 0 & 0\\ 1 & \frac{1}{v^{(1)}f^{(1)}} & 0\\ 1 & 0 & \frac{1}{v^{(2)}f^{(2)}}\end{pmatrix}\begin{pmatrix}e\\ -\zeta^{(1)}\\ -\zeta^{(2)}\end{pmatrix}\,,\end{aligned} \tag{2.53}$$

[8] Applying the divergence provides the longitudinal solutions, while the curl would provide the transverse solution.

where the eigenvalue $c^2 = \Omega^2/k^2$ is a real quantity in our case, because we assumed no viscous dissipation losses, it is independent of the frequency Ω but has the general physical significance of being the square of the complex wave velocity. With obvious definitions for the matrices $\mathbf{A}$, $\mathbf{P}$, and $\mathbf{R}$, while $\mathbf{V}$ was previously defined in (2.52), Eq. (2.53) becomes

$$\mathbf{A}\begin{pmatrix} e \\ -\zeta^{(1)} \\ -\zeta^{(2)} \end{pmatrix} = c^2 \mathbf{PRV}\begin{pmatrix} e \\ -\zeta^{(1)} \\ -\zeta^{(2)} \end{pmatrix} , \tag{2.54}$$

and then, the dispersion relation determining c^2 is

$$\det(\mathbf{A} - c^2\mathbf{PRV}) = 0 , \tag{2.55}$$

The solution of the dispersion relation (2.55) will give the three values of the velocities of the three longitudinal waves that propagate inside a double-porosity medium. Indeed, we expect three hybrid longitudinal waves to appear, that arise from the corresponding propagating modes in the three components of this double-porosity model (solid skeletal frame, matrix pores, and adjacent fractures), interacting between them.

2.4 Multipole expansion of the elastic field

The plane wave solutions (2.4) of Eqs. (2.2), (2.3), although commonly employed, are not always the most appropriate when one wants to study more complex structures than the homogeneous medium. Consequently, in systems with spherical symmetry (like those we shall consider in our study), it is convenient to express the solutions (2.4) as multipole expansions in a spherical wave basis. A complete basis of such solutions for Eq. (2.2), known as irrotational vector spherical waves, are given by [72]

$$\mathbf{J}_{L\ell m}(\mathbf{r}) = \frac{1}{Q_l}\nabla\left[j_\ell(Q_l r)Y_{\ell m}(\hat{\mathbf{r}})\right] , \ \mathbf{H}_{L\ell m}(\mathbf{r}) = \frac{1}{Q_l}\nabla\left[h_\ell^+(Q_l r)Y_{\ell m}(\hat{\mathbf{r}})\right] , \tag{2.56}$$

where $j_\ell(Q_l r)$ and $h_\ell^+(Q_l r)$ are the spherical Bessel and Hankel functions, respectively (see Appendix A), and $Y_{\ell m}(\hat{\mathbf{r}})$ the usual spherical harmonics (see Appendix B), with $\hat{\mathbf{r}}$ denoting the angular variables (θ, ϕ) of $\mathbf{r}$ in a spherical coordinate system. On the other hand, a complete basis of spherical wave solutions of Eq. (2.3) are [72]

$$\mathbf{J}_{M\ell m}(\mathbf{r}) = j_\ell(Q_t r)\mathbf{X}_{\ell m}(\hat{\mathbf{r}}) , \ \mathbf{H}_{M\ell m}(\mathbf{r}) = h_\ell^+(Q_t r)\mathbf{X}_{\ell m}(\hat{\mathbf{r}}) \tag{2.57}$$

and

$$\begin{aligned} \mathbf{J}_{N\ell m}(\mathbf{r}) &= \frac{\mathrm{i}}{Q_t}\nabla \times j_\ell(Q_t r)\mathbf{X}_{\ell m}(\hat{\mathbf{r}}) = \frac{\mathrm{i}}{Q_t}\nabla \times \mathbf{J}_{M\ell m}(\mathbf{r}) , \\ \mathbf{H}_{N\ell m}(\mathbf{r}) &= \frac{\mathrm{i}}{Q_t}\nabla \times h_\ell^+(Q_t r)\mathbf{X}_{\ell m}(\hat{\mathbf{r}}) = \frac{\mathrm{i}}{Q_t}\nabla \times \mathbf{H}_{M\ell m}(\mathbf{r}) , \end{aligned} \tag{2.58}$$

which are known as solenoidal vector spherical waves. The expressions of those solutions are based on the vector spherical harmonics, $\mathbf{X}_{\ell m}(\hat{\mathbf{r}})$ (see Appendix B). Each of the spherical wave solutions (2.56), (2.57), (2.58) is characterized, for a given frequency, from the angular momentum indices ℓ, m, and the index $P = L, M, N$. We note that the solutions $\mathbf{J}_{P\ell m}(\mathbf{r})$ exhibit a regular behavior at every point, unlike $\mathbf{H}_{P\ell m}(\mathbf{r})$ that diverge at the origin and have the form of outgoing spherical waves at $r \to \infty$. Their physical meaning will become clearer in the next chapter. The solutions $\mathbf{J}_{P\ell m}(\mathbf{r})$ also obey the following orthonormality relation

$$\int d^3 r \mathbf{J}^*_{P\ell m;Q}(\mathbf{r}) \cdot \mathbf{J}_{P'\ell' m';Q'}(\mathbf{r}) = \frac{\pi}{2Q^2}\delta(Q - Q')\delta_{PP'}\delta_{\ell\ell'}\delta_{mm'} \,, \tag{2.59}$$

where the dependence of the regular vector spherical waves on $Q(Q')$ is explicitly denoted in the subscripts.

In the general case, the elastic field in a homogeneous medium, at given frequency Ω, can be written as a linear combination of $\mathbf{J}_{P\ell m}(\mathbf{r})$ and $\mathbf{H}_{P\ell m}(\mathbf{r})$

$$\mathbf{u}(\mathbf{r}) = \sum_{P\ell m} \left[a^0_{P\ell m}\mathbf{J}_{P\ell m}(\mathbf{r}) + a^+_{P\ell m}\mathbf{H}_{P\ell m}(\mathbf{r}) \right] \,, \tag{2.60}$$

where the coefficients a^0_{L}, a^+_{L} are to be determined. Suppose, now, that we want to expand a plane, longitudinal ($\nu = l$) elastic wave of the form (2.4) with wavevector $\mathbf{Q}_\nu = Q_l \hat{\mathbf{e}}_1(\mathbf{Q}_l)$ in the spherical wave basis. Since a plane wave is finite everywhere, its multipole expansion, according to (2.56), (2.57), (2.58), can only contain $j_\ell(Q_l r)$. So, a longitudinal wave of the form (2.4) will be written as

$$\mathbf{u}(\mathbf{r}) = \sum_{\ell m} a^0_{L\ell m}\mathbf{J}_{L\ell m}(\mathbf{r}) \,. \tag{2.61}$$

Using the mathematical identity $\exp(\mathrm{i}\mathbf{Q}_l \cdot \mathbf{r}) = 4\pi \sum_{\ell m} \mathrm{i}^\ell j_\ell(Q_l r) Y_{\ell m}(\widehat{\mathbf{r}}) Y^*_{\ell m}(\widehat{\mathbf{Q}}_l)$, it can be readily shown that the coefficients $a^0_{L\ell m}$ are

$$a^0_{L\ell m} = 4\pi \mathrm{i}^{\ell+1}(-1)^{m+1} Y_{\ell -m}(\hat{\mathbf{Q}}_l)\, \hat{\mathbf{e}}_1(\mathbf{Q}_l) \cdot \mathbf{u}_0(\mathbf{Q}_l) \,. \tag{2.62}$$

The elastic field in a fluid-saturated poroelastic medium, at given frequency Ω, can be expanded into longitudinal and transverse vector spherical waves of appropriate wave number, as follows [23, 24]

$$\mathbf{u}(\mathbf{r}) = \sum_{\ell m} \left\{ a_{1L\ell m}\mathbf{J}_{L\ell m}(\mathbf{r}) + a_{2L\ell m}\mathbf{J}_{L\ell m}(\mathbf{r}) + a_{M\ell m}\mathbf{J}_{M\ell m}(\mathbf{r}) + a_{N\ell m}\mathbf{J}_{N\ell m}(\mathbf{r}) \right\} \,, \tag{2.63}$$

describing the displacement field of the solid. The first term in Eq. (2.63) describes fast longitudinal waves, the second slow longitudinal waves, which are unique to poroelastic

media, and the last two terms correspond to transverse waves. A similar to Eq. (2.63) expression holds for $\mathbf{U}(\mathbf{r})$, the displacement field for the saturated fluid, with expansion coefficients $A_1 a_{1L\ell m}$, $A_2 a_{2L\ell m}$, $A_3 a_{M\ell m}$, and $A_3 a_{N\ell m}$ instead of $a_{1L\ell m}$, $a_{2L\ell m}$, $a_{M\ell m}$, and $a_{N\ell m}$, respectively, where the coefficients A_1, A_2, A_3 are given by (2.21) and (2.24).

Chapter 3

Scattering by a spherical object

In this chapter we will deal with the scattering of acoustic waves by a single scatterer (elastic or poroelastic), immersed in a homogeneous fluid. This problem is essentially reduced to that of calculating the scattering T matrix that connects the amplitude of the scattered wave to that of the incident wave. We derive useful relations for the scattering cross section and the density of states induced by a single sphere, and demonstrate the applicability of the formalism on a simple example.

3.1 Scattering matrix of an elastic sphere in fluid

We shall examine the scattering of acoustic waves by a sphere of radius S, mass density ρ_s and propagation velocities of longitudinal and transverse waves c_l, c_t respectively, that is embedded in a fluid host with corresponding parameters ρ_h, c_h. We must calculate the scattered wave and the wave inside the sphere. As shown in section 2.4, elastic waves with longitudinal and transverse components, in general, can be expanded into a spherical wave basis. Therefore the incident wave will have the form

$$\mathbf{u}_0(\mathbf{r}) = \sum_{\ell m} a^0_{L\ell m} \frac{1}{Q_h} \boldsymbol{\nabla} \left[j_\ell(Q_h r) Y_{\ell m}(\hat{\mathbf{r}}) \right] \ , \tag{3.1}$$

i.e. Eq. (2.61), using $\mathbf{J}_{L\ell m}(\mathbf{r})$, vector spherical waves containing spherical Bessel functions, since the incident wave must be finite in all space. By $a^0_{L\ell m}$ we denote the incident wave coefficients [see Eq. (2.62)], obtained by projection of a plane wave onto the longitudinal vector spherical wave basis as described in § 2.4. In the fluid host, it exists, in addition to the incident wave, the scattered wave, expanded in the same way, with different expansion coefficients $a^+_{L\ell m}$ (that have to be determined) and where the radial part uses spherical Hankel functions of the first kind, because these asymptotically describe an outgoing

spherical wave: $h_\ell^+(x) \simeq (-\mathrm{i})^\ell \exp(\mathrm{i}x)/(\mathrm{i}x)$ as $x \to \infty$,

$$\mathbf{u}_{sc}(\mathbf{r}) = \sum_{\ell m} a^+_{L\ell m} \frac{1}{Q_h} \boldsymbol{\nabla} \left[h_\ell^+(Q_h r) Y_{\ell m}(\hat{\mathbf{r}}) \right] \ . \tag{3.2}$$

Both of those waves propagate in the same fluid host medium with $Q_h = \dfrac{\Omega}{c_h} = \Omega\sqrt{\dfrac{\rho_h}{\lambda_h}}$ thus, the total wave field in the host region is written as

$$\mathbf{u}^h(\mathbf{r}) = \mathbf{u}_0(\mathbf{r}) + \mathbf{u}_{sc}(\mathbf{r}) \ . \tag{3.3}$$

Inside the sphere both longitudinal and transverse waves exist, with different coefficients. Only spherical Bessel functions are used, since they are finite at $r = 0$. We write

$$\begin{aligned} \mathbf{u}(\mathbf{r}) = \sum_{\ell m} \Bigg\{ & a_{L\ell m} \frac{1}{Q_l} \boldsymbol{\nabla} \left[j_\ell(Q_l r) Y_{\ell m}(\hat{\mathbf{r}}) \right] + a_{M\ell m} j_\ell(Q_t r) \mathbf{X}_{\ell m}(\hat{\mathbf{r}}) + \\ & + a_{N\ell m} \frac{\mathrm{i}}{Q_t} \boldsymbol{\nabla} \times \left[j_\ell(Q_t r) \mathbf{X}_{\ell m}(\hat{\mathbf{r}}) \right] \Bigg\}, \quad r \le S, \end{aligned} \tag{3.4}$$

where $Q_\nu = \dfrac{\Omega}{c_\nu}, \nu = l, t$ and $c_l = \sqrt{\dfrac{\lambda_s + 2\mu_s}{\rho_s}}$, $c_t = \sqrt{\dfrac{\mu_s}{\rho_s}}$ and $a_{P\ell m}$ are appropriate coefficients to be determined. In general, in a linear scattering problem, the partial wave amplitudes of the scattered field and of the field inside the scatterer depend linearly on the corresponding amplitudes of the incident field

$$a^+_{L\ell m} = \sum_{\ell' m'} T_{L\ell m; L\ell' m'} a^0_{L\ell' m'} \ , \tag{3.5}$$

$$a_{P\ell m} = \sum_{\ell' m'} R_{P\ell m; L\ell' m'} a^0_{L\ell' m'} \ , \quad P = L, M, N \ . \tag{3.6}$$

where we defined the scattering T matrix and the corresponding R matrix for the partial wave amplitudes inside the sphere. In order to calculate the matrix elements we must apply appropriate boundary conditions on the surface of the sphere. These require continuity of two quantities: the displacement vector $\mathbf{u}$ and the surface traction $\boldsymbol{\tau}$, given by (1.46). The components of $\boldsymbol{\tau}$ depend on the field $\mathbf{u}$ so their form will change depending on the kind of waves propagating in the sphere and the host. In case of a solid sphere in a fluid host, both longitudinal and transverse waves exist inside the sphere, while only longitudinal waves can propagate in the host. This means that $c_t = 0$ and $\mu = 0$ and as a result the surface traction components τ_θ, τ_ϕ vanish.

A tangential displacement, with respect to the interface, in the solid cannot be connected with the corresponding in the fluid, because in fluids pure shear deformation does

not exist, and it is for this reason that we do not require continuity for the angular components of the elastic field at the interface, when at least one of the two media in contact is fluid. In this case, the boundary conditions are

$$\begin{aligned} u_r|_{r=S} &= u_r^h\Big|_{r=S} \\ \tau_r|_{r=S} &= \tau_r^h\Big|_{r=S} \\ \tau_\theta|_{r=S} &= 0 \\ \tau_\phi|_{r=S} &= 0 \end{aligned} \tag{3.7}$$

The expression for the field in the fluid host is given by Eqs. (3.1)-(3.3) and inside the sphere by (3.4). With the help of Appendix C, the expressions for the coefficients $\mathcal{B}_{\ell m}^{(i)}$ are simplified greatly in the case of fluid host (see Eq. C.4), because the coefficients of the transverse waves are eliminated. So the continuity of u_r results in

$$a_{L\ell m}^{+} h_\ell^{+'}(x_h) + a_{N\ell m}\sqrt{\ell(\ell+1)}\frac{j_\ell(x_t)}{x_t} - a_{L\ell m} j_\ell'(x_l) = -a_{L\ell m}^{0} j_\ell'(x_h). \tag{3.8}$$

From the continuity of τ_r we obtain

$$\begin{aligned} -a_{L\ell m}^{+}\frac{x_t^2}{2x_h}\frac{\rho_h}{\rho_s}h_\ell^{+}(x_h) + a_{N\ell m}\sqrt{\ell(\ell+1)}\frac{x_t j_\ell'(x_t) - j_\ell(x_t)}{x_t} - \\ - a_{L\ell m}\frac{\left[\ell(\ell+1) - x_t^2/2\right] j_\ell(x_l) - 2x_l j_\ell'(x_l)}{x_l} = a_{L\ell m}^{0}\frac{x_t^2}{2x_h}\frac{\rho_h}{\rho_s} j_\ell(x_h). \end{aligned} \tag{3.9}$$

In the above expressions we introduced the notation $x_h = Q_h S$, $x_l = Q_l S$, $x_t = Q_t S$. For the boundary condition concerning the angular components of $\boldsymbol{\tau}$ we obtain, with the help of (C.2) and (B.27), the following vector

$$\boldsymbol{\tau} - \boldsymbol{\tau}_r = \tau_\theta\hat{\theta} + \tau_\phi\hat{\phi} = \sum_{\ell m}\left[\mathcal{B}_{\ell m}^{(4)}\mathbf{X}_{\ell m}(\hat{\mathbf{r}}) + \mathcal{B}_{\ell m}^{(5)}\hat{\mathbf{r}}\times\mathbf{X}_{\ell m}(\hat{\mathbf{r}})\right] . \tag{3.10}$$

The advantage of this expression is that if we apply the boundary condition of continuity for the corresponding vectors inside and outside the sphere we will result in an expression of the form (B.37). This means that the difference of the coefficients $\mathcal{B}_{\ell m}^{(i)}, i = 4, 5$, inside and outside the sphere, must be zero. We obtain

$$a_{L\ell m}\sqrt{\ell(\ell+1)}\frac{x_l j_\ell'(x_l) - j_\ell(x_l)}{x_l} + a_{N\ell m}\frac{x_t j_\ell'(x_t) - [\ell(\ell+1) - 1 - x_t^2/2] j_\ell(x_t)}{x_t} = 0 , \tag{3.11}$$

$$a_{M\ell m}[x_t j_\ell'(x_t) - j_\ell(x_t)] = 0 . \tag{3.12}$$

From Eq. (3.8), (3.9), (3.11) and (3.12) it can be clearly seen that the T and R matrices, defined from (3.5), (3.6) are diagonal in $\{\ell, m\}$ and independent of m, i.e.

$$\begin{aligned} T_{L\ell m;L\ell' m'} &= T_{LL;\ell}\delta_{\ell\ell'}\delta_{mm'} \\ R_{P\ell m;L\ell' m'} &= R_{PL;\ell}\delta_{\ell\ell'}\delta_{mm'} \ . \end{aligned} \tag{3.13}$$

Moreover, Eq. (3.12), which involves only transverse M modes, is uncoupled from the rest [Eqs. (3.8), (3.9) and (3.11)] and leads to

$$R_{ML;\ell} = 0 \quad \text{or} \quad x_t j_\ell^{'}(x_t) - j_\ell(x_t) = 0. \tag{3.14}$$

The first from these two equations means that an incident L wave will not excite internal M waves within the sphere, i.e., the two subspaces $\{L, N\}$ and M are decoupled. The second one, when solved, will provide the so-called torsional eigenmodes [73]. These modes are localized in the sphere and cannot be excited by an externally incident acoustic wave. The sphere is oscillating, without change in its volume. The dimensionless eigenfrequencies $[x_t]_{\ell n}$, which arise as solutions $n = 1, 2, 3, ...$ of Eq. (3.14) for a given $\ell = 1, 2, ...$, are given in Table 3.1 for the first few values of n and ℓ. These are calculated by solving numerically the second of Eqs. (3.14) using bisection method, and are in agreement with the known values from the literature [73].

$\ell \backslash n$	1	2	3	4
1	5.76346	9.09501	12.3229	15.5146
2	2.50113	7.13601	10.5146	13.7717
3	3.86470	8.44492	11.8817	15.1754
4	5.09462	9.71250	13.2109	16.5445
5	6.26577	10.9506	14.5108	17.8858
6	7.40360	12.1664	15.7876	19.2042

Table 3.1: Dimensionless eigenfrequencies of torsional eigenstates.

The three remaining equations (3.8), (3.9) and (3.11) constitute a linear system for the unknowns $T_{LL;\ell}$, $R_{LL;\ell}$, and $R_{NL;\ell}$, which can be written as

$$\begin{bmatrix} d_{11} & d_{12} & d_{13} \\ d_{21} & d_{22} & d_{23} \\ d_{31} & d_{32} & d_{33} \end{bmatrix} \begin{bmatrix} T_{LL;\ell} \\ R_{NL;\ell} \\ R_{LL;\ell} \end{bmatrix} = \begin{bmatrix} b_1 \\ b_2 \\ b_3 \end{bmatrix} , \tag{3.15}$$

where

$$
\begin{aligned}
d_{11} &= h_\ell^{+\prime}(x_h) && (3.16)\\
d_{12} &= \sqrt{\ell(\ell+1)}\frac{j_\ell(x_t)}{x_t} && (3.17)\\
d_{13} &= -j_\ell^{'}(x_l) && (3.18)\\
d_{21} &= 0 && (3.19)\\
d_{22} &= \frac{x_t j_\ell^{'}(x_t) - [\ell(\ell+1) - 1 - x_t^2/2] j_\ell(x_t)}{x_t} && (3.20)\\
d_{23} &= \sqrt{\ell(\ell+1)}\frac{x_l j_\ell^{'}(x_l) - j_\ell(x_l)}{x_l} && (3.21)\\
d_{31} &= -\frac{x_t^2}{2x_h}\frac{\rho_h}{\rho_s} h_\ell^{+}(x_h) && (3.22)\\
d_{32} &= \sqrt{\ell(\ell+1)}\frac{x_t j_\ell^{'}(x_t) - j_\ell(x_t)}{x_t} && (3.23)\\
d_{33} &= -\frac{[\ell(\ell+1) - x_t^2/2] j_\ell(x_l) - 2x_l j_\ell^{'}(x_l)}{x_l} && (3.24)\\
b_1 &= -j_\ell^{'}(x_h) && (3.25)\\
b_2 &= 0 && (3.26)\\
b_3 &= \frac{x_t^2}{2x_h}\frac{\rho_h}{\rho_s} j_\ell(x_h). && (3.27)
\end{aligned}
$$

Solving this 3×3 system, we obtain the second kind of modes, so-called spheroidal, which are not bound but, as we will see in the example later in this chapter, they can be resonant with long lifetime (virtual bound states).

To summarize, the matrices T, R have the following properties:

1. they are diagonal with respect to ℓ, which means that the angular momentum is preserved,

2. they are independent of m, since the problem has azimuthal symmetry,

3. the subspace M is decoupled and provides the bound torsional eigenstates of the sphere, while the L, N subspaces are coupled. This means that an incident L wave will create scattered L waves in the fluid host and a linear combination of L and N waves inside the sphere (continuous spheroidal states).

3.2 Scattering matrix of a poroelastic sphere in fluid

We now consider a fluid-saturated poroelastic sphere of radius S, centered at the origin of coordinates, immersed in a fluid host medium characterized by mass density ρ_h and bulk modulus $K_h = \lambda_h$. A plane acoustic wave, of angular frequency Ω, incident on that sphere, gives rise to a scattered wave and the total displacement field outside the sphere, expanded into longitudinal spherical waves [23, 24], has a form similar to Eq. (3.3),

$$\mathbf{u}^h(\mathbf{r}) = \sum_{\ell m}\left\{a^0_{L\ell m}\frac{1}{Q_h}\nabla[j_\ell(Q_h r)Y_{\ell m}(\widehat{\mathbf{r}})] + a^+_{L\ell m}\frac{1}{Q_h}\nabla[h^+_\ell(Q_h r)Y_{\ell m}(\widehat{\mathbf{r}})]\right\}, \tag{3.28}$$

where $a^0_{L\ell m}$ and $a^+_{L\ell m}$ are the amplitudes of the spherical-wave components of the incident and scattered fields, respectively, $Q_h = \Omega\sqrt{\rho_h/K_h}$ is the wave number in the fluid host at given frequency. The associated (diagonal) stress tensor [see Eq. (1.24)]

$$\overleftrightarrow{\boldsymbol{\sigma}}^h = \overleftrightarrow{\boldsymbol{I}}\, K_h \nabla\cdot\mathbf{U}^h \equiv -\overleftrightarrow{\boldsymbol{I}}\, p_h \tag{3.29}$$

defines the pressure, p_h, in the fluid host. As we already explained in § 2.2 the displacement field inside a poroelastic sphere has two components, $\mathbf{u}(\mathbf{r})$ and $\mathbf{U}(\mathbf{r})$ for the solid and fluid component, respectively. These can be expanded into longitudinal and transverse vector spherical waves according to Eq. (2.63) with appropriate expansion coefficients

$$\begin{aligned}\mathbf{u}(\mathbf{r}) = \sum_{\ell m}\Bigg\{&a_{1L\ell m}\frac{1}{Q_1}\boldsymbol{\nabla}[j_\ell(Q_1 r)Y_{\ell m}(\widehat{\mathbf{r}})] + a_{2L\ell m}\frac{1}{Q_2}\boldsymbol{\nabla}[j_\ell(Q_2 r)Y_{\ell m}(\widehat{\mathbf{r}})]\\ &+ a_{M\ell m}j_\ell(Q_3 r)\mathbf{X}_{\ell m}(\widehat{\mathbf{r}}) + a_{N\ell m}\frac{\mathrm{i}}{Q_3}\boldsymbol{\nabla}\times[j_\ell(Q_3 r)\mathbf{X}_{\ell m}(\widehat{\mathbf{r}})]\Bigg\},\end{aligned} \tag{3.30}$$

$$\begin{aligned}\mathbf{U}(\mathbf{r}) = \sum_{\ell m}\Bigg\{&A_1 a_{1L\ell m}\frac{1}{Q_1}\boldsymbol{\nabla}[j_\ell(Q_1 r)Y_{\ell m}(\widehat{\mathbf{r}})] + A_2 a_{2L\ell m}\frac{1}{Q_2}\boldsymbol{\nabla}[j_\ell(Q_2 r)Y_{\ell m}(\widehat{\mathbf{r}})]\\ &+ A_3 a_{M\ell m}j_\ell(Q_3 r)\mathbf{X}_{\ell m}(\widehat{\mathbf{r}}) + A_3 a_{N\ell m}\frac{\mathrm{i}}{Q_3}\boldsymbol{\nabla}\times[j_\ell(Q_3 r)\mathbf{X}_{\ell m}(\widehat{\mathbf{r}})]\Bigg\},\end{aligned} \tag{3.31}$$

where Q_1, Q_2 are the solutions of Eq. (2.20), Q_3 is given by Eq. (2.23), A_1, A_2 are calculated in Eq. (2.21) and A_3 in Eq. (2.24).

The expansion coefficients in Eqs. (3.28), (3.30) and (3.31) are determined from those of the incident wave, $a^0_{L\ell m}$, uniquely from the following boundary conditions at the surface of the sphere [74].

(a): Continuity of the radial, azimuthal, and polar components of the surface traction

$$\overleftrightarrow{\boldsymbol{\sigma}}\widehat{\mathbf{r}} = \overleftrightarrow{\boldsymbol{\sigma}}^h\widehat{\mathbf{r}}\,. \tag{3.32}$$

(b): Continuity of the normal component of the filtration velocity

$$f(\dot{U}_r - \dot{u}_r) = \dot{u}_r^h - \dot{u}_r \ , \tag{3.33}$$

that ensures conservation of fluid mass.

(c): Consistency of the fluid pressure drop and the normal component of the filtration velocity (Darcy's law)

$$f(\dot{U}_r - \dot{u}_r) = -\kappa_s(p_h - p) \ , \tag{3.34}$$

where κ_s is a parameter that measures *interface permeability*. For a sealed interface, $\kappa_s = 0$, and, for an open interface, $\kappa_s = \infty$.

From the continuity of the radial component of the surface traction we obtain

$$d_{12}a_{1L\ell m} + d_{13}a_{2L\ell m} + d_{14}a_{N\ell m} = b_1 a^0_{L\ell m} - d_{11}a^+_{L\ell m} \ , \tag{3.35}$$

where

$$\begin{aligned}
d_{11} &= -x_h h_\ell^+(x_h) \\
d_{12} &= \{j_\ell(x_1)[x_1^2(\lambda_1 + 2\mu_b)/K_h - 2\ell(\ell+1)(\mu_b/K_h)] + 4x_1 j'_\ell(x_1)(\mu_b/K_h)\}/x_1 \\
d_{13} &= \{j_\ell(x_2)[x_2^2(\lambda_2 + 2\mu_b)/K_h - 2\ell(\ell+1)(\mu_b/K_h)] + 4x_2 j'_\ell(x_2)(\mu_b/K_h)\}/x_2 \\
d_{14} &= 2\sqrt{\ell(\ell+1)}[x_3 j'_\ell(x_3) - j_\ell(x_3)](\mu_b/K_h)/x_3 \\
b_1 &= x_h j_\ell(x_h) \ ,
\end{aligned} \tag{3.36}$$

with $x_\nu = Q_\nu S,\ \nu = 1,2,3,\ x_h = Q_h S$, and $\lambda_\nu = \mathcal{P} - 2\mu_b + \mathcal{Q} + A_\nu(\mathcal{Q} + \mathcal{R}),\ \nu = 1,2.$ Continuity of the tangential components of the surface traction yields

$$[x_3 j'_\ell(x_3) - j_\ell(x_3)]a_{M\ell m} = 0 \tag{3.37}$$

and

$$d_{22}a_{1L\ell m} + d_{23}a_{2L\ell m} + d_{24}a_{N\ell m} = 0 \ , \tag{3.38}$$

where

$$\begin{aligned}
d_{22} &= \sqrt{\ell(\ell+1)}[x_1 j'_\ell(x_1) - j_\ell(x_1)]/x_1 \\
d_{23} &= \sqrt{\ell(\ell+1)}[x_2 j'_\ell(x_2) - j_\ell(x_2)]/x_2 \\
d_{24} &= [(1 + x_3^2/2 - \ell(\ell+1)]j_\ell(x_3) + x_3 j'_\ell(x_3)]/x_3 \ .
\end{aligned} \tag{3.39}$$

From Eq. (3.33) we obtain

$$d_{32}a_{1L\ell m} + d_{33}a_{2L\ell m} + d_{34}a_{N\ell m} = b_3 a^0_{L\ell m} - d_{31}a^+_{L\ell m} \ , \tag{3.40}$$

where

$$\begin{aligned} d_{31} &= -h_\ell^{+\prime}(x_h) \\ d_{32} &= j_\ell'(x_1)[1+f(A_1-1)] \\ d_{33} &= j_\ell'(x_2)[1+f(A_2-1)] \\ d_{34} &= -\sqrt{\ell(\ell+1)}j_\ell(x_3)[1+f(A_3-1)]/x_3 \\ b_3 &= j_\ell'(x_h)\ . \end{aligned} \tag{3.41}$$

Finally, Eq. (3.34), in the case of an open interface ($\kappa_s = \infty \Rightarrow p = p_h$) that will concern us here, gives

$$d_{42}a_{1L\ell m} + d_{43}a_{2L\ell m} = b_4 a^0_{L\ell m} - d_{41}a^+_{L\ell m}\ , \tag{3.42}$$

where

$$\begin{aligned} d_{41} &= -x_h h_\ell^+(x_h) \\ d_{42} &= x_1 j_\ell(x_1)[1-K_b/K_s+f(A_1-1)]R/(f^2K_h) \\ d_{43} &= x_2 j_\ell(x_2)[1-K_b/K_s+f(A_2-1)]R/(f^2K_h) \\ b_4 &= x_h j_\ell(x_h)\ . \end{aligned} \tag{3.43}$$

Alternatively, for a finite value of κ_s, from Eq. (3.34) we obtain

$$d_{42}a_{1L\ell m} + d_{43}a_{2L\ell m} + d_{44}a_{N\ell m} = b_4 a^0_{L\ell m} - d_{41}a^+_{L\ell m}\ , \tag{3.44}$$

where

$$\begin{aligned} d_{41} &= \underline{\kappa}_s x_h h_\ell^+(x_h) \\ d_{42} &= \mathrm{i}x_h j_\ell'(x_1)f(1-A_1) - \underline{\kappa}_s x_1 j_\ell(x_1)[1-K_b/K_s+f(A_1-1)]R/(f^2K_h) \\ d_{43} &= \mathrm{i}x_h j_\ell'(x_2)f(1-A_2) - \underline{\kappa}_s x_2 j_\ell(x_2)[1-K_b/K_s+f(A_2-1)]R/(f^2K_h) \\ d_{44} &= -\mathrm{i}\sqrt{\ell(\ell+1)}x_h j_\ell(x_3)f(1-A_3)/x_3 \\ b_4 &= -\underline{\kappa}_s x_h j_\ell(x_h)\ , \end{aligned} \tag{3.45}$$

with $\underline{\kappa}_s = \kappa_s\sqrt{K_h\rho_h} = \kappa_s\rho_h c_h$ being a dimensionless interface permeability parameter.

For the fluid saturated poroelastic sphere, we define the T and R matrices as in the case of the elastic sphere [Eqs. (3.5), (3.6)] with the only difference that the polarization index for the internal (within the sphere) waves must include both slow and fast longitudinal waves, i.e. $P = 1L, 2L, M, N$. In analogy with what described in § 3.1 torsional modes, solutions of Eq. (3.37), are decoupled from the rest of the modes [Eqs. (3.35), (3.36), (3.38) - (3.40)]. These equations constitute a linear system for the unknowns $T_{LL;\ell}$, $R_{1LL;\ell}$, $R_{2LL;\ell}$, and $R_{NL;\ell}$, which can be written as

$$\begin{pmatrix} d_{11} & d_{12} & d_{13} & d_{14} \\ d_{21} & d_{22} & d_{23} & d_{24} \\ d_{31} & d_{32} & d_{33} & d_{34} \\ d_{41} & d_{42} & d_{43} & d_{44} \end{pmatrix} \begin{pmatrix} T_{LL;\ell} \\ R_{1LL;\ell} \\ R_{2LL;\ell} \\ R_{NL;\ell} \end{pmatrix} = \begin{pmatrix} b_1 \\ b_2 \\ b_3 \\ b_4 \end{pmatrix}\ , \tag{3.46}$$

where the various nonzero coefficients are given by Eqs. (3.36), (3.39), (3.41), and (3.43) or (3.45). Similar formulas for the scattering T matrix of the submerged fluid-saturated poroelastic sphere have also been reported by others [42, 75, 76], however, the explicit expressions derived here correspond to the specific basis of vector spherical waves used in our layer-multiple-scattering method [23, 24].

3.3 Scattering cross section and density of states

The usual definition [77] of the total scattering cross section σ is the integral $\int d\hat{\mathbf{r}}\sigma_{sc}(\hat{\mathbf{r}})$ where $\sigma_{sc}(\hat{\mathbf{r}})d\hat{\mathbf{r}}$ is the ratio of the number of particles scattered per unit time inside the solid angle $d\hat{\mathbf{r}}$, to the number of incident particles per time and surface unit. In case of scattering of elastic waves we do not refer to particles anymore and we replace it with the wave energy. For a plane wave incident on a spherical scatterer, along the z direction, we have

$$\sigma_{sc} = \lim_{r\to\infty} \int_S d\hat{\mathbf{r}} r^2 \frac{\langle P_r^{sc}\rangle}{\langle P_z^0\rangle} \tag{3.47}$$

The brackets denote time average in a period and P_α is the α-component of the Poynting vector, $\mathbf{P}$. For elastic waves we have [51]

$$\mathbf{P} = -\boldsymbol{\upsilon}\overleftrightarrow{\boldsymbol{\sigma}} = -\dot{\mathbf{u}}\overleftrightarrow{\boldsymbol{\sigma}} \tag{3.48}$$

where $\boldsymbol{\upsilon}$ is the wave velocity [1] and $\overleftrightarrow{\boldsymbol{\sigma}}$ is the stress tensor. Assuming a monochromatic wave, $\mathbf{u}(\mathbf{r},t) = \mathrm{Re}\{\mathbf{u}(\mathbf{r})e^{-\mathrm{i}\Omega t}\}$, we have

$$\overleftrightarrow{\boldsymbol{\sigma}}(\mathbf{r},t) = \mathrm{Re}\{\overleftrightarrow{\boldsymbol{\sigma}}(\mathbf{r})e^{-\mathrm{i}\Omega t}\} \tag{3.49}$$

and finally

$$\begin{aligned}\langle \mathbf{P}\rangle = \langle -\boldsymbol{\upsilon}\overleftrightarrow{\boldsymbol{\sigma}}\rangle &= \langle -\mathrm{Re}\{-\mathrm{i}\Omega\mathbf{u}(\mathbf{r})e^{-\mathrm{i}\Omega t}\}\,\mathrm{Re}\{\overleftrightarrow{\boldsymbol{\sigma}}(\mathbf{r})e^{-\mathrm{i}\Omega t}\}\rangle \\ &= \langle -\Omega\,\mathrm{Im}\{\mathbf{u}(\mathbf{r})e^{-\mathrm{i}\Omega t}\}\,\mathrm{Re}\{\overleftrightarrow{\boldsymbol{\sigma}}(\mathbf{r})e^{-\mathrm{i}\Omega t}\}\rangle\ .\end{aligned} \tag{3.50}$$

With the help of: $\langle \cos x \sin x\rangle = 0, \langle \cos^2 x\rangle = \langle \sin^2 x\rangle = \dfrac{1}{2}$, we end up to

$$\langle \mathbf{P}\rangle = \frac{\Omega}{2}\,\mathrm{Im}\{\mathbf{u}^*(\mathbf{r})\overleftrightarrow{\boldsymbol{\sigma}}(\mathbf{r})\}. \tag{3.51}$$

We will now calculate the Poynting vector for a longitudinal plane wave of the form $\mathbf{u}_0(\mathbf{r}) = u_0\hat{\mathbf{z}}e^{\mathrm{i}Q_l z}$ (as already stated the direction of propagation is $\hat{\mathbf{z}}$). The stress tensor is

[1] $\boldsymbol{\upsilon} = \dot{\mathbf{u}}$ is valid only if we assume perfect crystal with a single atom per lattice point and with no atoms in the interstitial space. The above equity denotes that we ignore phenomena associated with defects.

given by (1.37), where for a fluid medium ($\mu = 0$) it will be diagonal and more specifically $\boldsymbol{\sigma} = \lambda e = \lambda \boldsymbol{\nabla} \cdot \mathbf{u}$. We obtain

$$\begin{aligned} \langle P_z^0 \rangle &= \frac{\Omega}{2} \mathrm{Im}\{\hat{\mathbf{z}} \cdot [\mathbf{u}_0^*(\mathbf{r}) \overleftrightarrow{\boldsymbol{\sigma}}(\mathbf{r})]\} \\ &= \frac{\Omega}{2} \mathrm{Im}\{u_0^* e^{-\mathrm{i}Q_l z} \lambda \boldsymbol{\nabla} \cdot \mathbf{u}\} \\ &= \frac{\Omega}{2} Q_l \lambda |u_0|^2. \end{aligned} \tag{3.52}$$

The Poynting vector of the longitudinal scattered wave, which has the form of Eq. (3.2), i.e., $\mathbf{u}_{sc}(\mathbf{r}) = \sum_{\ell m} a_{L\ell m}^+ \frac{1}{Q_l} \boldsymbol{\nabla} \left[h_\ell^+(Q_l r) Y_{\ell m}(\hat{\mathbf{r}}) \right]$, is

$$\begin{aligned} \langle P_r^{sc} \rangle &= \frac{\Omega}{2} \mathrm{Im}\{\hat{\mathbf{r}} \cdot [\mathbf{u}_{sc}^*(\mathbf{r}) \overleftrightarrow{\boldsymbol{\sigma}}(\mathbf{r})]\} \\ &= \frac{\Omega}{2} \mathrm{Im}\{u_{sc;r}^* \tau_r + u_{sc;\theta}^* \tau_\theta + u_{sc;\phi}^* \tau_\phi\} \\ &= \frac{\Omega}{2} \mathrm{Im}\{u_{sc;r}^* \tau_r\}, \end{aligned} \tag{3.53}$$

since, we recall, that $\tau_\theta = \tau_\phi = 0$ for a fluid host. Using Eqs. (C.1), (C.2) into Eq. (3.53) and integrating over the solid angle $d\hat{\mathbf{r}}$, with use of the orthonormality of the spherical harmonics [see Eq. (B.8)], we obtain

$$\int d\hat{\mathbf{r}} r^2 \langle P_r^{sc} \rangle = \frac{\Omega}{2} \mathrm{Im}\{\sum_{\ell m} |a_{L\ell m}^+|^2 \lambda (-Q_l) h_\ell^{-\prime}(Q_l r) h_\ell^+(Q_l r) r^2\} \tag{3.54}$$

In the limit $r \to \infty$, the asymptotic forms of the spherical Hankel functions from (A.13), (A.14) lead to the following final expression

$$\int d\hat{\mathbf{r}} r^2 \langle P_r^{sc} \rangle = \frac{\Omega}{2} \frac{\lambda}{Q_l} \sum_{\ell m} |a_{L\ell m}^+|^2. \tag{3.55}$$

Replacing Eqs. (3.52), (3.55) into (3.47) leads to

$$\sigma_{sc} = \frac{1}{Q_l^2} \sum_{\ell m} \frac{|a_{L\ell m}^+|^2}{|u_0|^2} = \frac{1}{Q_l^2} \sum_{\ell m} |T_{LL;\ell}|^2 \frac{|a_{L\ell m}^0|^2}{|u_0|^2}. \tag{3.56}$$

Making use of Eq. (2.62) we express the expansion coefficient $a_{L\ell m}^0$ with respect to the plane wave amplitude u_0, $a_{L\ell m}^0 = -4\pi \mathrm{i}^{\ell+1} Y_{\ell m}^*(\widehat{\mathbf{Q}}_l) u_0$, and we can write

$$\sum_m \frac{|a_{L\ell m}^0|^2}{|u_0|^2} = 16\pi^2 \sum_m |Y_{\ell m}(\widehat{\mathbf{Q}}_l)|^2 = 4\pi(2\ell + 1). \tag{3.57}$$

Replacing Eq. (3.57) into (3.56) we finally obtain the total scattering cross section of the sphere, normalized to the geometric cross section πS^2

$$\frac{\sigma_{sc}}{\pi S^2} = \frac{4}{x_l^2}\sum_{\ell}(2\ell+1)|T_{LL;\ell}|^2. \tag{3.58}$$

Two other useful quantities are the *extinction* and *absorption cross sections*, given by the following expressions, that are shown in a straightforward manner, following a similar analysis,

$$\frac{\sigma_{ext}}{\pi S^2} = -\frac{4}{x_l^2}\sum_{\ell}(2\ell+1)\mathrm{Re}\{T_{LL;\ell}\}\ , \tag{3.59}$$

$$\sigma_{\mathrm{abs}} = \sigma_{\mathrm{ext}} - \sigma_{\mathrm{sc}}\ . \tag{3.60}$$

Another useful quantity, that can be directly calculated with the help of T matrix, is the change in the number of states of the acoustic field, up to an angular frequency Ω, induced by a single poroelastic sphere in an infinite host medium, and is given from the expression

$$\Delta N(\Omega) = \frac{1}{\pi}\sum_{\ell}(2\ell+1)\mathrm{Im}\ln\left[1+T_{LL;\ell}(\Omega)\right]\ . \tag{3.61}$$

Of more interest is the corresponding *density of states* induced by the sphere and given by $\Delta n(\Omega) = d\Delta N(\Omega)/d\Omega$.

3.4 Example

We will close this chapter with an example where we apply the previously developed theoretical tools in two cases: a solid homogeneous spherical scatterer and a fluid-saturated poroelastic spherical scatterer, both immersed in fluid host. First, we choose a solid homogeneous polystyrene sphere of mass density $\rho_s = 1050$ kg m^{-3}, longitudinal wave velocity $c_l = 2350$ m s^{-1} and transverse wave velocity $c_t = 1200$ m s^{-1}, immersed in water [mass density $\rho_h = 1000$ kg m^{-3} and (longitudinal) wave velocity $c_h = 1480$ m s^{-1}]. Figure 3.1 depicts the dimensionless scattering cross section $\sigma_{sc}/\pi S^2$ and the dimensionless change in the density of states $\Delta n c_h/S$. We note that two characteristic scattering peaks appear, one at $\Omega S/c_h = 3.076$, corresponding to angular momentum $\ell = 2$ and the second with lower intensity at $\Omega S/c_h = 4.492$, corresponding to angular momentum $\ell = 3$. These resonant states manifest themselves as Lorentzian peaks at the same frequency in the change in the density of states, as expected. An important comment has to be made at this point: the lorentzian-shaped curves in the density of states correspond to an area $\Delta N(\omega)$ of 5 and 7 states for the individual modes $\ell = 2$ and $\ell = 3$ respectively. This confirms that every single ℓ mode is $(2\ell+1)$-degenerated due to the azimuthal symmetry of the spherical particle, in accordance with the factor $(2\ell+1)$ appearing in Eq. (3.61).

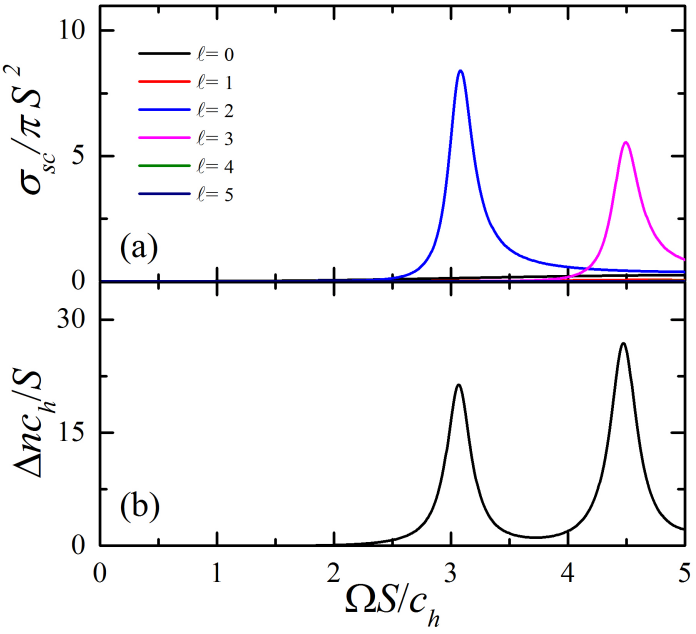

Figure 3.1: (a) Reduced scattering cross section of an acoustic plane wave incident on a homogeneous polystyrene sphere of radius S immersed in water and (b) change in the density of states of the acoustic field induced by this sphere.

It is, also, worth noting that our results, in the way they are presented, do not depend explicitly on the radius S of the particle and apply to any radius as long as the different quantities $(\Omega, \sigma_{sc}, \Delta n)$ are appropriately scaled.

In the second case, we consider a water-saturated polystyrene porous sphere immersed in water. The elastic parameters for the solid component of the sphere are identical to those of the solid homogeneous polystyrene; the elastic parameters for the fluid inside the porous and in the host region are those of water. We need in addition the values of the elastic moduli of the bare skeletal frame of the porous polystyrene sphere, K_b and μ_b, which are evaluated using Berryman's self-consistent effective medium theory for a polystyrene/void elastic composite, assuming that the pores are modeled by randomly distributed needles, as appropriate for the low-porosity limit that will concern us here [78, 79]. For $f = 10\%$ that we will consider in our study, we find $K_b = 2.602$ GPa and $\mu_b = 1.186$ GPa. Accordingly, the tortuosity is given by $\xi = f^{-2/3}$, for a random array of needles [59].

In Biot's theory [25, 26], by which we describe the individual porous spheres, there are two distinct limits. When the viscous skin depth, $\delta = \sqrt{2\eta/(\Omega\rho_f)}$, is much larger than the radius, R_p, of the (cylindrical) pores, viscous drag prevents the efficient formation of slow longitudinal waves, which are associated with an out-of-phase relative motion of

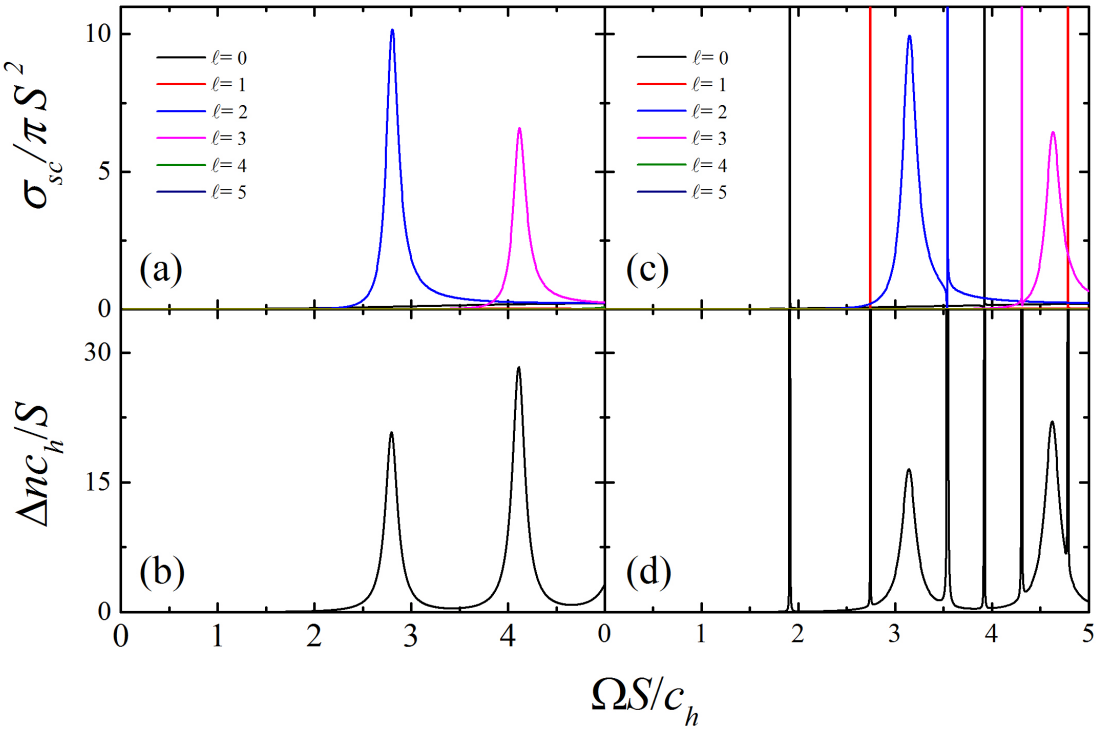

Figure 3.2: (a),(c) Reduced scattering cross section of an acoustic plane wave incident on a water-saturated porous polystyrene sphere of radius S immersed in water, and, (b),(d) change in the density of states of the acoustic field induced by this sphere treated as effectively homogeneous (left panel) and in the limit of $\eta = 0$ (right panel). The slow waves are manifested as very sharp resonances.

the solid frame and infiltrated liquid. In this so-called *viscous-coupling* limit, the porous material behaves as an effective homogeneous medium, the elastic parameters of which can be evaluated, e.g., by the self-consistent homogenization method of Berryman [78,79], while dissipative losses are quite small and can be neglected [42]. On the other hand, when $\delta \ll R_p$, we are in the so-called *inertial-coupling* limit where all three bulk acoustic modes in the porous material (transverse, fast and slow longitudinal) become nondispersive and attenuation free, as one would have in the absence of viscous losses ($\eta = 0$). In Fig. 3.2, we present two cases corresponding to those two limits. In the case $\delta \gg R_p$ [left panel in Fig. 3.2] we treat the porous sphere as effectively homogeneous, with elastic parameters $\rho_s^{eff} = 1045$ kg m^{-3}, $c_l^{eff} = 2222$ m s^{-1}, and, $c_t^{eff} = 1073$ m s^{-1}, lower than those of the corresponding homogeneous sphere, calculated by the self-consistent homogenization method of Berryman [78,79]. We observe the same peaks appearing as in the case of the

homogeneous solid sphere, except that they are sharper and red-shifted [at $\Omega S/c_h = 2.807$ and $\Omega S/c_h = 4.124$ for the modes $\ell = 2$ and $\ell = 3$, respectively]. In the case $\delta \ll R_p$ [right panel in Fig. 3.2] we treat the sphere as poroelastic, using the results of § 3.2, considering the limit $\eta = 0$. Here, additional very sharp resonances appear that originate from the manifestation of the slow waves in the absence of viscous losses.

Chapter 4

Layer Multiple Scattering

Among the methods developed for the theoretical study of periodic phononic structures, the LMS method is especially attractive because it provides many advantages, such as being fast and numerically accurate. It combines the expansion into spherical waves for the description of scattering by single particles and 2D structures with the expansion into plane waves for the scattering between such consecutive layers. The only restriction is that the layers must have the same 2D periodicity. This method calculates the reflectance and transmittance of finite slabs and also the complex band structure of an infinite crystal. In this chapter we describe in a concise but rigorous manner our LMS method [23, 24], which we recently extended to include porous fluid-saturated scatterers [80, 81], by adapting it in the case of interest, i.e., for acoustic scattering.

4.1 Scattering by a plane of spheres

In our study we will deal with structures consisting of consecutive layers, say perpendicular to the z direction. Whether these structures are finite or infinite in this direction, the basic component is a composite slab, consisting, in general, of one or more layers, each of them containing spherical non-overlapping scatterers arranged in a 2D lattice, parallel to the xy plane. The layers can be displaced (slided), parallel to the xy plane, and/or along z direction, the only restriction being to keep the same 2D periodicity throughout the slab. The 2D lattice defined by the vectors

$$\mathbf{R}_n = n_1\mathbf{a}_1 + n_2\mathbf{a}_2 \ , \tag{4.1}$$

where $n_1, n_2 = 0, \pm1, \pm2, \pm3, \ldots$, and $\mathbf{a}_1$, $\mathbf{a}_2$ are the primitive lattice vectors in the xy plane. Next, we define the corresponding 2D reciprocal lattice as follows

$$\mathbf{g} = m_1\mathbf{b}_1 + m_2\mathbf{b}_2 \ , \tag{4.2}$$

with $m_1, m_2 = 0, \pm 1, \pm 2, \pm 3, \ldots$ and the primitive vectors of the reciprocal lattice $\mathbf{b}_1$, $\mathbf{b}_2$, defined from

$$\mathbf{b}_i \cdot \mathbf{a}_j = 2\pi\delta_{ij} \ , \quad i,j = 1,2 \ . \tag{4.3}$$

Since the structures under study present 2D periodicity perpendicular to the z direction, we write the parallel to the xy plane component of the wave vector of an incident plane wave as follows

$$\mathbf{q}_\parallel = \mathbf{k}_\parallel + \mathbf{g}' \ , \tag{4.4}$$

where $\mathbf{k}_\parallel$ is the reduced wave vector inside the Surface Brillouin Zone (SBZ) of the 2D lattice and $\mathbf{g}'$ an appropriate vector of the reciprocal lattice (4.2), so that for a given $\mathbf{q}_\parallel$, the vector $\mathbf{q}_\parallel - \mathbf{g}'$ will lie within the SBZ, after successive subtractions of vectors of the reciprocal space. From Eqs. (4.3) and (4.4) it follows immediately that $\exp(\mathrm{i}\mathbf{q}_\parallel \cdot \mathbf{R}_n) = \exp(\mathrm{i}\mathbf{k}_\parallel \cdot \mathbf{R}_n)$.

We now consider at $z = 0$ a plane of nonoverlapping submerged fluid-saturated poroelastic spheres, which are centered on the sites $\mathbf{R}_n$ of a given 2D lattice. The wavevector of the incident wave, using Eq. (4.4), has the form

$$\mathbf{K}^{\pm}_{\mathbf{g}'} = \mathbf{k}_\parallel + \mathbf{g}' \pm \hat{\mathbf{z}}[Q_h^2 - (\mathbf{k}_\parallel + \mathbf{g}')^2]^{1/2} \tag{4.5}$$

where $Q_h = \Omega\sqrt{\rho_h/K_h}$ is the wavenumber in the medium surrounding the scatterers (host medium) and the $+$ or $-$ sign refers to incidence from the left ($z < 0$) or from the right ($z > 0$), respectively. The corresponding displacement field is written as

$$\mathbf{u}^{\pm}_{in}(\mathbf{r}) = [u_{in}]^{\pm}_{\mathbf{g}'} \exp(\mathrm{i}\mathbf{K}^{\pm}_{\mathbf{g}'} \cdot \mathbf{r})\widehat{\mathbf{K}}^{\pm}_{\mathbf{g}'} \tag{4.6}$$

and the coefficients in the respective spherical wave expansion, according to Eq. (2.62), are $a^0_{L\ell m} = 4\pi\mathrm{i}^{\ell+1}(-1)^{m+1}Y_{\ell -m}(\widehat{\mathbf{K}}^{\pm}_{\mathbf{g}'})[u_{in}]^{\pm}_{\mathbf{g}'}$.

Because of the 2D periodicity of the array of spheres, the wave scattered by it, when the wave given by Eq. (4.6) is incident upon it, has the following form

$$\mathbf{u}_{sc}(\mathbf{r}) = \sum_{\mathbf{R}_n} \exp(\mathrm{i}\mathbf{k}_\parallel \cdot \mathbf{R}_n) \sum_{\ell m} b^+_{L\ell m} \frac{1}{Q_h} \nabla[h^+_\ell(Q_h r_n) Y_{\ell m}(\widehat{\mathbf{r}}_n)] \ , \tag{4.7}$$

where $\mathbf{r}_n = \mathbf{r} - \mathbf{R}_n$ and the coefficients $b^+_{L\ell m}$ are obtained by solving the following system of linear equations [23]

$$\sum_{\ell' m'} (\delta_{\ell\ell'}\delta_{mm'} - T_{LL;\ell}\ Z^{\ell m}_{\ell' m'}) b^+_{L\ell' m'} = T_{LL;\ell}\ a^0_{L\ell m} \ , \tag{4.8}$$

with

$$Z^{\ell' m'}_{\ell m} = 4\pi \sum_{\mathbf{R}_n \neq 0} \exp(\mathrm{i}\mathbf{k}_\parallel \cdot \mathbf{R}_n) \sum_{\ell'' m''} (-1)^{(\ell - \ell' - \ell'')/2} (-1)^{m' + m''} h^+_{\ell''}(Q_h R_n) Y_{\ell'' -m''}(-\widehat{\mathbf{R}}_n)$$
$$\times \int d\widehat{\mathbf{r}} Y_{\ell m}(\widehat{\mathbf{r}}) Y_{\ell' -m'}(\widehat{\mathbf{r}}) Y_{\ell'' m''}(\widehat{\mathbf{r}}) \ . \tag{4.9}$$

Since Ω and $\mathbf{k}_\parallel$ are conserved quantities in the scattering process, the scattered field, given by Eq. (4.7), will consist of a series of plane waves with wave vectors

$$\mathbf{K}_\mathbf{g}^\pm = \mathbf{k}_\parallel + \mathbf{g} \pm \widehat{\mathbf{z}}[Q_h^2 - (\mathbf{k}_\parallel + \mathbf{g})^2]^{1/2} \ , \forall \mathbf{g} \ . \tag{4.10}$$

Indeed, with the help of the mathematical identity

$$\sum_{\mathbf{R}_n} \exp(\mathrm{i}\mathbf{k}_\parallel \cdot \mathbf{R}_n) h_\ell^+(Q_h r_n) Y_{\ell m}(\widehat{\mathbf{r}}_n) = \sum_\mathbf{g} \frac{2\pi(-\mathrm{i})^\ell}{Q_h A_0 K_{\mathbf{g}z}^+} Y_{\ell m}(\widehat{\mathbf{K}}_\mathbf{g}^s) \exp(\mathrm{i}\mathbf{K}_\mathbf{g}^s \cdot \mathbf{r}) \ , \tag{4.11}$$

where A_0 is the area of the unit cell of the 2D lattice and $s = +$ or $-$ corresponds to $z > 0$ or $z < 0$, respectively, it is straightforward to show that

$$\mathbf{u}_{sc}(\mathbf{r}) = \sum_\mathbf{g} [u_{sc}]_\mathbf{g}^s \exp(\mathrm{i}\mathbf{K}_\mathbf{g}^s \cdot \mathbf{r}) \widehat{\mathbf{K}}_\mathbf{g}^s \ , \tag{4.12}$$

with

$$[u_{sc}]_\mathbf{g}^s = \sum_{\ell m} \Delta_{L\ell m}(\mathbf{K}_\mathbf{g}^s) b_{L\ell m}^+ \ ,$$

where

$$\Delta_{L\ell m}(\mathbf{K}_\mathbf{g}^s) = \frac{2\pi(-\mathrm{i})^{\ell-1}}{Q_h A_0 K_{\mathbf{g}z}^+} Y_{\ell m}(\widehat{\mathbf{K}}_\mathbf{g}^s) \ .$$

It is worth noting that, though the scattered field consists, in general, of a number of diffracted beams corresponding to different 2D reciprocal lattice vectors $\mathbf{g}$, only beams for which $K_{\mathbf{g}z}^s$ is real constitute propagating waves. When $(\mathbf{k}_\parallel + \mathbf{g})^2 > Q_h^2$ the corresponding wave decays to the right for $s = +$, and to the left for $s = -$. We also note that $[u_{sc}]_\mathbf{g}^s$ depend on the incident plane wave through the coefficients $b_{L\ell m}^+$, which are evaluated from Eqs. (4.8) for a given plane wave component of wavevector $\mathbf{K}_{\mathbf{g}'}^{s'}$. For example, when a plane wave given by Eq. (4.6) is incident on the plane of spheres from the left, the transmitted wave (incident+scattered) on the right of the plane is given by

$$\mathbf{u}_{tr}^+(\mathbf{r}) = \sum_\mathbf{g} [u_{tr}]_\mathbf{g}^+ \exp(\mathrm{i}\mathbf{K}_\mathbf{g}^+ \cdot \mathbf{r}) \widehat{\mathbf{K}}_\mathbf{g}^+ \ , \ z > 0 \ , \tag{4.13}$$

with

$$[u_{tr}]_\mathbf{g}^+ = [u_{in}]_{\mathbf{g}'}^+ \delta_{\mathbf{g}\mathbf{g}'} + [u_{sc}]_\mathbf{g}^+ \equiv S_{\mathbf{g}\mathbf{g}'}^{++} [u_{in}]_{\mathbf{g}'}^+ \ ,$$

and the reflected wave on the left of the plane by

$$\mathbf{u}_{rf}^-(\mathbf{r}) = \sum_\mathbf{g} [u_{rf}]_\mathbf{g}^- \exp(\mathrm{i}\mathbf{K}_\mathbf{g}^- \cdot \mathbf{r}) \widehat{\mathbf{K}}_\mathbf{g}^- \ , \ z < 0 \ , \tag{4.14}$$

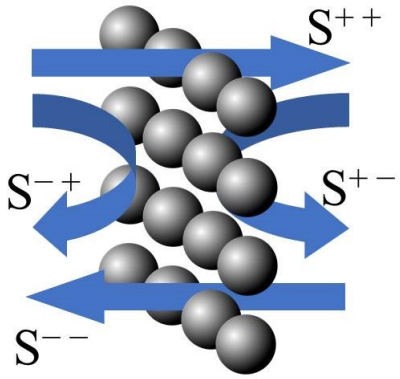

Figure 4.1: Transmittance and reflectance matrices for a plane of spheres.

with

$$[u_{rf}]^{-}_{\mathbf{g}} = [u_{sc}]^{-}_{\mathbf{g}} \equiv S^{-+}_{\mathbf{g}\mathbf{g}'}[u_{in}]^{+}_{\mathbf{g}'} \ .$$

Similarly we can define the transmission matrix elements $S^{--}_{\mathbf{g}\mathbf{g}'}$ and the reflection matrix elements $S^{+-}_{\mathbf{g}\mathbf{g}'}$ for a plane wave incident on the plane of spheres from the right. Using Eq. (4.12) we obtain

$$S^{ss'}_{\mathbf{g}\mathbf{g}'} = \delta_{ss'}\delta_{\mathbf{g}\mathbf{g}'} + \sum_{\ell m} \Delta_{L\ell m}(\mathbf{K}^{s}_{\mathbf{g}}) b^{+}_{L\ell m}(\mathbf{K}^{s'}_{\mathbf{g}'})([u_{in}]^{s'}_{\mathbf{g}'})^{-1} \ , \tag{4.15}$$

where we explicitly denoted the dependence of $b^{+}_{L\ell m}$ on $\mathbf{K}^{s'}_{\mathbf{g}'}$. We note that the matrix elements $S^{ss'}_{\mathbf{g}\mathbf{g}'}$ obey the symmetry relation $S^{-s-s'}_{\mathbf{g}\mathbf{g}'} = S^{ss'}_{\mathbf{g}\mathbf{g}'}$. The physical meaning of these matrices is depicted in Fig. 4.1.

The difference in the number of states up to a given frequency Ω, between the system under consideration (a plane of particles in a homogeneous medium) and that of the host medium extending over all space is given by

$$\Delta N(\Omega) = \frac{N}{A} \int \int_{SBZ} d^2\mathbf{k}_{\|} \Delta N(\Omega, \mathbf{k}_{\|}) \ , \tag{4.16}$$

where N is the number of surface unit cells of the plane particles and A the area of the SBZ. The $\mathbf{k}_{\|}$-resolved change in the number of states is given, in the spherical-wave representation, by [82]

$$\Delta N(\Omega, \mathbf{k}_{\|}) = \frac{1}{\pi} \mathrm{Im} \ln \det(\mathbf{I} + \mathbf{T}) - \frac{1}{\pi} \mathrm{Im} \ln \det(\mathbf{I} - \mathbf{T}\mathbf{Z}) \ , \tag{4.17}$$

where $\mathbf{I}$ is the unit matrix, $\mathbf{Z}$ is the matrix whose elements are defined by Eq. (4.9), and in the plane wave representation by

$$\Delta N(\Omega, \mathbf{k}_\parallel) = \frac{1}{2\pi} \mathrm{Im} \ln \det \mathbf{S} \ , \tag{4.18}$$

where

$$\mathbf{S} = \begin{pmatrix} \mathbf{S}^{++} & \mathbf{S}^{+-} \\ \mathbf{S}^{-+} & \mathbf{S}^{--} \end{pmatrix} . \tag{4.19}$$

We note that the S matrix is defined in the basis of those reciprocal-lattice vectors which correspond to propagating beams and that the resulting $\Delta N(\Omega, \mathbf{k}_\parallel)$, contrary to that obtained through Eq. (4.17), does not include possible bound states of the system. The corresponding $\mathbf{k}_\parallel$-resolved change in the density of states is obtained through $\Delta n(\Omega, \mathbf{k}_\parallel) = \partial \Delta N(\Omega, \mathbf{k}_\parallel)/\partial\Omega$.

4.2 Scattering by a slab

In order to describe scattering by multilayers of particles with the same 2D periodicity, it is convenient to express the waves on the left of a given layer with respect to an origin, $\mathbf{A}_l$, on the left of the layer at $-\mathbf{d}_l$ from its center and the waves on the right of this layer with respect to an origin, $\mathbf{A}_r$, on the right of the layer at $\mathbf{d}_r$ from its center, i.e., a plane wave on the left of the layer will be written as $u^s_{\mathbf{g}} \exp[\mathrm{i}\mathbf{K}^s_{\mathbf{g}} \cdot (\mathbf{r} - \mathbf{A}_l)]\widehat{\mathbf{K}}^s_{\mathbf{g}}$ and a plane wave on the right of the layer will be written as $u^s_{\mathbf{g}} \exp[\mathrm{i}\mathbf{K}^s_{\mathbf{g}} \cdot (\mathbf{r} - \mathbf{A}_r)]\widehat{\mathbf{K}}^s_{\mathbf{g}}$. With the above choice of origins the transmission (reflection) matrix elements of a layer become

$$\begin{aligned} Q^{\mathrm{I}}_{\mathbf{g}\mathbf{g}'} &= S^{++}_{\mathbf{g}\mathbf{g}'} \exp\left[\mathrm{i}(\mathbf{K}^+_{\mathbf{g}} \cdot \mathbf{d}_r + \mathbf{K}^+_{\mathbf{g}'} \cdot \mathbf{d}_l)\right] \\ Q^{\mathrm{II}}_{\mathbf{g}\mathbf{g}'} &= S^{+-}_{\mathbf{g}\mathbf{g}'} \exp\left[\mathrm{i}(\mathbf{K}^+_{\mathbf{g}} \cdot \mathbf{d}_r - \mathbf{K}^-_{\mathbf{g}'} \cdot \mathbf{d}_r)\right] \\ Q^{\mathrm{III}}_{\mathbf{g}\mathbf{g}'} &= S^{-+}_{\mathbf{g}\mathbf{g}'} \exp\left[-\mathrm{i}(\mathbf{K}^-_{\mathbf{g}} \cdot \mathbf{d}_l - \mathbf{K}^+_{\mathbf{g}'} \cdot \mathbf{d}_l)\right] \\ Q^{\mathrm{IV}}_{\mathbf{g}\mathbf{g}'} &= S^{--}_{\mathbf{g}\mathbf{g}'} \exp\left[-\mathrm{i}(\mathbf{K}^-_{\mathbf{g}} \cdot \mathbf{d}_l + \mathbf{K}^-_{\mathbf{g}'} \cdot \mathbf{d}_r)\right] . \end{aligned} \tag{4.20}$$

The transmission (reflection) matrices for a multilayer slab are obtained from the corresponding matrices of the individual layers.

A composite slab may consist of a finite number of elements, where each element can be a plane of scatterers, a planar interface, or a homogeneous slab. We remind that if two consecutive layers are immersed in different hosts, separated by a planar interface, then this interface should be considered as an extra element that will cause scattering. The reflection and transmission matrices, $\mathbf{Q}$, for a pair of consecutive elements, let us denote them '1' and '2', are calculated by combining the matrices $\mathbf{Q}(1)$ and $\mathbf{Q}(2)$ of the two elements as shown in Fig. 4.2. Here it must be noted that, even though the choice of $\mathbf{d}_l$

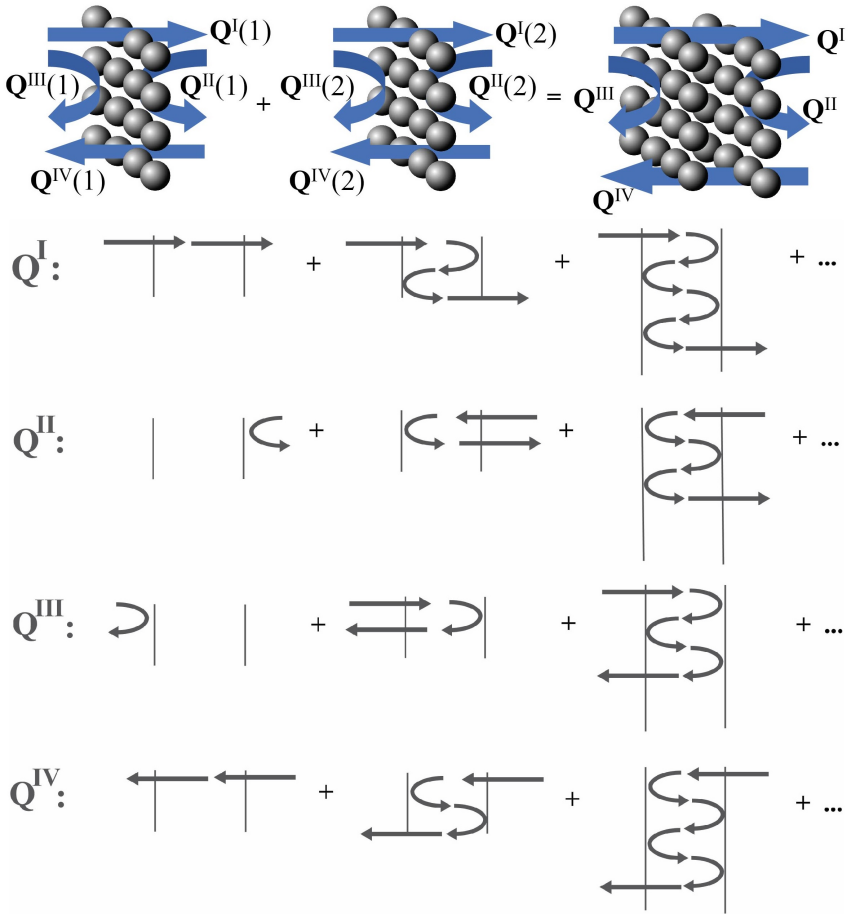

Figure 4.2: Transmittance and reflectance matrices for a multilayer slab.

and $\mathbf{d}_r$ is somehow arbitrary, it must respect the matching between consecutive elements, i.e., $\mathbf{A}_r(1) = \mathbf{A}_l(2)$. It is easy to prove, after taking into consideration all the processes of multiple scattering, described schematically in Fig. 4.2, that

$$\begin{aligned}
\mathbf{Q}^{\mathrm{I}} &= \mathbf{Q}^{\mathrm{I}}(2)[1 - \mathbf{Q}^{\mathrm{II}}(1)\mathbf{Q}^{\mathrm{III}}(2)]^{-1}\mathbf{Q}^{\mathrm{I}}(1) \\
\mathbf{Q}^{\mathrm{II}} &= \mathbf{Q}^{\mathrm{II}}(2) + \mathbf{Q}^{\mathrm{I}}(2)\mathbf{Q}^{\mathrm{II}}(1)[1 - \mathbf{Q}^{\mathrm{III}}(2)\mathbf{Q}^{\mathrm{II}}(1)]^{-1}\mathbf{Q}^{\mathrm{IV}}(2) \\
\mathbf{Q}^{\mathrm{III}} &= \mathbf{Q}^{\mathrm{III}}(1) + \mathbf{Q}^{\mathrm{IV}}(1)\mathbf{Q}^{\mathrm{III}}(2)[1 - \mathbf{Q}^{\mathrm{II}}(1)\mathbf{Q}^{\mathrm{III}}(2)]^{-1}\mathbf{Q}^{\mathrm{I}}(1) \\
\mathbf{Q}^{\mathrm{IV}} &= \mathbf{Q}^{\mathrm{IV}}(1)[1 - \mathbf{Q}^{\mathrm{III}}(2)\mathbf{Q}^{\mathrm{II}}(1)]^{-1}\mathbf{Q}^{\mathrm{IV}}(2)\ . \qquad (4.21)
\end{aligned}$$

All the matrices refer to the same Ω and $\mathbf{k}_{\|}$. We remind that the waves on the left and the right of the pair of elements are expanded with respect to the point defined by the position

vector $-\mathbf{d}_l(1,2) = -\mathbf{d}_l(1)$ from the center of the left element and $\mathbf{d}_r(1,2) = \mathbf{d}_r(2)$ from the center of the right element, respectively. The same procedure can, obviously, be used to calculate the transmission and reflection matrices from three consecutive elements, by combining the matrices of the pair of two elements with those of the third. In this way, we can find the scattering matrices of a composite slab consisting by any (finite) number of elements.

For a finite slab of a phononic crystal, consisting of a large number of repeating identical composite unit slabs, a technique can be used to double consecutively the size of the system, that allows the fast and effective calculation of the scattering matrices characterizing the whole system. Let us assume that we have 2^M $(M = 0, 1, 2, ...)$ consecutive unit slabs. Having calculated the $\mathbf{Q}$ matrices of a unit slab, the corresponding matrices for a pair of such slabs are calculated by the way described in Eqs. (4.21). Next, using as units the $\mathbf{Q}$ matrices of the pair, those of four consecutive unit slabs can be deduced, and so on; by doubling the number of the unit slabs in each step, we finally obtain the $\mathbf{Q}$ matrices for the whole slab of the crystal. If this slab is immersed in a different homogeneous host, without absorption, the scattering on the left and right side must be taken into consideration by handling these surfaces as extra elements contributing to the multiple scattering. It is worth noting that the (semi-infinite) medium on the left of the slab of the crystal can be different from that at its right.

For a plane wave $[u_{in}]^+_{\mathbf{g}'} \exp[\mathrm{i}\mathbf{K}^+_{\mathbf{g}'} \cdot (\mathbf{r} - \mathbf{A}_L)]\widehat{\mathbf{K}}^+_{\mathbf{g}'}$, incident on the slab from the left, we finally obtain a reflected wave $\sum_{\mathbf{g}} [u_{rf}]^-_{\mathbf{g}} \exp[\mathrm{i}\mathbf{K}^-_{\mathbf{g}} \cdot (\mathbf{r} - \mathbf{A}_L)]\widehat{\mathbf{K}}^-_{\mathbf{g}}$ on the left of the slab and a transmitted wave $\sum_{\mathbf{g}} [u_{tr}]^+_{\mathbf{g}} \exp[\mathrm{i}\mathbf{K}^+_{\mathbf{g}} \cdot (\mathbf{r} - \mathbf{A}_R)]\widehat{\mathbf{K}}^+_{\mathbf{g}}$ on the right of the slab, where $\mathbf{A}_L$ $(\mathbf{A}_R)$ is the position vector of the appropriate origin at the left (right) interface of the slab. We have

$$[u_{tr}]^+_{\mathbf{g}} = Q^{\mathrm{I}}_{\mathbf{g}\mathbf{g}'} [u_{in}]^+_{\mathbf{g}'} \tag{4.22}$$

and

$$[u_{rf}]^-_{\mathbf{g}} = Q^{\mathrm{III}}_{\mathbf{g}\mathbf{g}'} [u_{in}]^+_{\mathbf{g}'} \ , \tag{4.23}$$

where $\mathbf{Q}^{\mathrm{I}}$ and $\mathbf{Q}^{\mathrm{III}}$ are the appropriate transmission and reflection matrices of the whole slab. After calculating the transmitted and reflected waves on the right and left of the slab, we can obtain the corresponding transmittance $\mathcal{T}(\Omega, \mathbf{k}_\parallel + \mathbf{g}')$ and reflectance $\mathcal{R}(\Omega, \mathbf{k}_\parallel + \mathbf{g}')$ from Eqs. (4.24) and (4.25), respectively.

These are defined as the ratio of the transmitted, respectively the reflected, energy flux to the energy flux associated with the incident wave. Assuming, e.g., incidence from

the left we obtain with the help of Eq. (3.52)

$$\mathcal{T} = \frac{\sum_{\mathbf{g}} |[u_{tr}]^+_{\mathbf{g}}|^2 K^+_{\mathbf{g}z}}{|[u_{in}]^+_{\mathbf{g}'}|^2 K^+_{\mathbf{g}'z}} \tag{4.24}$$

and

$$\mathcal{R} = \frac{\sum_{\mathbf{g}} |[u_{rf}]^-_{\mathbf{g}}|^2 K^+_{\mathbf{g}z}}{|[u_{in}]^+_{\mathbf{g}'}|^2 K^+_{\mathbf{g}'z}} \ . \tag{4.25}$$

The above expressions are valid for the case of a slab having the same (semi-infinite) medium at its left and at its right. We remember that only propagating beams (those with $K^+_{\mathbf{g}z}$ real) enter the numerators of the above equations. Finally we note that if absorption is present it can be calculated from the requirement of energy conservation, $\mathcal{A} = 1 - \mathcal{T} - \mathcal{R}$.

On the other hand, the change in the number of states between the slab and the homogeneous host medium extending all over the space can be calculated from Eqs. (4.16) and (4.18), where the elements of the S matrix in the plane-wave representation are given by

$$\begin{aligned}
S^{++}_{\mathbf{g}\mathbf{g}'} &= \exp\left[-\mathrm{i}(\mathbf{K}^+_{\mathbf{g}} \cdot \mathbf{A}_R - \mathbf{K}^+_{\mathbf{g}'} \cdot \mathbf{A}_L)\right] Q^{\mathrm{I}}_{\mathbf{g}\mathbf{g}'} \\
S^{+-}_{\mathbf{g}\mathbf{g}'} &= \exp\left[-\mathrm{i}(\mathbf{K}^+_{\mathbf{g}} \cdot \mathbf{A}_R - \mathbf{K}^-_{\mathbf{g}'} \cdot \mathbf{A}_R)\right] Q^{\mathrm{II}}_{\mathbf{g}\mathbf{g}'} \\
S^{-+}_{\mathbf{g}\mathbf{g}'} &= \exp\left[-\mathrm{i}(\mathbf{K}^-_{\mathbf{g}} \cdot \mathbf{A}_L - \mathbf{K}^+_{\mathbf{g}'} \cdot \mathbf{A}_L)\right] Q^{\mathrm{III}}_{\mathbf{g}\mathbf{g}'} \\
S^{--}_{\mathbf{g}\mathbf{g}'} &= \exp\left[-\mathrm{i}(\mathbf{K}^-_{\mathbf{g}} \cdot \mathbf{A}_L - \mathbf{K}^-_{\mathbf{g}'} \cdot \mathbf{A}_R)\right] Q^{\mathrm{IV}}_{\mathbf{g}\mathbf{g}'} \ ,
\end{aligned} \tag{4.26}$$

for the given Ω and $\mathbf{k}_{\|}$. The phase factors in Eq. (4.26) arise from the need to refer all waves to a common origin. The possible eigenmodes of the slab are obtained by requiring existence of a wave field localized within the slab in the absence of incident wave. Dividing the slab into a left and a right part, described by reflection matrices $\mathbf{Q}^{\mathrm{II}}_1$ and $\mathbf{Q}^{\mathrm{III}}_2$, respectively, this requirement leads to the secular equation

$$\det[\mathbf{I} - \mathbf{Q}^{\mathrm{II}}_1 \mathbf{Q}^{\mathrm{III}}_2] = 0 \ . \tag{4.27}$$

4.3 Complex band structure of an infinite crystal

For a three-dimensional crystal consisting of an infinite periodic sequence of layers stacked along the z-direction, the wave field in the host region between the n-th and the $(n+1)$-th unit slabs has the form

$$\mathbf{u}(\mathbf{r}) = \sum_{\mathbf{g}} \{u^+_{\mathbf{g}n} \exp[\mathrm{i}\mathbf{K}^+_{\mathbf{g}} \cdot (\mathbf{r} - \mathbf{A}_n)] \widehat{\mathbf{K}}^+_{\mathbf{g}} + u^-_{\mathbf{g}n} \exp[\mathrm{i}\mathbf{K}^-_{\mathbf{g}} \cdot (\mathbf{r} - \mathbf{A}_n)] \widehat{\mathbf{K}}^-_{\mathbf{g}}\} \ , \tag{4.28}$$

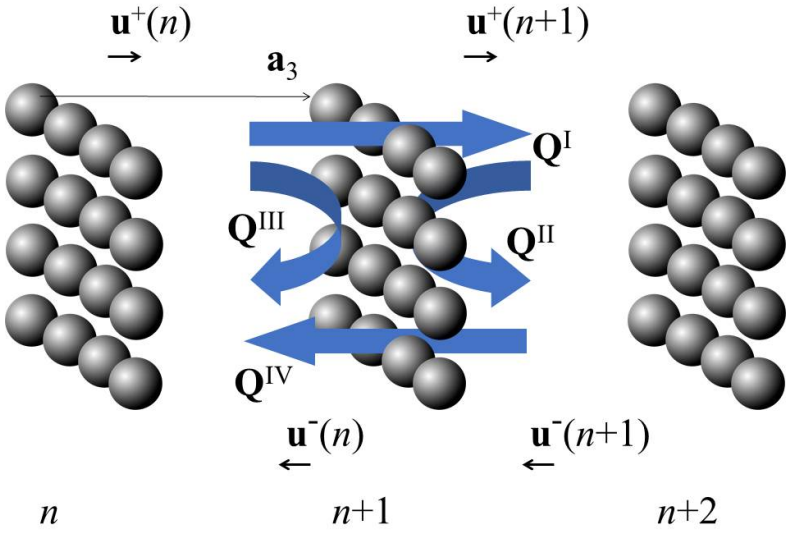

Figure 4.3: Q matrices for an infinite periodic phononic structure.

where $\mathbf{A}_n$ is an appropriate origin between the n-th and the $(n+1)$-th unit slabs (see Fig. 4.3). The coefficients $u^{\pm}_{\mathbf{g}n}$ are obviously related to $u^{\pm}_{\mathbf{g}n+1}$ through the Q matrices of the unit slab as follows

$$\begin{aligned} u^{+}_{\mathbf{g}n+1} &= \sum_{\mathbf{g}'} [Q^{\mathrm{I}}_{\mathbf{g}\mathbf{g}'} u^{+}_{\mathbf{g}'n} + Q^{\mathrm{II}}_{\mathbf{g}\mathbf{g}'} u^{-}_{\mathbf{g}'n+1}] \,, \\ u^{-}_{\mathbf{g}n} &= \sum_{\mathbf{g}'} [Q^{\mathrm{III}}_{\mathbf{g}\mathbf{g}'} u^{+}_{\mathbf{g}'n} + Q^{\mathrm{IV}}_{\mathbf{g}\mathbf{g}'} u^{-}_{\mathbf{g}'n+1}] \,. \end{aligned} \tag{4.29}$$

On the other hand Bloch's theorem implies that $u^{\pm}_{\mathbf{g}n+1} = \exp(\mathrm{i}\mathbf{k}\cdot\mathbf{a}_3) u^{\pm}_{\mathbf{g}n}$, where $\mathbf{k} = (\mathbf{k}_{\|}, k_z(\Omega, \mathbf{k}_{\|}))$ and $\mathbf{a}_3$ is a vector which connects a point in the n-th slab to an equivalent point in the $(n+1)$-th slab (Fig. 4.3). For given Ω and $\mathbf{k}_{\|}$ one can obtain k_z from the following eigenvalue equation

$$\begin{pmatrix} \mathbf{Q}^{\mathrm{I}} & \mathbf{Q}^{\mathrm{II}} \\ -[\mathbf{Q}^{\mathrm{IV}}]^{-1}\mathbf{Q}^{\mathrm{III}}\mathbf{Q}^{\mathrm{I}} & [\mathbf{Q}^{\mathrm{IV}}]^{-1}[\mathbf{I} - \mathbf{Q}^{\mathrm{III}}\mathbf{Q}^{\mathrm{II}}] \end{pmatrix} \begin{pmatrix} \mathbf{u}^{+}_{n} \\ \mathbf{u}^{-}_{n+1} \end{pmatrix} = \exp(\mathrm{i}\mathbf{k}\cdot\mathbf{a}_3) \begin{pmatrix} \mathbf{u}^{+}_{n} \\ \mathbf{u}^{-}_{n+1} \end{pmatrix} , \tag{4.30}$$

which follows directly from Eq. (4.29) and Bloch's theorem. Alternatively, one can formulate an eigenvalue equation for the transfer matrix

$$\begin{pmatrix} \mathbf{Q}^{\mathrm{I}} - \mathbf{Q}^{\mathrm{II}}[\mathbf{Q}^{\mathrm{IV}}]^{-1}\mathbf{Q}^{\mathrm{III}} & \mathbf{Q}^{\mathrm{II}}[\mathbf{Q}^{\mathrm{IV}}]^{-1} \\ -[\mathbf{Q}^{\mathrm{IV}}]^{-1}\mathbf{Q}^{\mathrm{III}} & [\mathbf{Q}^{\mathrm{IV}}]^{-1} \end{pmatrix} \begin{pmatrix} \mathbf{u}^{+}_{n} \\ \mathbf{u}^{-}_{n} \end{pmatrix} = \exp(\mathrm{i}\mathbf{k}\cdot\mathbf{a}_3) \begin{pmatrix} \mathbf{u}^{+}_{n} \\ \mathbf{u}^{-}_{n} \end{pmatrix} . \tag{4.31}$$

The solutions $k_z(\Omega, \mathbf{k}_\parallel)$ resulting from Eq. (4.30) or, equivalently, Eq. (4.31), looked upon as functions of real Ω, define for each $\mathbf{k}_\parallel$ lines in the complex k_z plane, which all together constitute the complex band structure of the infinite crystal associated with the given crystallographic plane. It is worth noting that the band structure exhibits periodicity in the reciprocal space since replacing $\mathbf{k}_\parallel$ with $\mathbf{k}_\parallel + \mathbf{g}$ renames the coefficients without changing the form of the wave function. Moreover, because the eigenvalues of Eq. (4.30) are of the form $\exp(\mathrm{i}\mathbf{k}\cdot\mathbf{a}_3)$, values of k_z that differ by an integer multiple of $2\pi/a_{3z}$ correspond to the same Bloch wave. We can choose, as a result, the reduced band of $\mathbf{k}$ in the reciprocal space as following: $(\mathbf{k}_\parallel, \mathrm{Re}k_z)$ with $\mathbf{k}_\parallel = (k_x, k_y)$ extending over all the surface Brillouin zone (SBZ) of the given crystallographic plane, and with $-|\mathbf{b}_3|/2 < \mathrm{Re}k_z \leq |\mathbf{b}_3|/2$, where $\mathbf{b}_3 = 2\pi(\mathbf{a}_1 \times \mathbf{a}_2)/[\mathbf{a}_1 \cdot (\mathbf{a}_2 \times \mathbf{a}_3)] = 2\pi/a_{3z}\widehat{\mathbf{z}}$, while $|\mathbf{a}_1| \equiv a_0$ (see Fig. 4.4). Here we should also note that when a plane of mirror symmetry, associated with the crystallographic plane under study, exists then the solutions (Bloch waves) of Eq. (4.30) appear in pairs: $k_z(\Omega; \mathbf{k}_\parallel)$ and $k_z(\Omega; -\mathbf{k}_\parallel)$. A line of given $\mathbf{k}_\parallel$ may be real (in the sense that k_z is real) over certain frequency regions, and be complex (in the sense that k_z is complex) for Ω outside these regions. It turns out that, for given $\mathbf{k}_\parallel$ and Ω, out of the solutions $k_z(\Omega, \mathbf{k}_\parallel)$, none or, at best, a few are real and the corresponding eigenvectors represent propagating modes of the acoustic field in the given infinite crystal. The remaining solutions $k_z(\Omega, \mathbf{k}_\parallel)$ are complex and the corresponding eigenvectors represent evanescent waves. These have an amplitude which increases exponentially in the positive or negative z-direction and, unlike the propagating waves, do not exist as physical entities in the infinite crystal. However, they are an essential part of the physical solutions of the acoustic field in the case of a surface or a slab of finite thickness. A region of frequency where propagating waves do not exist, for given $\mathbf{k}_\parallel$, constitutes a frequency gap of the acoustic field for the given $\mathbf{k}_\parallel$. If over a frequency region no propagating wave exists whatever the value of $\mathbf{k}_\parallel$, then this region constitutes an *absolute frequency gap*.

Finally, for the sake of completeness, we note that the transfer matrix on the left hand side of Eq. (4.31) can also provide the reflection matrix, $\mathbf{R}_\infty$, of the corresponding semi-infinite crystal and, through $\mathbf{R}_\infty$, one can find the surface states of the crystal, if such exist. In order to obtain $\mathbf{R}_\infty$, the eigenvectors of the transfer matrix need to be arranged in a matrix $\mathbf{F}$ which projects the space of forward and backward Bloch eigenmodes, $\mathbf{V}^+$ and $\mathbf{V}^-$, onto the original plane-wave basis, as follows [83, 84]

$$\begin{pmatrix} \mathbf{u}_0^+ \\ \mathbf{u}_0^- \end{pmatrix} = \begin{pmatrix} \mathbf{F}^{++} & \mathbf{F}^{+-} \\ \mathbf{F}^{-+} & \mathbf{F}^{--} \end{pmatrix} \begin{pmatrix} \mathbf{V}^+ \\ \mathbf{V}^- \end{pmatrix} . \tag{4.32}$$

By definition, each eigenmode propagates through the crystal without changing its state and, on the other hand, for a semi-infinite crystal, there is no rear surface to reflect the forward into backward Bloch waves. Therefore, the appropriate boundary condition for the scattering problem of an acoustic wave incident on a semi-infinite phononic crystal from the homogeneous host material that extends to infinity is $\mathbf{V}^- = 0$ [84]. Therefore

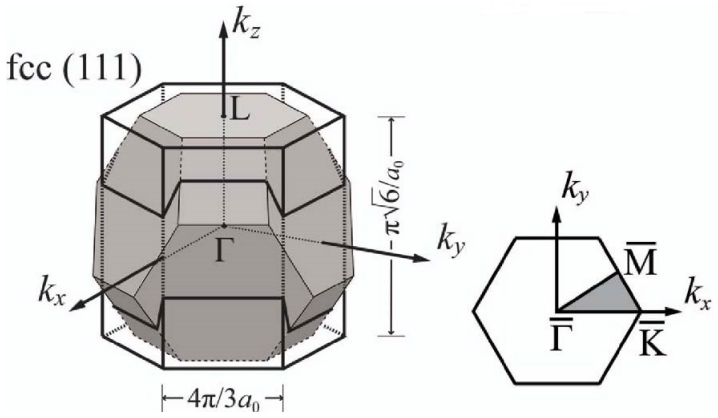

Figure 4.4: The reduced **k** zone associated with the *fcc* (111) crystallographic plane (left panel) and the corresponding SBZ (right panel). The (bulk) *fcc* Brillouin zone (shaded tetradecahedron) is also shown for comparison.

Eq. (4.32) yields

$$\mathbf{u}_0^- = \mathbf{F}^{-+}[\mathbf{F}^{++}]^{-1}\mathbf{u}_0^+ \equiv \mathbf{R}_\infty \mathbf{u}_0^+ \ . \tag{4.33}$$

On the other hand, the condition for the occurrence of surface states translates to the existence of non-zero forward Bloch modes ($\mathbf{V}^+ \neq 0$) in the absence of incoming field ($\mathbf{u}_0^+ = 0$) [85, 86]. Then Eq. (4.32) gives $\mathbf{F}^{++}\mathbf{V}^+ \equiv \mathbf{u}_0^+ = 0$, which is satisfied when $\det[\mathbf{F}^{++}] = 0$.

Chapter 5

Phononic crystals of poroelastic spheres

In this chapter we demonstrate the applicability of the LMS method for phononic crystals of poroelastic spheres on two specific examples, namely close-packed *fcc* crystals of porous silica [80] and polymer spheres immersed in water [81]. From another point of view, and indeed in a different perspective, these crystals can be considered as double-porosity granular materials.

5.1 Close-packed periodic structures of porous silica spheres

In the present section, we shall consider water-saturated porous silica as poroelastic material, in which case the values of the relevant parameters of the solid (denoted by an index s) and fluid (denoted by an index f), which coincides with the host (denoted by an index h), materials involved are: mass density $\rho_s = 2200$ kg m^{-3}, longitudinal wave velocity $c_l = \sqrt{(K_s + 4\mu_s/3)/\rho_s} = 5970$ m s^{-1}, transverse wave velocity $c_t = \sqrt{\mu_s/\rho_s} = 3760$ m s^{-1}, for silica; and mass density $\rho_f = 1000$ kg m^{-3}, (longitudinal) wave velocity $c_f = \sqrt{K_f/\rho_f} = 1480$ m s^{-1}, and fluid viscosity $\eta = 10^{-3}$ Pa s, for water. The elastic moduli of the bare skeletal frame, K_b and μ_b, can be experimentally measured independently. However, since there are no experimental data available, following Kargl and Lim [42], we evaluate them using Berryman's self-consistent effective medium theory for a silica-void elastic composite, assuming that the pores are modeled by randomly distributed needles, as appropriate for the low-porosity limit that will concern us here [78]. For $f = 10\%$ we find $K_b = 28.9$ GPa and $\mu_b = 23.8$ GPa. Accordingly, the tortuosity is given by $\xi = f^{-2/3}$, for a random array of needles [59].

We consider an *fcc* structure, with lattice constant a, of close-packed porous silica spheres immersed in water and view the crystal structure as a sequence of (111) crystallo-

graphic planes. In each plane, the spheres are arranged on an hexagonal lattice with lattice constant $a_0 = a\sqrt{2}/2$ while consecutive planes are separated by a distance $d = a_0\sqrt{6}/3$. We assume that the spheres have a radius $S = a_0/2 = 2.5$ μm. Such mesoporous and macroporous microspheres can be easily synthesized in the laboratory and are promising candidates for diverse applications in many areas ranging from chromatography and catalysis to biology, drug delivery, and medicine [87–95].

We study the acoustic response and phononic eigenmodes of this crystal by means of full elastodynamic calculations using the LMS method, developed in Chapter 4, which is ideally suited for the case under consideration. Besides the complex phononic band structure of the infinite crystal [see Eq. (4.31)], the method allows one to calculate, also, the transmittance ($\mathcal{T}$), reflectance ($\mathcal{R}$), and absorbance ($\mathcal{A} = 1 - \mathcal{T} - \mathcal{R}$) of a finite slab of the crystal at any angle of incidence [see Eqs. (4.24), (4.25)] and, in this respect, it can describe an actual acoustic transmission experiment. Another advantage of the method is that it solves the elastodynamic equations in the frequency domain and, therefore, it can treat dispersion and viscous losses, which naturally occur in poroelastic materials, in a straightforward manner. The properties of the individual poroelastic scatterers enter only through the corresponding T matrix, explicit expression for which are derived in Chapter 3. We recall that, a region of frequency where propagating waves do not exist, for given $\mathbf{k}_\parallel$, constitutes a frequency gap of the acoustic field, for this $\mathbf{k}_\parallel$. If over a frequency region no propagating wave exists whatever the value of $\mathbf{k}_\parallel$, then this region constitutes an absolute frequency gap. In order to ensure good convergence in our calculations, it is sufficient to truncate the spherical-wave expansions at $\ell_{\max} = 8$ and take into account 37 two-dimensional reciprocal lattice vectors in the relevant plane-wave expansions [24], in all cases we examine here.

In Fig. 5.1, we display the calculated transmission and absorption spectra of an eight-layers-thick (111) slab of the crystal under consideration, at normal incidence, for given porosity $f = 10\%$ but different pore sizes. As we already mentioned in § 3.4, in Biot's theory there are two distinct limits. In the small pore-size limit with respect to the viscous skin depth $\delta = \sqrt{2\eta/(\Omega\rho_f)}$ [see Fig. 5.1(a)], within the considered range of frequencies, Poiseuille flow occurs. Locking of fluid and solid motion arises from the fluid viscosity and results in propagation of a fast wave while the out-of-phase relative motion of the solid frame and infiltrated liquid, required for slow wave propagation, cannot be efficiently realized. In this regime, the porous material behaves as a homogeneous medium with effective elastic parameters that can be calculated using the self-consistent effective-medium theory of Berryman for elastic composites [78]. Nevertheless, also in this case, the absorptive losses are associated with the slow wave modes and cannot be accounted for by effective-medium theory, even when retaining the energy dissipation mechanism by attributing a shear modulus $\mu_f = -\mathrm{i}\Omega\eta$ to the fluid component. Since there is no significant difference to the final results of the effective-medium calculations with and without losses in the frequency range studied, we neglect, for convenience, the viscosity of water so all effective

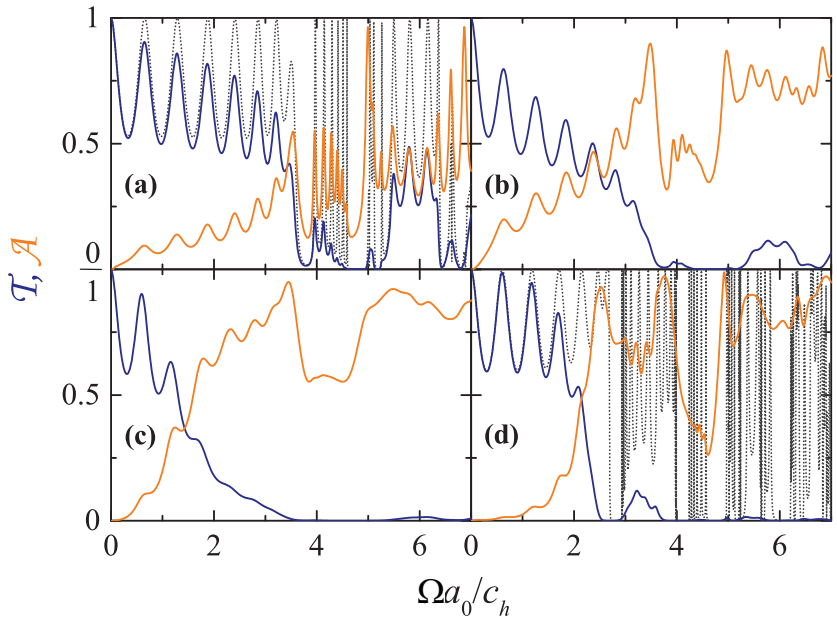

Figure 5.1: Transmittance and absorbance of an acoustic plane wave incident normally on a slab consisting of eight *fcc* (111) planes of submerged water-saturated close-packed porous silica spheres of radius $S = 2.5$ μm, with porosity $f = 10\%$, for different pore sizes: $R_p = 10$ nm (a), $R_p = 30$ nm (b), $R_p = 100$ nm (c), and $R_p = 500$ nm (d). The dotted lines in diagrams (a) and (d) display the corresponding transmission spectra for crystals made of homogeneous spheres with elastic parameters calculated using self-consistent effective-medium theory for (lossless) composite elastic media [78] and of water-saturated porous spheres neglecting viscous losses ($\eta = 0$), respectively.

material parameters are dispersionless and real valued. We obtain: $\overline{\rho} = 2080$ kg m^{-3}, $\overline{c_l} = 5449$ m s^{-1}, $\overline{c_t} = 3389$ m s^{-1}. It is interesting to note that frictional dissipation due to the slow waves is in this case much larger than in the corresponding single sphere ($\sigma_{\rm abs}$ is very small) due to multiple-scattering effects. As the pore size increases, the out-of-phase relative motion of the solid and fluid is not impeded by viscous drag so that the slow waves can propagate, giving rise to enhanced absorptive losses and consequent drastic drop of the transmittance [see Figs. 5.1(b) and (c)]. On the other hand, for very large pores, if the viscous skin depth is negligible with respect to the pore size, the three density parameters in Eqs. (2.20) and (2.23) become real and all three bulk modes become nondispersive and attenuation free, as one would have in the absence of viscous losses ($\eta = 0$). This trend can be clearly seen in Fig. 5.1(d). In this regime Poiseuille flow is not established and fast wave propagation is driven by inertial coupling which locks the solid and fluid components

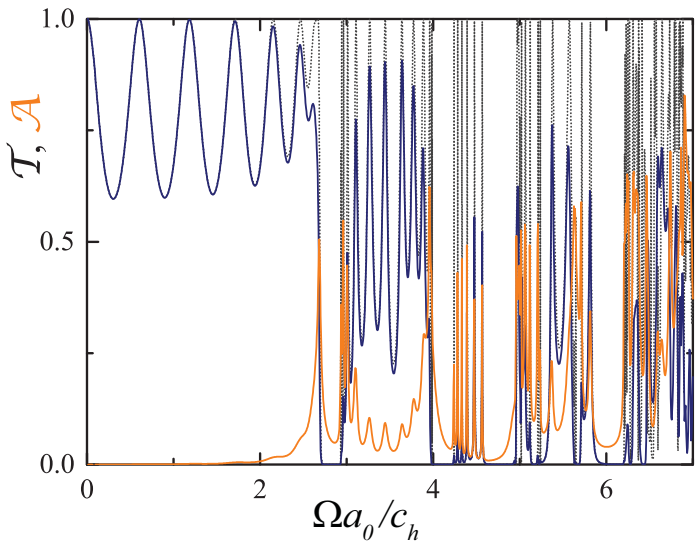

Figure 5.2: The same as in Fig. 5.1(d) for spheres of porosity $f = 10\%$ but of radius $S = 2.5$ mm and pore radius $R_p = 500$ μm.

together. It becomes clear from the above that porous silica nanoparticles, immersed in a water-like liquid, at hypersonic (GHz) frequencies are in the viscous coupling regime. This explains why, treating such particles as effectively homogeneous with elastic parameters smaller than those of pure solid silica, one can successfully explain BLS experiments on corresponding colloidal crystals [18].

We can approach more closely the inertial coupling limit if we increase all characteristic length parameters of the system by a factor of t, i.e. $R_p \to tR_p$, $S \to tS$, $a \to ta$, in which case the viscous-length-to-porous-size ratio decreases by a factor of $\sqrt{t}$ ($\frac{\delta}{R_p} \to \frac{1}{\sqrt{t}}\frac{\delta}{R_p}$) in the same region of reduced frequency $\Omega a_0/c_h$. For example, it can be seen in Fig. 5.2 that for submerged water-saturated close-packed porous silica spheres of radius $S = 2.5$ mm, porosity $f = 10\%$, and pore radius $R_p = 500$ μm, the transmission spectrum is very similar to that of the corresponding lossless case ($\eta = 0$) while the absorbance is overall strongly suppressed and exhibits sharp peaks only at the resonances where the wavefield is predominantly localized at the spheres.

The transmission spectra of the reference lossless structures in the viscous and inertial coupling regimes, shown by dotted lines in Fig. 5.1(a), (d) and replotted in Figs. 5.3(c) and 5.4(c), can be interpreted in conjunction with relevant dispersion diagrams for the corresponding infinite crystals, depicted in Figs. 5.3(b) and 5.4(b), respectively. We note that in these lossless cases there is no characteristic length scale in the problem, the results apply to different regions of frequency provided that the dimensions of the structural units are

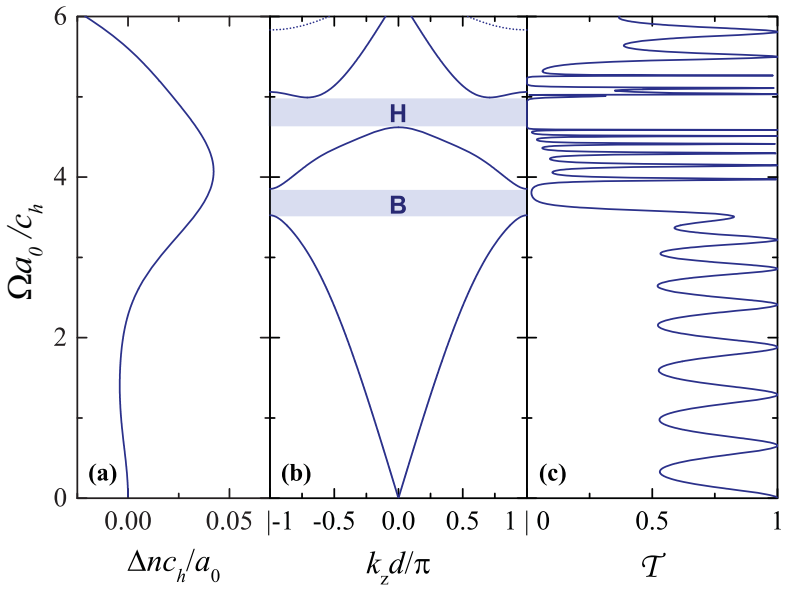

Figure 5.3: (a) Change in the density of states of the acoustic field induced by a submerged water-saturated porous silica sphere with porosity $f = 10\%$, treated as a lossless homogeneous sphere with elastic parameters calculated using self-consistent effective-medium theory for composite elastic media [78]. (b) The phononic band structure of an *fcc* crystal of such close-packed homogeneous spheres, in water, along the [111] direction. Solid (dotted) lines refer to nondegenerate (doubly degenerate) bands of Λ_1 (Λ_3) symmetry. The shaded areas mark the Bragg (B) and hybridization (H) gaps. (c) Transmittance of an acoustic plane wave incident normally on a (111) slab of this crystal, eight-layers thick.

scaled accordingly. That is why we choose to represent our results using $\Omega a_0/c_h$ as dimensionless frequency. It can be seen that the transmittance exhibits Fabry-Perot oscillations in regions of acoustically active bands, due to multiple reflections at the surfaces of the slab, and drops down to small values outside these regions. The phononic band structure of these crystals can be understood as follows. An extended acoustic band, that would be in a corresponding effective homogeneous medium, is folded within the first Brillouin zone as a result of structure periodicity and Bragg gaps open up at the zone boundaries. In addition, there are narrow bands originating from localized modes of the individual spheres, weakly interacting between them. These modes are manifested as resonance peaks in the corresponding density of states, as shown in Figs. 5.3(a) and 5.4(a). When bands of the same symmetry cross each other, a band gap, so-called hybridization gap, opens up about the crossing point due to level repulsion. The bands along the *fcc* [111] direction have the symmetry of the irreducible representations of the C_{3v} point group [96]. Therefore they

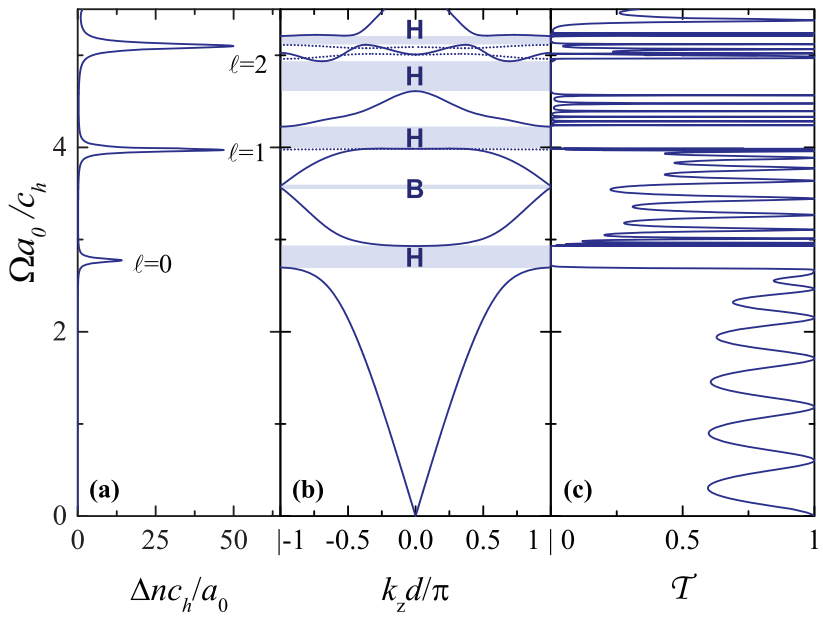

Figure 5.4: The same as Fig. 5.3 but for submerged water-saturated porous silica spheres described by Biot's theory, ignoring viscous losses ($\eta = 0$). The peaks in (a) correspond to resonances of given multipole order ℓ denoted in the diagram.

are either nondegenerate, if they have the Λ_1 or the Λ_2 symmetry, or doubly degenerate if they have the Λ_3 symmetry. Only the Λ_1 bands are acoustically active in the sense that they can be excited by an acoustic plane wave with appropriate frequency incident normally on a (111) slab of the crystal because they have the proper symmetry [97]. It is expected that strong absorption will appear in band regions with large admixture of modes localized in and about the spheres when the dissipation mechanism triggered by the slow waves in the porous material is switched on. It can be seen that this is the case, for example, in the flat band regions originating from the multipole resonances of the spheres (see Fig. 5.4), where high absorption is attained as shown in Fig. 5.1(d).

The above porous-based phononic crystal exhibits interesting absorptive properties and can be used as an efficient filter through an appropriate selection not only of the pore size, but also of the porosity level. In Fig. 5.5 we show the transmittance, absorbance, and reflectance of an acoustic plane wave incident normally on a slab of this crystal, consisting of eight *fcc* (111) layers, for different pore sizes R_p, as a function of the porosity f. Broadband high-level absorbance can be attained for rather intermediate values of the ratio R_p/δ ($R_p = 100$ nm) and relatively low porosity values, varying from $f = 10\%$ to 25%. The porosity f, as an additional degree of freedom, can be chosen to achieve for rather moderate R_p/δ the appearance of regions of frequency where both the transmittance and

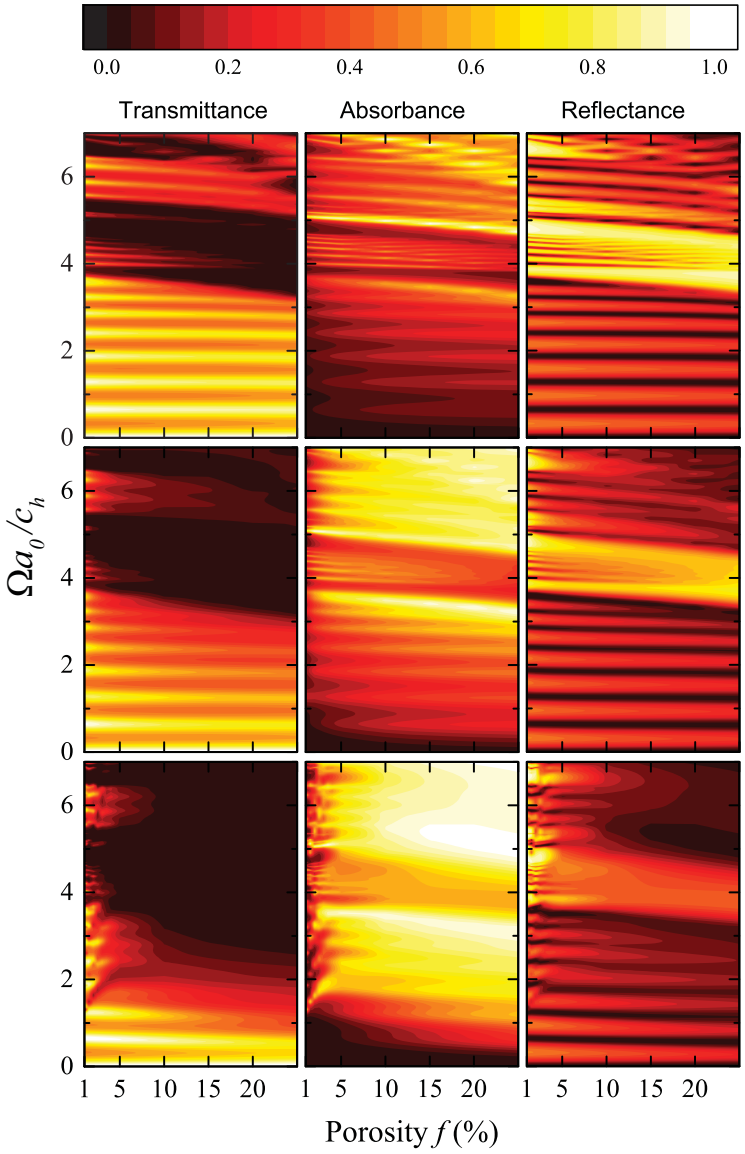

Figure 5.5: Transmittance, absorbance and reflectance of an acoustic plane wave incident normally on a slab consisting of eight *fcc* (111) planes of submerged water-saturated close-packed porous silica spheres, of radius $S = 2.5$ μm, versus the porosity f, for different pore sizes. Pore radius (from top to bottom): $R_p = 10$, 30, and 100 nm.

reflectance practically vanish, leading to $\mathcal{A} \simeq 1$. It is interesting to note that broadband acoustic isolation occurs not only for waves incident normally but also at an angle on a slab

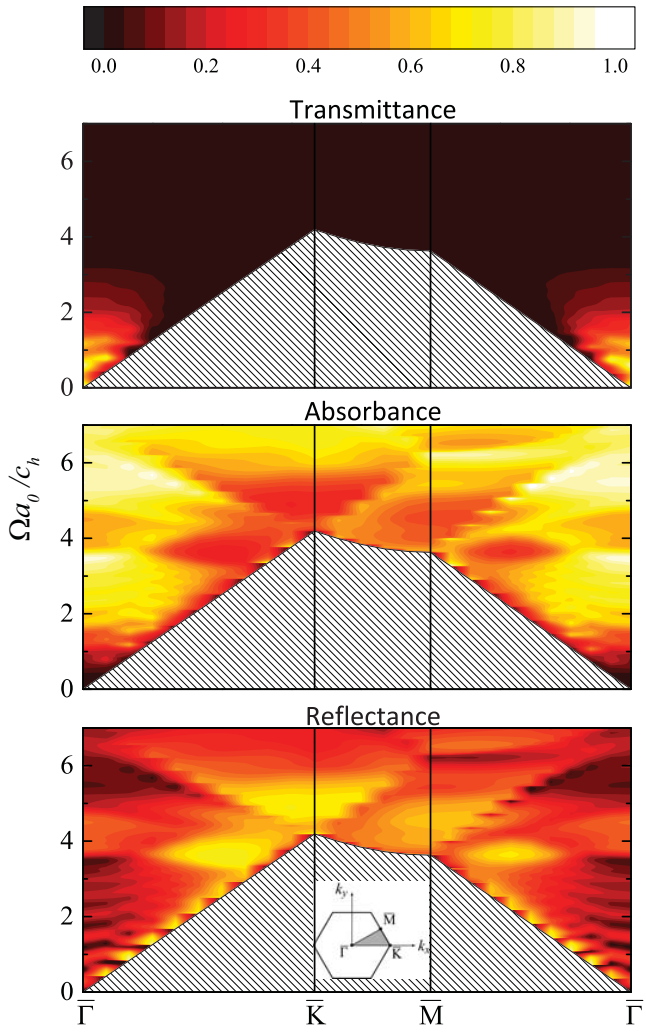

Figure 5.6: Transmittance, absorbance, and reflectance of an acoustic plane wave incident on a slab consisting of eight *fcc* (111) planes of submerged water-saturated close-packed porous silica spheres ($S = 2.5$ μm, $f = 10\%$, and $R_p = 100$ nm) with $\mathbf{k}_\parallel$ along high symmetry lines of the *fcc* (111) surface Brillouin zone, shown in the inset. $\overline{\Gamma}$: $\mathbf{k}_\parallel = \frac{2\pi}{a_0}(0,0)$, $\overline{\mathrm{K}}$: $\mathbf{k}_\parallel = \frac{2\pi}{a_0}\left(\frac{2}{3},0\right)$, $\overline{\mathrm{M}}$: $\mathbf{k}_\parallel = \frac{2\pi}{a_0}\left(\frac{1}{2},\frac{\sqrt{3}}{6}\right)$.

of the material. This is shown in Fig. 5.6, which displays the variation of the transmission spectra of an eight-layers-thick *fcc* (111) slab of submerged water-saturated close-packed porous silica spheres, with $S = 2.5$ μm, $f = 10\%$, and $R_p = 100$ nm, for different $\mathbf{k}_\parallel$ along

high symmetry lines of the *fcc* (111) surface Brillouin zone. The direction of incidence is specified by the corresponding polar and azimuthal angles, $\theta = \arccos\left(\sqrt{1 - c_h^2 k_\parallel^2/\Omega^2}\right)$ and $\phi = \arctan(k_y/k_x)$, respectively. Obviously, at given $\mathbf{k}_\parallel$, propagating incident waves exist above an angular frequency threshold $\Omega_{inf} = c_h|\mathbf{k}_\parallel|$ (delimiting the hatched area in Fig. 5.6). It can be seen (and we verified it for other arbitrary points $\mathbf{k}_\parallel$ within the surface Brillouin zone as well) that, above $\Omega a_0/c_h \simeq 2$, the transmittance practically vanishes, whatever the direction of incidence.

In summary, we applied the LMS method for phononic crystals of poroelastic spheres immersed in a fluid medium to close-packed *fcc* crystals of submerged water-saturated meso- and macroporous silica microspheres, encompassing the viscous and inertial coupling regimes. It is worth noting that our formalism remains invariant under a transformation $\Omega \to \xi\Omega$ and $R_p \to R_p/\xi$, $S \to S/\xi$, $a \to a/\xi$, $\eta \to \eta/\xi$, where ξ is an arbitrary constant factor. Therefore, the results obtained here apply to different regions of frequency of the acoustic field, provided that all size parameters as well as the viscosity coefficient are scaled accordingly. Our results are analyzed by reference to phononic dispersion diagrams, appropriate to the viscous and inertial coupling limits, in conjunction with corresponding transmission spectra, providing a consistent interpretation of the underlying physics. For intermediate pore sizes, it is shown that, with increasing porosity, strong absorption leads to negligible transmission over an extended frequency range, which might be useful for broadband acoustic shielding applications. Our results corroborate that these novel phononic crystals of porous building units exhibit unprecedented properties driven by the slow longitudinal waves, which are unique to poroelastic materials, and multiple scattering effects. These structures cannot be described by treating the poroelastic material as an effective homogeneous medium and rigorous methods based on Biot's theory, such as that developed in the present thesis, are required.

5.2 Double porosity granular polymers

In this section we report a thorough theoretical study of the acoustic properties of a specific water-saturated double-porosity granular polymeric structure consisting of close-packed porous polystyrene spheres, with porosity f and radius $S = a_0/2 = 2.5$ mm, in the [111] *fcc* stacking. This is the same geometry as that described in section 5.1. We recall that $a_0 = a\sqrt{2}/2$ is the lattice constant and $d = a_0\sqrt{6}/3$ the distance between consecutive lattice planes. The values of the relevant parameters of the solid material (polystyrene) are: $\rho_s = 1050$ kg m^{-3}, $c_l = \sqrt{(K_s + 4\mu_s/3)/\rho_s} = 2350$ m s^{-1}, $c_t = \sqrt{\mu_s/\rho_s} = 1200$ m s^{-1}, and we use the same values as in section 5.1 for water. We calculate the elastic moduli of the bare skeletal frame in the same way as in the previous section, using Berryman's self-consistent effective medium theory for a polystyrene/void elastic composite, and for $f = 10\%$ that we will consider in our study, and find $K_b = 2.602$ GPa and $\mu_b = 1.186$ GPa.

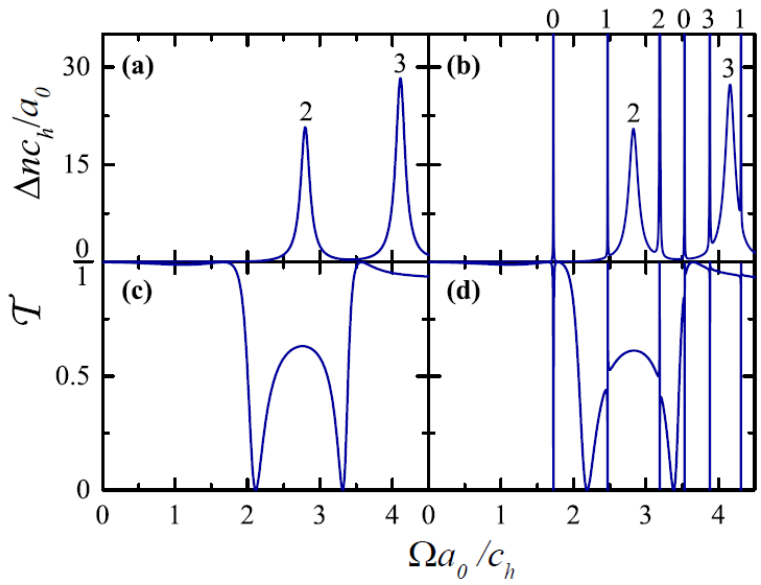

Figure 5.7: (Upper diagrams) Change in the density of states of the acoustic field [Eq. (3.61)] induced by a submerged water-saturated porous polystyrene sphere, with porosity $f = 10\%$, (a) treated as a lossless homogeneous sphere with elastic parameters evaluated using self-consistent effective-medium theory for composite elastic media [58,78] and (b) described by Biot's theory, ignoring viscous losses ($\eta = 0$). The peaks in (a) and (b) correspond to resonances of given multipole order, ℓ, denoted in the diagrams. (Lower diagrams) Transmittance of an acoustic plane wave [Eq. (4.24)] incident normally on an hexagonal array, i.e, a single *fcc* (111) plane, of the above spheres. In (c) and (d) the spheres are described as in (a) and (b), respectively.

Accordingly, the tortuosity is given by $\xi = f^{-2/3}$, for a random array of needles [59]. Our numerical calculations are carried out by the LMS method, where we truncated the spherical-wave expansions at $\ell_{max} = 7$ and took into account 43 2D reciprocal lattice vectors in the relevant plane-wave expansions, thus ensuring good convergence in all cases examined.

The change in the density of states of the acoustic field induced by a submerged water-saturated porous polystyrene sphere and the acoustic transmission spectrum of a 2D hexagonal array of such close-packed spheres, at normal incidence, in the two distinct limits ($\delta \ll R_p$ and $\delta \gg R_p$) discussed in the previous section are depicted in Fig. 5.7. It can be seen that resonance peaks appear in the density of states. Their presence is explained as follows. The eigenmodes of the acoustic field in the case of a single sphere, i.e., solutions of Eq. (3.5) in the absence of an incident field, are obtained at the poles of the scattering T

matrix. Besides the torsional bound states with real eigenfrequencies, which are confined in the sphere and cannot be excited by an externally incident wave [see Eq. (3.37)], there are resonant modes at the poles of the T matrix in the lower complex frequency half-plane, near the real axis, at $z_\ell = \Omega_\ell - \mathrm{i}\gamma_\ell$; Ω_ℓ is the eigenfrequency while γ_ℓ denotes the inverse of the lifetime of the respective 2^ℓ-pole resonant mode. The corresponding change in the density of states can be deduced from Eq. (3.61) through a Laurent expansion in the vicinity of z_ℓ on the real axis, which yields $\Delta n_\ell(\Omega) \simeq \frac{(2\ell+1)}{\pi}\gamma_\ell/[(\Omega-\Omega_\ell)^2+\gamma_\ell^2]$, i.e., the change of the partial density of states, $\Delta n_\ell(\Omega)$, is a lorentzian centered at Ω_ℓ with a half width at half maximum equal to γ_ℓ. These resonant modes, when the spheres are assembled in a 2D lattice, form bands $\Omega_\nu(\mathbf{k}_\parallel)$, $\nu = 1, 2, \ldots$ of corresponding collective modes of the plane. In our case, at $\mathbf{k}_\parallel = 0$, the hexagonal symmetry of the structure implies that there will be a partial lift of the $(2\ell+1)$-fold degeneracy of the resonant modes of the individual spheres and the corresponding modes of the plane will have the symmetry of the irreducible representations of the C_{6v} point group: $L_1, L_{1'}, L_2, L_{2'}$ (one-dimensional) and $L_3, L_{3'}$ (two-dimensional) [96]. Therefore they will be either nondegenerate or doubly degenerate, respectively. We note that only the L_1 modes are acoustically active in the sense that they can be excited by an acoustic plane wave with appropriate frequency incident normally on the given plane, because they have the proper symmetry [97], and manifest themselves as resonance structures in the corresponding transmission spectrum. The acoustically inactive, so-called *deaf*, modes are bound states with infinite lifetime, confined in the plane, and cannot be excited by an externally incident wave. However, for $\mathbf{k}_\parallel \neq 0$ a general non-high-symmetry point, all modes belong to the identity representation of the trivial group and, therefore, are acoustically active.

$O(3)$	$\ell = 0$	$\ell = 1$	$\ell = 2$	$\ell = 3$
C_{6v}	L_1	$L_1\ L_{3'}$	$L_1\ L_3\ L_{3'}$	$L_1\ L_2\ L_{2'}\ L_3\ L_{3'}$
C_{3v}	Λ_1	$\Lambda_1\ \Lambda_{3'}$	$\Lambda_1\ \Lambda_3\ \Lambda_{3'}$	$\Lambda_1\ \Lambda_2\ \Lambda_{2'}\ \Lambda_3\ \Lambda_{3'}$

Table 5.1: Compatibility relations between irreducible representations of the $O(3)$, C_{6v}, and C_{3v} point symmetry groups.

As shown in Figs. 5.7(a) and (c), in the viscous-coupling limit, we obtain the typical acoustic response of non-porous polymer spheres characterized by well-formed resonances, which originate from the spheroidal modes of the individual particles [see Eq. (3.46)] and move to lower frequencies with increasing porosity. On the contrary, in the inertial-coupling limit, interestingly, additional very sharp resonances appear in the transmission spectrum of an hexagonal array, i.e., a single *fcc* (111) plane, of submerged water-saturated close-packed porous polystyrene spheres, with porosity $f = 10\%$, as can be seen in Fig. 5.7(d). These resonances stem from corresponding single-particle modes [see

Fig. 5.7(b)] with a very long lifetime, which are strongly localized in the spheres and have a predominant character of slow longitudinal waves. Therefore these modes, which are pushed up to higher frequencies with increasing porosity, should be unambiguously ascribed to the existence of slow longitudinal waves in the poroelastic particles. As expected from a group-theory analysis [96], each sphere mode of $\ell = 0, 1, 2, 3$ gives one acoustically active L_1 mode of the given planar array for $\mathbf{k}_\parallel = 0$, as can be seen in Fig. 5.7. In addition, there are acoustically inactive plane modes of different symmetry, as implied from the appropriate compatibility relations (see Table 5.1).

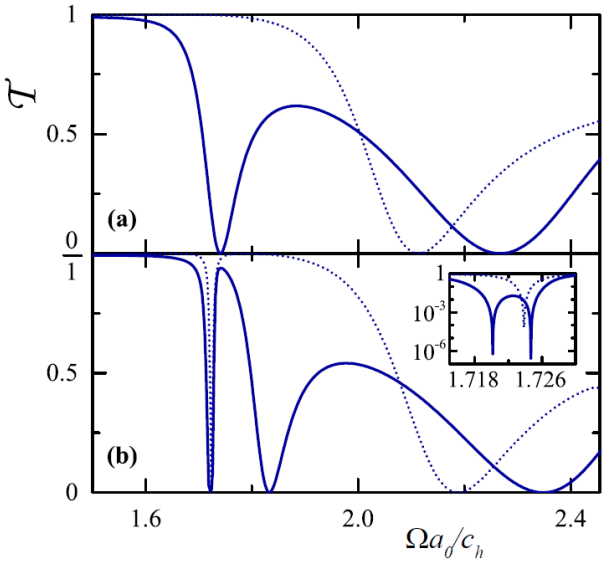

Figure 5.8: Transmittance of an acoustic plane wave incident normally on a bilayer of consecutive *fcc* (111) planes of submerged water-saturated close-packed porous polystyrene spheres, with porosity $f = 10\%$, (a) treated as lossless homogeneous spheres with elastic parameters calculated using self-consistent effective-medium theory for composite elastic media [78, 79] and (b) described by Biot's theory, ignoring viscous losses ($\eta = 0$). The dotted lines in (a) and (b) display the corresponding transmission spectra for a single *fcc* (111) plane of such spheres. The inset to (b) shows an enlarged view about the sharp resonances in the low frequency part of the spectrum, in logarithmic scale.

In the case of a pair of two consecutive *fcc* (111) planes of the spheres under consideration, for given $\mathbf{k}_\parallel$, each plane mode gives rise to two modes due to interlayer coupling, by analogy to the formation of bonding and antibonding orbitals of a diatomic molecule from the corresponding electronic states of the individual atoms, as depicted in Fig. 5.8 for $\mathbf{k}_\parallel = 0$. By the same token, stacking consecutive hexagonal arrays so as to grow an

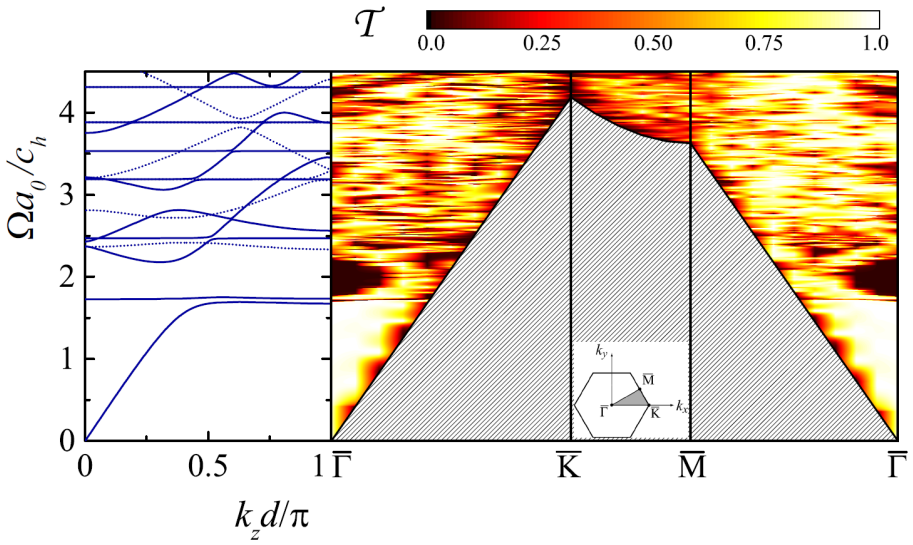

Figure 5.9: (Left-hand diagram) Phononic dispersion diagram of an *fcc* crystal of submerged water-saturated close-packed porous polystyrene spheres, with porosity $f = 10\%$, described by Biot's theory without viscous losses ($\eta = 0$), along the [111] direction. (Right-hand diagram) Transmittance of an acoustic plane wave incident on a (111) slab of this crystal, eight-layer-thick, with $\mathbf{k}_\parallel$ along the high-symmetry lines of the corresponding SBZ, shown in the inset. $\overline{\Gamma}$: $\mathbf{k}_\parallel = \frac{2\pi}{a_0}(0,0)$, $\overline{\mathrm{K}}$: $\mathbf{k}_\parallel = \frac{2\pi}{a_0}(\frac{2}{3},0)$, $\overline{\mathrm{M}}$: $\mathbf{k}_\parallel = \frac{2\pi}{a_0}(\frac{1}{2},\frac{\sqrt{3}}{6})$. The direction of incidence is specified by the corresponding polar and azimuthal angles, $\theta = \arccos\left(\sqrt{1 - c_h^2 k_\parallel^2/\Omega^2}\right)$ and $\phi = \arctan(k_y/k_x)$, respectively. Obviously, at given $\mathbf{k}_\parallel$, propagating incident waves exist above an angular frequency threshold $\Omega_{inf} = c_h|\mathbf{k}_\parallel|$ (hatched area).

infinite *fcc* crystal of submerged water-saturated close-packed porous polystyrene spheres, the modes of the individual planes will form corresponding bands. These are the narrow bands appearing in the left-hand diagram of Fig. 5.9. For $\mathbf{k}_\parallel = 0$ the bands have the symmetry of the irreducible representations of the C_{3v} point group [96]. Therefore they are either nondegenerate, if they have the Λ_1 or the Λ_2 symmetry, or doubly degenerate if they have the Λ_3 symmetry. We note that only the Λ_1 bands are acoustically active in the sense that they can be excited by an acoustic plane wave with appropriate frequency incident normally on a (111) slab of the crystal, which is then transmitted through the slab, because they have the proper symmetry [97]. In addition to the above relatively narrow bands, there is an extended acoustic band, of Λ_1 symmetry, which would be in a corresponding effective homogeneous medium, folded within the first Brillouin zone be-

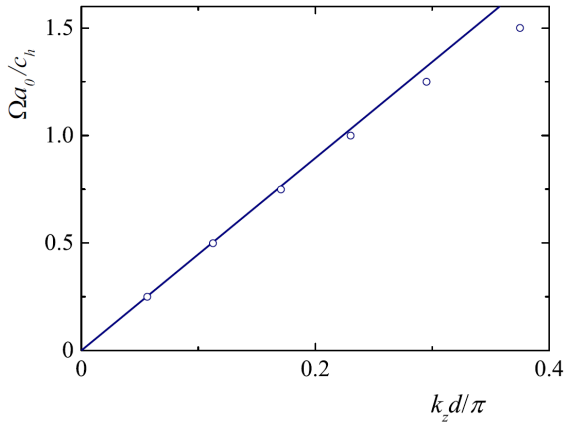

Figure 5.10: An enlarged view of the left-hand diagram of Fig. 5.9 in the long-wavelength limit (symbols). The solid line shows the linear dispersion curve with slope $\bar{c}$ calculated by Eq. (E.10).

cause of structure periodicity, with Bragg gaps appearing at the zone boundaries, as we already mentioned in § 5.1. Besides the Bragg gaps, when the extended acoustic band crosses a narrow band of the same symmetry, level repulsion leads, also, to the opening of a frequency gap about the crossing point, so-called *hybridization gap*. Such a relatively wide hybridization gap appears, e.g., in the dispersion diagram, obtained by solving the eigenvalue problem (4.31), displayed in Fig. 5.9 about $\Omega a_0/c_h = 2$ for $\mathbf{k}_{\|} = 0$. However, as can be seen in Fig. 5.9, this gap is not omnidirectional. It progressively shrinks as we deviate from $\mathbf{k}_{\|} = 0$ and finally closes thus allowing for acoustic transmission through a finite slab of the crystal.

It is worth noting that specific features of the phononic band structure depicted in Fig. 5.9, such as anisotropy, flat bands and frequency gaps driven by coherent multiple scattering, cannot be accounted for by any local effective-medium theory for double-porosity media. These theories are valid when the wavelength is much longer than the size of the representative elementary volume and describe the composite medium in terms of effective quantities. For example, the model of Berryman and Wang [66,67], in the absence of viscous losses ($\eta = 0$) as appropriate for the case under consideration in Fig. 5.9, predicts the existence of one transverse and three longitudinal acoustic waves with frequency-independent propagation velocities. This model assumes a fluid-saturated double-porosity medium consisting of a porous matrix with fractures, where each of the three components, i.e., solid skeletal frame, matrix pores, and adjacent fractures, forms a percolating network. Therefore, there are indeed one transverse wave propagating in the solid frame and three hybrid longitudinal waves, which arise from the corresponding propagating modes

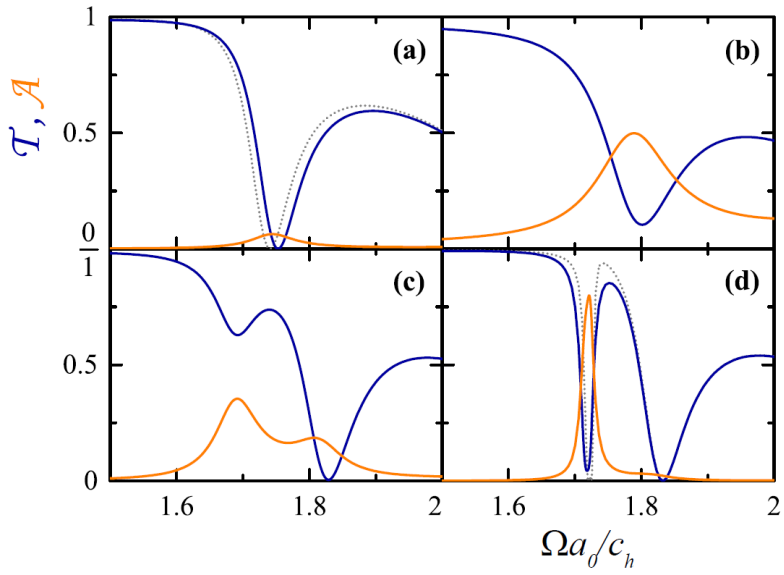

Figure 5.11: Transmittance and absorbance of an acoustic plane wave incident normally on bilayer of consecutive *fcc* (111) planes of submerged water-saturated close-packed porous polystyrene spheres of radius $S = 2.5$ mm, with porosity $f = 10\%$, for different pore sizes: $R_p = 500$ nm (a), $R_p = 5$ μm (b), $R_p = 50$ μm (c), and $R_p = 500$ μm (d). The dotted lines in (a) and (d) display the corresponding transmission spectra for homogeneous spheres with elastic parameters calculated using self-consistent effective-medium theory for (lossless) composite elastic media [78,79] and for water-saturated porous spheres described by Biot's theory, neglecting viscous losses ($\eta = 0$), respectively.

in the above three components interacting between them. In our case of unconsolidated porous polymer grains, the continuous network topology of the solid frame and the matrix pores is broken, and thus only the longitudinal acoustic wave propagating in the fluid-filled fractures will survive. The propagation velocity, $\bar{c}$, of this wave in the particular morphology of the granular double-porosity medium that concerns us here (and corresponds to vanishing elastic moduli of the solid skeletal frame [43]) can be deduced from the model of Berryman and Wang [66,67] (see Appendix E). As shown in Fig. 5.10, $\bar{c}$, evaluated by Eq. (E.10), is in excellent agreement with the slope of the dispersion curve obtained by our LMS calculations in the long-wavelength limit.

Viscous losses are described by Biot's theory [25,26], which properly combines both mechanical and hydrodynamic properties of a composite comprising a porous elastic medium filled with a viscous fluid. Strong absorption is expected in frequency regions where resonant modes localized in the spheres exist, especially if these modes have strong ad-

mixture of slow longitudinal waves, which correspond to an out-of-phase relative motion of the solid frame and infiltrated liquid in the porous material. As a typical example, in Fig. 5.11 we display the evolution of the absorption spectrum of a bilayer of consecutive *fcc* (111) planes of submerged water-saturated close-packed porous polystyrene spheres of radius $S = 2.5$ mm, with porosity $f = 10\%$, for different pore sizes, in the frequency region of the first resonant modes. For narrow pores ($R_p = 500$ nm), we are in the viscous-coupling regime where slow longitudinal waves are not efficiently excited and thus a very weak absorption band is observed at the resonance which originates from the quadrupole spheroidal-like particle modes [see Fig. 5.11(a)]. As the pore radius increases, the slow-wave component of these modes is clearly manifested in a stronger absorption peak, which becomes prominent at $R_p = 5$ μm [see Fig. 5.11(b)]. By further increasing the pore radius well beyond the viscous length, which is about 2 μm in the frequency region under consideration, the losses associated with the spheroidal-like particle modes are gradually suppressed. At the same time, the sharp particle modes, which have an almost

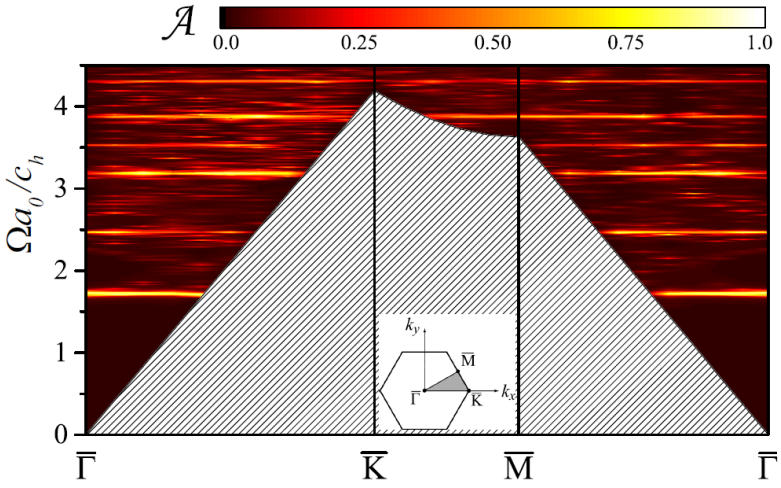

Figure 5.12: Absorbance of an acoustic plane wave incident on a slab consisting of eight *fcc* (111) planes of submerged water-saturated close-packed porous polystyrene spheres ($S = 2.5$ mm, $f = 10\%$, and $R_p = 500$ μm) with $\mathbf{k}_\parallel$ along the high-symmetry lines of the corresponding SBZ, shown in the inset. $\overline{\Gamma} : \mathbf{k}_\parallel = \frac{2\pi}{a_0}(0,0)$, $\overline{\mathrm{K}} : \mathbf{k}_\parallel = \frac{2\pi}{a_0}(\frac{2}{3},0)$, $\overline{\mathrm{M}} : \mathbf{k}_\parallel = \frac{2\pi}{a_0}(\frac{1}{2},\frac{\sqrt{3}}{6})$. The direction of incidence is specified by the corresponding polar and azimuthal angles, $\theta = \arccos\left(\sqrt{1 - c_h^2 k_\parallel^2/\Omega^2}\right)$ and $\phi = \arctan(k_y/k_x)$, respectively. Obviously, at given $\mathbf{k}_\parallel$, propagating incident waves exist above an angular frequency threshold $\Omega_{inf} = c_h|\mathbf{k}_\parallel|$ (hatched area).

exclusively slow-wave character in the spheres, are developed and manifest themselves as strong peaks in the absorption spectrum, as shown in Figs. 5.11(c) and (d) for the lowest monopole mode of this type in the range of frequencies considered. For wide pores, in the inertial-coupling regime, we obtain very narrow and dispersionless bands of strong absorption at the frequencies of these modes in the double-porosity polymeric material under consideration, as shown in Fig. 5.12.

In summary, we reported a thorough theoretical study of the acoustic response of a particular class of double-porosity liquid-saturated granular polymeric material, formed by close-packed porous polymer spheres assembled in an *fcc* lattice, by means of numerical calculations using our LMS method. Calculated transmission and absorption spectra of finite slabs of these materials are analyzed by reference to the acoustic modes of the constituent spheres as well as to the dispersion diagrams of corresponding infinite crystals, providing a consistent interpretation of the observed features. In particular, our results reveal the existence of unprecedented resonant modes with very long lifetime, localized in the spheres, in the inertial-coupling regime, i.e., when the radius of the spheres' pores is much larger than the viscous length. These modes, which can be easily tuned in frequency by adjusting the intrinsic porosity of the spheres, induce narrow dispersionless absorption bands as well as directional gaps in the transmission spectrum of finite slabs of the double-porosity material.

Chapter 6

Brillouin Light Scattering

In this chapter we review some of the basic principles of BLS by lattice vibrations and present a formalism for the calculation of the BLS intensities. Our theoretical formalism, which provides the basis for a rigorous description of the BLS by colloidal phononic crystals, is applied in two cases: a homogeneous fluid and an isolated solid sphere.

6.1 Basic principles of Brillouin light scattering

The spontaneous BLS method is an efficient non-destructive experimental technique to study acoustic phonons in micro- and nanostructures, in the region of upper ultrasounds (frequencies in GHz range). It is based on the interaction of the photons of an incident monochromatic laser beam with the thermally excited acoustic phonons in the structure, which propagate in a specific direction chosen from the scattering geometry. The scattering vector $\mathbf{q} = \mathbf{k}_s - \mathbf{k}_i$ is defined from the wavevectors of the scattered ($\mathbf{k}_s$) and the incident ($\mathbf{k}_i$) photon.

In case of homogeneous and isotropic materials, the law of conservation of momentum dictates the wave number of the phonon, $\mathbf{Q}$, to be equal to the scattering vector $\mathbf{q}$. So the BLS spectrum, for given $\mathbf{q}$, exhibits pairs of peaks originating from the inelastic photon scattering, that change their frequency by $\pm c_l Q$ or $\pm c_t Q$, where c_l, c_t are the propagation velocities of longitudinal and transverse elastic waves, respectively, in the material (see Fig. 6.1). The peaks corresponding to an increase in the photon frequency originate from absorption of one phonon of frequency $\Omega_\nu(Q) = c_\nu Q, \quad \nu = l, t$, and wave vector $\mathbf{Q}$ (anti-Stokes processes), while the peaks corresponding to a decrease in the photon frequency originate from emission of one phonon (Stokes processes). In macroscopic structures of micro- or nanoparticles, the acoustic phonon states exhibit, in general, complicated dispersion relations, which can be identified through BLS experiments.

The physical mechanism causing BLS is the photoelastic effect, which relates the me-

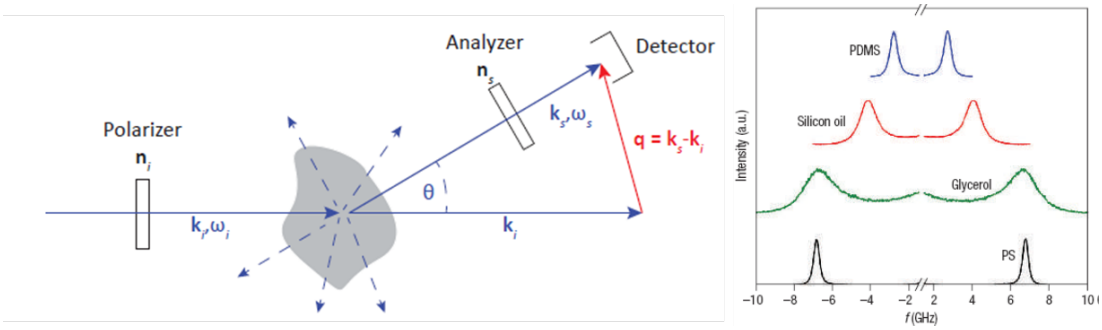

Figure 6.1: Schematic representation of a general BLS experimental setup. An incident laser beam of polarization $\mathbf{n}_i$, frequency ω_i and wave number $\mathbf{k}_i$ is scattered towards all directions. Only scattered light of wave vector $\mathbf{k}_s$ and polarization $\mathbf{n}_s$ arrives at the detector. The scattering vector $\mathbf{q} = \mathbf{k}_s - \mathbf{k}_i$ is defined by the geometry. The right-hand diagram shows some typical examples of BLS spectra for homogeneous fluids and for polystyrene recorded at $q = 0.017$ nm^{-1} [45].

chanical deformations $e_{ik}(\mathbf{r}, t)$, which are formed in a material due to thermally excited elastic waves (phonons), to changes of the dielectric function. In general, for small deformations, we can express the change in the component of the dielectric tensor $\delta\epsilon_{ik}(\mathbf{r}, t)$ linearly with respect to the components of the strain tensor [99]

$$\delta\epsilon_{ik}(\mathbf{r}, t) = \sum_{jl} k_{ikjl} e_{jl}(\mathbf{r}, t). \tag{6.1}$$

The photoelastic coefficients k_{ikjl} are related to the *Pockels elasto-optic* coefficients p_{ikjl}, defined from

$$[\delta\epsilon^{-1}]_{ik} \equiv [\epsilon^{-1}]_{ik} - [\epsilon_r^{-1}]_{ik} = \sum_{jl} p_{ikjl} e_{jl}, \tag{6.2}$$

where $\overleftrightarrow{\boldsymbol{\epsilon}}$ and $\overleftrightarrow{\boldsymbol{\epsilon}}_r$ are the dielectric tensors of the material under mechanical stress and free of stress (reference medium), respectively. Differentiating the tensor identity $\overleftrightarrow{\boldsymbol{\epsilon}}_r^{-1}\overleftrightarrow{\boldsymbol{\epsilon}}_r = \overleftrightarrow{\mathbf{I}}$ we get $\delta\overleftrightarrow{\boldsymbol{\epsilon}}^{-1}\overleftrightarrow{\boldsymbol{\epsilon}}_r + \overleftrightarrow{\boldsymbol{\epsilon}}_r^{-1}\delta\overleftrightarrow{\boldsymbol{\epsilon}} = 0$ and, multiplying from the left with $\overleftrightarrow{\boldsymbol{\epsilon}}_r$, we can write $\delta\overleftrightarrow{\boldsymbol{\epsilon}} = -\overleftrightarrow{\boldsymbol{\epsilon}}_r\delta\overleftrightarrow{\boldsymbol{\epsilon}}^{-1}\overleftrightarrow{\boldsymbol{\epsilon}}_r$. Therefore, using Eq. (6.2), we obtain

$$\begin{aligned} \delta\epsilon_{ik} &= -\sum_{\mu\nu} [\epsilon_r]_{i\mu} [\delta\epsilon^{-1}]_{\mu\nu} [\epsilon_r]_{\nu k} \\ &= -\sum_{\mu\nu jl} [\epsilon_r]_{i\mu} p_{\mu\nu jl} e_{jl} [\epsilon_r]_{\nu k} \,. \end{aligned} \tag{6.3}$$

Comparing Eqs. (6.1) and (6.3), we have

$$k_{ikjl} = -\sum_{\mu\nu}[\epsilon_r]_{i\mu}p_{\mu\nu jl}[\epsilon_r]_{\nu k} \ . \tag{6.4}$$

By making use of tensor inversion operations we obtain

$$\begin{aligned}\sum_{ik}[\epsilon_r^{-1}]_{\alpha i}k_{ikjl}[\epsilon_r^{-1}]_{k\beta} &= -\sum_{ik}\sum_{\mu\nu}[\epsilon_r^{-1}]_{\alpha i}[\epsilon_r]_{i\mu}p_{\mu\nu jl}[\epsilon_r]_{\nu k}[\epsilon_r^{-1}]_{k\beta} \\ &= -\sum_{\mu\nu}\delta_{\alpha\mu}p_{\mu\nu jl}\delta_{\nu\beta} \\ \Rightarrow p_{\alpha\beta jl} &= -\sum_{ik}[\epsilon_r^{-1}]_{\alpha i}k_{ikjl}[\epsilon_r^{-1}]_{k\beta} \ .\end{aligned} \tag{6.5}$$

For isotropic materials, $[\epsilon_r]_{ik} = \delta_{ik}\epsilon_r$ and Eqs. (6.4) and (6.5) reduce to the simpler form

$$k_{ikjl} = -\epsilon_r^2 p_{ikjl}, \qquad p_{ikjl} = -\frac{k_{ikjl}}{\epsilon_r^2} \ . \tag{6.6}$$

It can be shown that the elasto-optic coefficients obey the general permutation symmetry relations

$$p_{ikjl} = p_{kijl}, \quad \text{and} \quad p_{ikjl} = p_{iklj} \ , \tag{6.7}$$

therefore, the notation can be shortened by introducing new collective indices: $1 = (11)$, $2 = (22)$, $3 = (33)$, $4 = (23) = (32)$, $5 = (13) = (31)$, $6 = (12) = (21)$. For isotropic materials, like polycrystalline or amorphous solids and fluids, there are only two independent such coefficients and the tensor $\overleftrightarrow{\mathbf{p}}$ takes the form

$$\overleftrightarrow{\mathbf{p}} = \begin{pmatrix} p_{11} & p_{12} & p_{12} & 0 & 0 & 0 \\ p_{12} & p_{11} & p_{12} & 0 & 0 & 0 \\ p_{12} & p_{12} & p_{11} & 0 & 0 & 0 \\ 0 & 0 & 0 & \dfrac{p_{11}-p_{12}}{2} & 0 & 0 \\ 0 & 0 & 0 & 0 & \dfrac{p_{11}-p_{12}}{2} & 0 \\ 0 & 0 & 0 & 0 & 0 & \dfrac{p_{11}-p_{12}}{2} \end{pmatrix} . \tag{6.8}$$

Therefore, Eq. (6.1), with the help of Eqs. (6.6), (6.8), becomes

$$\delta\overleftrightarrow{\boldsymbol{\epsilon}} = -\epsilon_r^2 \begin{pmatrix} p_{11} & p_{12} & p_{12} & 0 & 0 & 0 \\ p_{12} & p_{11} & p_{12} & 0 & 0 & 0 \\ p_{12} & p_{12} & p_{11} & 0 & 0 & 0 \\ 0 & 0 & 0 & (p_{11}-p_{12})/2 & 0 & 0 \\ 0 & 0 & 0 & 0 & (p_{11}-p_{12})/2 & 0 \\ 0 & 0 & 0 & 0 & 0 & (p_{11}-p_{12})/2 \end{pmatrix} \begin{pmatrix} e_{11} \\ e_{22} \\ e_{33} \\ e_{23} \\ e_{13} \\ e_{12} \end{pmatrix}$$

$$= -\epsilon_r^2 \begin{pmatrix} p_{11}e_{11} + p_{12}e_{22} + p_{12}e_{33} \\ p_{12}e_{11} + p_{11}e_{22} + p_{12}e_{33} \\ p_{12}e_{11} + p_{12}e_{22} + p_{11}e_{33} \\ \dfrac{p_{11}-p_{12}}{2}e_{23} \\ \dfrac{p_{11}-p_{12}}{2}e_{13} \\ \dfrac{p_{11}-p_{12}}{2}e_{12} \end{pmatrix}$$

or, equivalently, in 3×3 matrix form

$$\delta\overleftrightarrow{\boldsymbol{\epsilon}} = -\epsilon_r^2 \begin{pmatrix} p_{11}e_{11} + p_{12}e_{22} + p_{12}e_{33} & \dfrac{p_{11}-p_{12}}{2}e_{12} & \dfrac{p_{11}-p_{12}}{2}e_{13} \\ \dfrac{p_{11}-p_{12}}{2}e_{12} & p_{12}e_{11} + p_{11}e_{22} + p_{12}e_{33} & \dfrac{p_{11}-p_{12}}{2}e_{23} \\ \dfrac{p_{11}-p_{12}}{2}e_{13} & \dfrac{p_{11}-p_{12}}{2}e_{23} & p_{12}e_{11} + p_{12}e_{22} + p_{11}e_{33} \end{pmatrix} .$$

In our study we assume, for simplicity, $p_{11} \cong p_{12} \equiv p$ and the tensor $\delta\overleftrightarrow{\boldsymbol{\epsilon}}$ reduces to a scalar

$$\delta\epsilon_{ik}(\mathbf{r},t) = -\epsilon_r^2 p \boldsymbol{\nabla}\cdot\mathbf{u}(\mathbf{r},t)\delta_{ik} \; . \tag{6.9}$$

6.2 Calculation of Brillouin light scattering intensities

According to Maxwell equations, the electric field of an electromagnetic wave (EM), in absence of macroscopic currents, satisfies the vector differential equation

$$\boldsymbol{\nabla}\times[\boldsymbol{\nabla}\times\mathbf{E}(\mathbf{r},t)] = \frac{-\mu}{c^2}\frac{\partial^2}{\partial t^2}\overleftrightarrow{\epsilon}(\mathbf{r},t)\mathbf{E}(\mathbf{r},t) \; , \tag{6.10}$$

where c is the velocity of light in vacuum and we assumed a constant magnetic permeability μ, that we set equal to unity in the following, because we shall be concerned with non-magnetic materials. Since the time variation of $\epsilon_{ik}(\mathbf{r},t)$ is relatively slow (it lies in the acoustic phonon range), we can ignore this variation compared to that of the EM field[1].

[1]The propagation velocity of the EM wave is much greater than that of the elastic wave (phonons), so the time variation of the elastic field is slow and can be considered constant.

This allows us, by setting $\epsilon_{ik}(\mathbf{r},t) = \epsilon_r(\mathbf{r}) + \delta\epsilon_{ik}(\mathbf{r},t)$ with $\epsilon_r(\mathbf{r})$ being the dielectric constant of the static reference system and $\delta\epsilon_{ik}(\mathbf{r},t)$ the dynamical change induced by the phonons, to rewrite Eq. (6.10) as follows

$$\sum_j \mathcal{L}_{ij}(\mathbf{r},t) E_j(\mathbf{r},t) = \frac{1}{c^2} \sum_k \delta\epsilon_{ik}(\mathbf{r},t) \frac{\partial^2}{\partial t^2} E_k(\mathbf{r},t) \ , \tag{6.11}$$

where

$$\mathcal{L}_{ij}(\mathbf{r},t) = -[\boldsymbol{\nabla} \times \boldsymbol{\nabla} \times]_{ij} - \delta_{ij} \frac{\epsilon_r(\mathbf{r})}{c^2} \frac{\partial^2}{\partial t^2} \ . \tag{6.12}$$

The inhomogeneous differential equation (6.11) can be solved using a Green's function technique. Introducing the (tensor) Green's function through

$$\sum_j \mathcal{L}_{ij}(\mathbf{r},t) G_{jk}(\mathbf{r},t;\mathbf{r}',t') = -\delta_{ik}\delta(\mathbf{r}-\mathbf{r}')\delta(t-t') \ , \tag{6.13}$$

it is straightforward to show that the solution of Eq. (6.11) can be written in the form

$$E_i(\mathbf{r},t) = E_{r;i}(\mathbf{r},t) - \frac{1}{c^2} \sum_{kj} \int d^3r' \int dt' G_{ik}(\mathbf{r},t;\mathbf{r}',t') \delta\epsilon_{kj}(\mathbf{r}',t') \frac{\partial^2}{\partial t'^2} E_j(\mathbf{r}',t') \ , \tag{6.14}$$

where $\mathbf{E}_r(\mathbf{r},t)$ is the solution of the corresponding homogeneous equation. Eq. (6.14) has the form of the Lippmann-Schwinger equation.

We shall deal with inelastic light scattering which involves absorption or emission of only one phonon by a photon. Therefore, we proceed in solving Eq. (6.14) to the first-order Born approximation. This approximation yields an expression for the scattered field to first order with respect to the relevant operators of the phonon field, and thus describes scattering of radiation with the participation of only one phonon. The expression for the scattered field is

$$\mathbf{E}_s(\mathbf{r},t) \equiv \mathbf{E}(\mathbf{r},t) - \mathbf{E}_r(\mathbf{r},t) \ , \tag{6.15}$$

thus, from Eq. (6.14) we write

$$E_{s;i}(\mathbf{r},t) = -\frac{1}{c^2} \sum_{kj} \int d^3r' \int dt' G_{ik}(\mathbf{r},t;\mathbf{r}',t') \delta\epsilon_{kj}(\mathbf{r}',t') \frac{\partial^2}{\partial t'^2} E_{r;j}(\mathbf{r}',t') \ . \tag{6.16}$$

Assuming that the initial field is a monochromatic wave with harmonic time dependence $\exp(-\mathrm{i}\omega_i t)$, Eq. (6.16) takes the form

$$E_{s;i}(\mathbf{r},t) = \frac{\omega_i^2}{c^2} \sum_{kj} \int d^3r' \int dt' G_{ik}(\mathbf{r},t;\mathbf{r}',t') \delta\epsilon_{kj}(\mathbf{r}',t') E_{r;j}(\mathbf{r}',t') \ . \tag{6.17}$$

or

$$\mathbf{E}_s(\mathbf{r},t) = \frac{\omega_i^2}{c^2}\int d^3r' \int dt' \overleftrightarrow{\mathbf{G}}(\mathbf{r},t;\mathbf{r}',t')\delta\overleftrightarrow{\boldsymbol{\epsilon}}(\mathbf{r}',t')\mathbf{E}_r(\mathbf{r}',t') \; . \tag{6.18}$$

It can be shown that the time-dependent Green's function $\overleftrightarrow{\mathbf{G}}(\mathbf{r},t;\mathbf{r}',t')$ is the inverse Fourier transform of the corresponding time-independent Green's function,

$$\overleftrightarrow{\mathbf{G}}(\mathbf{r},t;\mathbf{r}',t') = \frac{1}{2\pi}\int_{-\infty}^{\infty} d\omega \overleftrightarrow{\mathbf{G}}(\mathbf{r},\mathbf{r}';\omega)e^{-\mathrm{i}\omega(t-t')} \; , \tag{6.19}$$

which satisfies the equation

$$\left[-\boldsymbol{\nabla}\times\boldsymbol{\nabla}\times + \frac{\epsilon_r(\mathbf{r})\omega^2}{c^2}\overleftrightarrow{\mathbf{I}}\right]\overleftrightarrow{\mathbf{G}}(\mathbf{r},\mathbf{r}';\omega) = -\overleftrightarrow{\mathbf{I}}\delta(\mathbf{r}-\mathbf{r}') \; . \tag{6.20}$$

We shall consider the simplest case where the reference system is optically homogeneous, i.e., $\epsilon_r(\mathbf{r}) = \epsilon_r$ is constant in space. This can be achieved if, for example, in an assembly of particles we fill the intermediate space with some liquid which has the same refractive index as that of the particles. In this case, by setting $k = \sqrt{\epsilon_r}\omega/c$, the Green's function is given by

$$\overleftrightarrow{\mathbf{G}}(\mathbf{r},\mathbf{r}';\omega) = \left[\overleftrightarrow{\mathbf{I}} + \frac{1}{k^2}\boldsymbol{\nabla}_{\mathbf{r}'}\boldsymbol{\nabla}_{\mathbf{r}'}\right]\frac{e^{\mathrm{i}k|\mathbf{r}-\mathbf{r}'|}}{4\pi|\mathbf{r}-\mathbf{r}'|} \; , \tag{6.21}$$

where for the tensor $\boldsymbol{\nabla}_{\mathbf{r}'}\boldsymbol{\nabla}_{\mathbf{r}'}$ we used dyadic notation[2] and $\boldsymbol{\nabla}_{\mathbf{r}'}$ denotes differentiation with respect to x_i'. At distances far away from the source, $r \gg r'$, we have

$$|\mathbf{r}-\mathbf{r}'| = (r^2 + r'^2 - 2\mathbf{r}\cdot\mathbf{r}')^{1/2} = r\left(1 - 2\hat{\mathbf{r}}\cdot\frac{\mathbf{r}'}{r} + \frac{r'^2}{r^2}\right)^{1/2} \; ,$$

thus

$$\frac{e^{\mathrm{i}k|\mathbf{r}-\mathbf{r}'|}}{|\mathbf{r}-\mathbf{r}'|} \simeq \frac{1}{r}e^{\mathrm{i}kr}e^{-\mathrm{i}(k\hat{\mathbf{r}})\cdot\mathbf{r}'} \tag{6.22}$$

and Eq. (6.21) becomes

$$\overleftrightarrow{\mathbf{G}}(\mathbf{r},\mathbf{r}';\omega) \simeq \frac{e^{\mathrm{i}kr}}{4\pi r}\left[\overleftrightarrow{\mathbf{I}} + \frac{1}{k^2}\boldsymbol{\nabla}_{\mathbf{r}'}\boldsymbol{\nabla}_{\mathbf{r}'}\right]e^{-\mathrm{i}\mathbf{k}\cdot\mathbf{r}'} = \frac{e^{\mathrm{i}kr}}{4\pi r}e^{-\mathrm{i}\mathbf{k}\cdot\mathbf{r}'}\left[\overleftrightarrow{\mathbf{I}} - \hat{\mathbf{k}}\hat{\mathbf{k}}\right] \; , \tag{6.23}$$

where $\mathbf{k} = k\hat{\mathbf{r}}$. It is straightforward to prove that $\left[\overleftrightarrow{\mathbf{I}} - \hat{\mathbf{k}}\hat{\mathbf{k}}\right]\mathbf{A} \equiv -\hat{\mathbf{k}}\times(\hat{\mathbf{k}}\times\mathbf{A})$ and thus Eq. (6.23) can be written as

$$\overleftrightarrow{\mathbf{G}}(\mathbf{r},\mathbf{r}';\omega) \simeq -\frac{e^{\mathrm{i}kr}}{4\pi r}e^{-\mathrm{i}\mathbf{k}\cdot\mathbf{r}'}\hat{\mathbf{k}}\times\hat{\mathbf{k}}\times \; . \tag{6.24}$$

[2] In dyadic form $\overleftrightarrow{\mathbf{C}} = \mathbf{AB}$ is equivalent to $C_{ij} = A_iB_j$.

Replacing Eq. (6.19) into Eq. (6.18) and considering as initial field an incident plane wave $\mathbf{E}_r(\mathbf{r}',t') = \hat{\mathbf{n}}_i E_0 e^{\mathrm{i}(\mathbf{k}_i\cdot\mathbf{r}'-\omega_i t')}$ we have

$$\mathbf{E}_s(\mathbf{r},t) = \frac{\omega_i^2}{c^2}\int d^3r' \int dt' \int \frac{d\omega}{2\pi}\overleftrightarrow{\mathbf{G}}(\mathbf{r},\mathbf{r}';\omega)e^{-\mathrm{i}\omega(t-t')}\delta\overleftrightarrow{\boldsymbol{\epsilon}}(\mathbf{r}',t')\hat{\mathbf{n}}_i E_0 e^{\mathrm{i}(\mathbf{k}_i\cdot\mathbf{r}'-\omega_i t')} \,. \quad (6.25)$$

In the limit $r \gg r'$ we substitute Eq. (6.24) into Eq. (6.25) and obtain

$$\begin{aligned}\mathbf{E}_s(\mathbf{r},t) = \frac{-\omega_i^2}{c^2}\frac{E_0}{4\pi r}\int d^3r' \int dt' \int \frac{d\omega}{2\pi} e^{\mathrm{i}kr}e^{-\mathrm{i}(\mathbf{k}-\mathbf{k}_i)\cdot\mathbf{r}'} \\ \hat{\mathbf{k}}\times\hat{\mathbf{k}}\times\left[\delta\overleftrightarrow{\boldsymbol{\epsilon}}(\mathbf{r}',t')\hat{\mathbf{n}}_i\right]e^{-\mathrm{i}\omega t}e^{\mathrm{i}(\omega-\omega_i)t'} \,.\end{aligned} \quad (6.26)$$

We now expand $\delta\overleftrightarrow{\boldsymbol{\epsilon}}(\mathbf{r}',t')$ in the basis of eigenstates, p, of the elastic field

$$\delta\overleftrightarrow{\boldsymbol{\epsilon}}(\mathbf{r}',t') = \sum_p \delta\overleftrightarrow{\boldsymbol{\epsilon}}_p(\mathbf{r}')e^{-\mathrm{i}\Omega_p t'} \quad (6.27)$$

and perform the integration over t' in Eq. (6.26), which yields

$$\begin{aligned}\mathbf{E}_s(\mathbf{r},t) = &\frac{-\omega_i^2}{c^2}\frac{E_0}{4\pi r}\sum_p\int d^3r' \int d\omega e^{\mathrm{i}kr}e^{-\mathrm{i}(\mathbf{k}-\mathbf{k}_i)\cdot\mathbf{r}'}\hat{\mathbf{k}}\times\hat{\mathbf{k}}\times \\ &[\delta\overleftrightarrow{\boldsymbol{\epsilon}}_p(\mathbf{r}')\hat{\mathbf{n}}_i]e^{-\mathrm{i}\omega t}\delta(\omega-\omega_i-\Omega_p)\end{aligned} \quad (6.28)$$

and, integrating over ω, we recall $k = k(\omega)$, we finally obtain

$$\mathbf{E}_s(\mathbf{r},t) = \frac{-\omega_i^2}{c^2}\frac{E_0}{4\pi r}\int d^3r' e^{\mathrm{i}k_f r}e^{-\mathrm{i}(\mathbf{k}_f-\mathbf{k}_i)\cdot\mathbf{r}'}\hat{\mathbf{k}}_f\times\hat{\mathbf{k}}_f\times\underbrace{\sum_p\delta\overleftrightarrow{\boldsymbol{\epsilon}}_p(\mathbf{r}')e^{-\mathrm{i}\Omega_p t}}_{\delta\overleftrightarrow{\boldsymbol{\epsilon}}(\mathbf{r}',t)}\hat{\mathbf{n}}_i e^{-\mathrm{i}\omega_i t} \,, \quad (6.29)$$

where $k_f = \sqrt{e_r}(\omega_i+\Omega_p)/c \simeq k_i$, $\mathbf{k}_f = k_f\hat{\mathbf{k}}_f (= k_f\hat{\mathbf{r}})$. Defining the scattering vector $\mathbf{q} = \mathbf{k}_f - \mathbf{k}_i$ and using the Fourier transform

$$\delta\overleftrightarrow{\boldsymbol{\epsilon}}(\mathbf{q},t) = \int d^3r'\delta\overleftrightarrow{\boldsymbol{\epsilon}}(\mathbf{r}',t)e^{-\mathrm{i}\mathbf{q}\cdot\mathbf{r}'} \,, \quad (6.30)$$

Eq. (6.29) takes the form

$$\mathbf{E}_s(\mathbf{r},t) = \frac{-\omega_i^2}{c^2}\frac{E_0}{4\pi r}e^{\mathrm{i}(k_f r-\omega_i t)}\hat{\mathbf{k}}_f\times\hat{\mathbf{k}}_f\times[\delta\overleftrightarrow{\boldsymbol{\epsilon}}(\mathbf{q},t)\hat{\mathbf{n}}_i] \,. \quad (6.31)$$

Projecting on a specific polarization direction $\hat{\mathbf{n}}_f$ we have

$$E_s(\mathbf{r},t) = \hat{\mathbf{n}}_f\cdot\mathbf{E}_s(\mathbf{r},t) = \frac{-\omega_i^2}{c^2}\frac{E_0}{4\pi r}e^{\mathrm{i}(k_f r-\omega_i t)}\hat{\mathbf{n}}_f\cdot\{\hat{\mathbf{k}}_f\times\hat{\mathbf{k}}_f\times[\delta\overleftrightarrow{\boldsymbol{\epsilon}}(\mathbf{q},t)\hat{\mathbf{n}}_i]\} \quad (6.32)$$

and, using the identity $\mathbf{A}\times(\mathbf{B}\times\mathbf{C})=\mathbf{B}(\mathbf{A}\cdot\mathbf{C})-\mathbf{C}(\mathbf{A}\cdot\mathbf{B})$ and the fact that $\hat{\mathbf{n}}_f\perp\hat{\mathbf{k}}_f$ for transverse waves, we obtain

$$E_s(\mathbf{r},t)=\frac{\omega_i^2}{c^2}\frac{E_0}{4\pi r}e^{\mathrm{i}(k_f r-\omega_i t)}\underbrace{\hat{\mathbf{n}}_f\cdot[\delta\overleftrightarrow{\boldsymbol{\epsilon}}(\mathbf{q},t)\hat{\mathbf{n}}_i]}_{\delta\epsilon_{if}(\mathbf{q},t)}\ . \tag{6.33}$$

Since in the present study, as noted above, the tensor $\delta\overleftrightarrow{\boldsymbol{\epsilon}}$ reduces to a scalar [see Eq. (6.9)], the polarization of the incident beam does not change because the elements $\delta\epsilon_{if}(\mathbf{q},t)$ are zero if the initial and the final polarization states are orthogonal. Therefore we will consider $\hat{\mathbf{n}}_f=\hat{\mathbf{n}}_i$ and $\delta\epsilon_{if}(\mathbf{q},t)=\delta\epsilon_{ii}(\mathbf{q},t)=\delta\epsilon(\mathbf{q},t)$ where we have omitted the indices for simplicity. Also, $k_i^2=\epsilon_r\omega_i^2/c^2\simeq k_f^2$, and thus Eq. (6.33) becomes

$$E_s(\mathbf{r},t)=\frac{E_0k_f^2}{4\pi\epsilon_r r}e^{\mathrm{i}(k_f r-\omega_i t)}\delta\epsilon(\mathbf{q},t)\ . \tag{6.34}$$

The spectral density of light scattered into the detector positioned at a large distance R along the direction $\mathbf{r}$ is given by the Fourier transform of the correlation function of the electric field [100]

$$\begin{aligned}I(\mathbf{q},\omega_f)&\equiv\frac{1}{2\pi}\int dt e^{\mathrm{i}\omega_f t}<E_s^*(R\hat{\mathbf{r}},0)E_s(R\hat{\mathbf{r}},t)>\\&=\frac{|E_0|^2k_f^4}{32\pi^3\epsilon_r^2R^2}\int dt<\delta\epsilon^*(\mathbf{q},0)\delta\epsilon(\mathbf{q},t)>e^{\mathrm{i}(\omega_f-\omega_i)t}\ .\end{aligned} \tag{6.35}$$

The time-correlation function is defined by

$$<\delta\epsilon^*(\mathbf{q},0)\delta\epsilon(\mathbf{q},t)>=\lim_{T\to\infty}\frac{1}{T}\int_{-T/2}^{+T/2}dt'\delta\epsilon^*(\mathbf{q},t')\delta\epsilon(\mathbf{q},t'+t)\ , \tag{6.36}$$

thus, substituting into Eq. (6.35) and introducing the new variable $\omega=\omega_f-\omega_i$ we have

$$\begin{aligned}I(\mathbf{q},\omega)&=\frac{|E_0|^2k_f^4}{32\pi^3\epsilon_r^2R^2}\int dt<\delta\epsilon^*(\mathbf{q},0)\delta\epsilon(\mathbf{q},t)>e^{\mathrm{i}\omega t}\\&=\frac{|E_0|^2k_f^4}{32\pi^3\epsilon_r^2R^2}\int dte^{\mathrm{i}\omega t}\lim_{T\to\infty}\frac{1}{T}\int_{-T/2}^{+T/2}dt'\sum_p\delta\epsilon_p^*(\mathbf{q})e^{\mathrm{i}\Omega_p t'}\sum_{p'}\delta\epsilon_{p'}(\mathbf{q})e^{-\mathrm{i}\Omega_{p'}(t'+t)}\\&=\frac{|E_0|^2k_f^4}{32\pi^3\epsilon_r^2R^2}\int dte^{\mathrm{i}\omega t}\sum_{p,p'}\delta\epsilon_p^*(\mathbf{q})\delta\epsilon_{p'}(\mathbf{q})e^{-\mathrm{i}\Omega_{p'}t}\underbrace{\lim_{T\to\infty}\frac{1}{T}\int_{-T/2}^{+T/2}dt'e^{\mathrm{i}(\Omega_p-\Omega_{p'})t'}}_{\delta_{\Omega_p\Omega_{p'}}}\\&=\frac{|E_0|^2k_f^4}{16\pi^2\epsilon_r^2R^2}\sum_p\delta\epsilon_p^*(\mathbf{q})\sum_{p'}\delta\epsilon_{p'}(\mathbf{q})\delta(\omega-\Omega_{p'})\delta_{\Omega_p\Omega_{p'}}\ ,\end{aligned} \tag{6.37}$$

where $\delta\epsilon_p(\mathbf{q})$ is the time-independent part of Eq. (6.30) if we make use of Eq. (6.27), and by introducing Eq. (6.9) we can easily show that

$$\delta\epsilon_p(\mathbf{q}) = -\epsilon_r^2 p \int d^3r e^{-\mathrm{i}\mathbf{q}\cdot\mathbf{r}} \boldsymbol{\nabla}\cdot\mathbf{u}_p(\mathbf{r}) \tag{6.38}$$

or, alternatively, using again the Fourier transform $\mathbf{u}_p(\mathbf{r}) = \frac{1}{(2\pi)^3}\int dq'^3 \mathbf{u}_p(\mathbf{q}') e^{\mathrm{i}\mathbf{q}'\cdot\mathbf{r}}$ we write

$$\delta\epsilon_p(\mathbf{q}) = -\mathrm{i}\epsilon_r^2 p\mathbf{q}\cdot\mathbf{u}_p(\mathbf{q}) = -\mathrm{i}\epsilon_r^2 p \int d^3r e^{-\mathrm{i}\mathbf{q}\cdot\mathbf{r}} \mathbf{q}\cdot\mathbf{u}_p(\mathbf{r}) \,. \tag{6.39}$$

Substituting Eq. (6.38) or Eq. (6.39) into Eq. (6.37) we obtain two equivalent expressions for the intensity of the scattered radiation

$$I(\mathbf{q},\omega) = \frac{|E_0|^2 k_f^4 \epsilon_r^2 p^2}{16\pi^2 R^2} \sum_{p,p'} \int d^3r \left[e^{-\mathrm{i}\mathbf{q}\cdot\mathbf{r}} \boldsymbol{\nabla}\cdot\mathbf{u}_p(\mathbf{r})\right]^* \int d^3r e^{-\mathrm{i}\mathbf{q}\cdot\mathbf{r}} \boldsymbol{\nabla}\cdot\mathbf{u}_{p'}(\mathbf{r}) \delta(\omega-\Omega_{p'}) \delta_{\Omega_p\Omega_{p'}} \,, \tag{6.40}$$

and

$$I(\mathbf{q},\omega) = \frac{|E_0|^2 k_f^4 \epsilon_r^2 p^2}{16\pi^2 R^2} \sum_{p,p'} \int d^3r \left[e^{-\mathrm{i}\mathbf{q}\cdot\mathbf{r}} \mathbf{q}\cdot\mathbf{u}_p(\mathbf{r})\right]^* \int d^3r e^{-\mathrm{i}\mathbf{q}\cdot\mathbf{r}} \mathbf{q}\cdot\mathbf{u}_{p'}(\mathbf{r}) \delta(\omega-\Omega_{p'}) \delta_{\Omega_p\Omega_{p'}} \,. \tag{6.41}$$

We should note that these equations describe absorption processes of only one phonon by a photon ($\omega = \omega_f - \omega_i = \Omega_p$) and they manifest as delta functions (anti-Stokes peaks). The corresponding emission processes of a phonon (Stokes) result from the conjugate expression of Eq. (6.27), which arises from the definition of the displacement field, as $\mathbf{u}(\mathbf{r},t) = \mathrm{Re}[\mathbf{u}(\mathbf{r})\exp(-\mathrm{i}\Omega t)]$.

6.3 Homogeneous fluid

The displacement field associated with an acoustic wave propagating in a homogeneous fluid medium, of density ρ, can be written, in general, in the plane wave basis as[3]

$$\mathbf{u}(\mathbf{r},t) = \sum_{\mathbf{Q}} \mathrm{Re}\{C_{\mathbf{Q}}\widehat{\mathbf{Q}} e^{\mathrm{i}(\mathbf{Q}\cdot\mathbf{r}-\Omega_Q t)}\} = \sum_{\mathbf{Q}} \frac{1}{2}[C_{\mathbf{Q}}\widehat{\mathbf{Q}} e^{\mathrm{i}(\mathbf{Q}\cdot\mathbf{r}-\Omega_Q t)} + C^*_{\mathbf{Q}}\widehat{\mathbf{Q}} e^{-\mathrm{i}(\mathbf{Q}\cdot\mathbf{r}-\Omega_Q t)}] \tag{6.42}$$

where $C_{\mathbf{Q}}$ are complex expansion coefficients and $\Omega_Q = cQ$, c being the propagation velocity in the fluid. Assuming a large rectangular volume $V = L_x L_y L_z$ and periodic

[3]The actual displacement field is the real part of the complex field.

boundary conditions, we obtain in the limit $V \to \infty$

$$\mathbf{u}(\mathbf{r},t) = \frac{V}{8\pi^3}\int dQQ^2 \int d\widehat{\mathbf{Q}} \quad \frac{1}{2}[C_{\mathbf{Q}} \underbrace{\widehat{\mathbf{Q}} e^{\mathrm{i}(\mathbf{Q}\cdot\mathbf{r}-\Omega_Q t)}}_{\frac{-\mathrm{i}}{Q}\nabla e^{\mathrm{i}\mathbf{Q}\cdot\mathbf{r}}e^{-\mathrm{i}\Omega_Q t}} + C^*_{\mathbf{Q}}\widehat{\mathbf{Q}} e^{-\mathrm{i}(\mathbf{Q}\cdot\mathbf{r}-\Omega_Q t)}] \tag{6.43}$$

and, using the mathematical identity

$$e^{\mathrm{i}\mathbf{Q}\cdot\mathbf{r}} = 4\pi\sum_{\ell m}\mathrm{i}^\ell j_\ell(Qr)Y_{\ell m}(\hat{\mathbf{r}})Y^*_{\ell m}(\hat{\mathbf{Q}}) \;, \tag{6.44}$$

we obtain

$$\mathbf{u}(\mathbf{r},t) = \frac{2V}{\pi}\sum_{\ell m}\int dQQ^2\frac{1}{2Q}\{a_{\ell mQ}\boldsymbol{\nabla}[j_\ell(Qr)Y_{\ell m}(\hat{\mathbf{r}})]e^{-\mathrm{i}\Omega_Q t} + a^*_{\ell mQ}\boldsymbol{\nabla}[j_\ell(Qr)Y^*_{\ell m}(\hat{\mathbf{r}})]e^{\mathrm{i}\Omega_Q t}\} \tag{6.45}$$

in the spherical wave representation, with corresponding field amplitudes

$$a_{\ell mQ} = \frac{1}{4\pi}\int d\hat{\mathbf{Q}}\mathrm{i}^{\ell-1}Y^*_{\ell m}(\hat{\mathbf{Q}})C_{\mathbf{Q}} \;. \tag{6.46}$$

We need to calculate the phonon population. The time average of the total oscillation energy of the wave field is given from the equipartition theorem for harmonic oscillators

$$\langle E\rangle_t = 2\langle T\rangle_t = 2\cdot\frac{1}{2}\langle\int_V d^3r\rho\dot{\mathbf{u}}^2(\mathbf{r},t)\rangle_t \;. \tag{6.47}$$

We have from (6.43)

$$\dot{\mathbf{u}}(\mathbf{r},t) = \frac{V}{8\pi^3}\int d^3Q\;\frac{1}{2}\left[-\mathrm{i}\Omega_Q C_{\mathbf{Q}}e^{\mathrm{i}(\mathbf{Q}\cdot\mathbf{r}-\Omega_Q t)}\hat{\mathbf{Q}} + \mathrm{i}\Omega_Q C^*_{\mathbf{Q}}e^{-\mathrm{i}(\mathbf{Q}\cdot\mathbf{r}-\Omega_Q t)}\hat{\mathbf{Q}}\right] \;, \tag{6.48}$$

so that

$$\begin{aligned}\langle E\rangle_t = \frac{\rho}{4}\int_V d^3r\frac{1}{T}\int_0^T dt\frac{V}{8\pi^3}\int d^3Q\left[-\mathrm{i}\Omega_Q C_{\mathbf{Q}}e^{\mathrm{i}(\mathbf{Q}\cdot\mathbf{r}-\Omega_Q t)}\hat{\mathbf{Q}} + \mathrm{i}\Omega_Q C^*_{\mathbf{Q}}e^{-\mathrm{i}(\mathbf{Q}\cdot\mathbf{r}-\Omega_Q t)}\hat{\mathbf{Q}}\right]\\ \cdot\frac{V}{8\pi^3}\int d^3Q'\left[-\mathrm{i}\Omega_{Q'}C_{\mathbf{Q}'}e^{\mathrm{i}(\mathbf{Q}'\cdot\mathbf{r}-\Omega_{Q'}t)}\hat{\mathbf{Q}}' + \mathrm{i}\Omega_{Q'}C^*_{\mathbf{Q}'}e^{-\mathrm{i}(\mathbf{Q}'\cdot\mathbf{r}-\Omega_{Q'}t)}\hat{\mathbf{Q}}'\right] \;.\end{aligned} \tag{6.49}$$

Integration with respect to $\mathbf{r}$ gives $\int_V d^3re^{\mathrm{i}(\mathbf{Q}-\mathbf{Q}')\cdot\mathbf{r}} = V\delta_{\mathbf{Q}\mathbf{Q}'}$ while the integrals over a time period eliminate the time-dependent terms because $\int_0^T dte^{\pm\mathrm{i}2\Omega_Q t} = 0$. Finally, we obtain

$$\langle E\rangle_t = \frac{V}{8\pi^3}\int d^3Q\;\frac{\rho V}{2}\Omega_Q^2|C_{\mathbf{Q}}|^2 \equiv \sum_{\mathbf{Q}}\langle E_{\mathbf{Q}}\rangle \;, \tag{6.50}$$

where we note that the magnitudes $C_{\mathbf{Q}}$ are the components of the normal oscillation modes of the lattice. Defining $\langle E_{\mathbf{Q}} \rangle$ as the average thermal energy of each normal mode we have

$$\langle E_{\mathbf{Q}} \rangle = \left[\langle n_{\mathbf{Q}} \rangle + \frac{1}{2} \right] \hbar \Omega_{\mathbf{Q}} = \left[\frac{1}{e^{\frac{\hbar \Omega_{\mathbf{Q}}}{k_B T}} - 1} + \frac{1}{2} \right] \hbar \Omega_{\mathbf{Q}} \simeq k_B T \, , \tag{6.51}$$

since $\hbar \Omega_{\mathbf{Q}} \ll k_B T$ [4]. From (6.50), (6.51) it turns out

$$|C_{\mathbf{Q}}|^2 = \frac{2 k_B T}{\rho V \Omega_Q^2} \, , \tag{6.52}$$

which, we note, is independent of $\widehat{\mathbf{Q}}$. From (6.46) and (6.52) and with the help of completeness relation (B.9) we obtain

$$\sum_{\ell m} |a_{\ell m Q}|^2 = \frac{1}{4\pi} \frac{2 k_B T}{\rho V \Omega_Q^2} \, . \tag{6.53}$$

Alternatively substituting into Eq. (6.47) the displacement field from Eq. (6.45) and following the same procedure in the spherical wave representation we derive exactly the same relation

$$\langle E \rangle_t = \rho \left(\frac{2V}{\pi} \right)^2 \sum_{\ell m} \int dQ Q^2 \frac{\pi}{4} \Omega_Q^2 |a_{\ell m Q}|^2 = \frac{V}{8\pi^3} \int d^3 Q k_B T \Rightarrow \sum_{\ell m} |a_{\ell m Q}|^2 = \frac{1}{4\pi} \frac{2 k_B T}{\rho V \Omega_Q^2} \, . \tag{6.54}$$

The BLS spectral density is obtained, in general, through Eq. (6.37)

$$I(\mathbf{q}, \omega) \propto \sum_p \delta \epsilon_p^*(\mathbf{q}) \sum_{p'} \delta \epsilon_{p'}(\mathbf{q}) \delta(\omega - \Omega_{p'}) \delta_{\Omega_p \Omega_{p'}} \tag{6.55}$$

In the specific case of an isotropic homogeneous fluid medium the subscript p denotes either the index $\mathbf{Q}$ (in the plane wave representation) or the discrete angular momentum indices ℓm and the continuum index Q (in the spherical wave representation) and we have already noted that $\Omega_p = \Omega_Q = cQ$. Therefore we should be careful in handling (6.55) and the correct formula for the BLS spectral density is

$$I(\mathbf{q}, \omega) \propto \sum_p \delta \epsilon_p^*(\mathbf{q}) \sum_{p'} \delta \epsilon_{p'}(\mathbf{q}) \delta(\omega - \Omega_{Q'}) \delta_{QQ'} \tag{6.56}$$

[4] Indeed at room temperature ($T = 300$ K) $k_B T = 0.02585$ eV while $\hbar \Omega_Q \sim 10^{-6}$ eV in the range of GHz.

In the plane wave basis ($\sum_p = \frac{V}{8\pi^3}\int d^3Q$) and by using the second of Eqs. (6.39), (we omit the constant factor $\dfrac{|E_0|^2 k_f^4 \epsilon_r^2 p^2}{16\pi^2 R^2}$ for simplicity) we obtain

$$\begin{aligned} I(\mathbf{q},\omega) &\propto \left(\frac{V}{8\pi^3}\right)^2 \int d^3Q \int d^3r e^{-\mathrm{i}\mathbf{q}\cdot\mathbf{r}} \mathbf{q}\cdot C_{\mathbf{Q}}\widehat{\mathbf{Q}} e^{\mathrm{i}\mathbf{Q}\cdot\mathbf{r}} \int d^3Q' \int d^3r e^{\mathrm{i}\mathbf{q}\cdot\mathbf{r}} \mathbf{q}\cdot C^*_{\mathbf{Q}'}\widehat{\mathbf{Q}}' e^{-\mathrm{i}\mathbf{Q}'\cdot\mathbf{r}} \times \\ &\times \delta(\omega-\Omega_{Q'})\delta_{QQ'} \\ &= \left(\frac{V}{8\pi^3}\right)^2 \int d^3Q 8\pi^3\delta(\mathbf{q}-\mathbf{Q})\mathbf{q}\cdot\widehat{\mathbf{Q}}C_{\mathbf{Q}} \int d^3Q' 8\pi^3\delta(\mathbf{q}-\mathbf{Q}')\mathbf{q}\cdot\widehat{\mathbf{Q}}'C^*_{\mathbf{Q}'} \\ &\times \delta(\omega-\Omega_{Q'})\delta_{QQ'} \\ &= V^2q^2|C_{\mathbf{q}}|^2\delta(\omega-\Omega_q) \\ &= \frac{2k_BTV}{\rho c^2}\delta(\omega-\Omega_q)\ . \end{aligned} \tag{6.57}$$

Correspondingly, in the spherical wave basis ($\sum_p = \frac{2V}{\pi}\sum_{\ell m}\int dQQ^2$) and by using Eq. (6.38) we obtain

$$\begin{aligned} I(\mathbf{q},\omega) &\propto \frac{2V}{\pi}\sum_{\ell m}\int dQQ^2 \int d^3r e^{-\mathrm{i}\mathbf{q}\cdot\mathbf{r}} \boldsymbol{\nabla}\cdot\{a_{\ell mQ}\frac{1}{Q}\boldsymbol{\nabla}[j_\ell(Qr)Y_{\ell m}(\widehat{\mathbf{r}})]\} \\ &\times \frac{2V}{\pi}\sum_{\ell' m'}\int dQ'Q'^2 \int d^3r e^{\mathrm{i}\mathbf{q}\cdot\mathbf{r}} \boldsymbol{\nabla}\cdot\{a^*_{\ell' m' Q'}\frac{1}{Q'}\boldsymbol{\nabla}[j_{\ell'}(Q'r)Y^*_{\ell' m'}(\widehat{\mathbf{r}})]\} \\ &\times \delta(\omega-\Omega_{Q'})\delta_{QQ'}\ . \end{aligned} \tag{6.58}$$

Using the identities (6.44), (B.8), (A.22) and substituting the coefficient $a_{\ell mQ}$ from Eq. (6.46), Eq. (6.58) becomes

$$\begin{aligned} I(\mathbf{q},\omega) &\propto \frac{2V}{\pi}\sum_{\ell m}\int dQQ^2(-\mathrm{i})^\ell 4\pi\frac{\pi}{2qQ}\delta(q-Q)(-Q)Y_{\ell m}(\widehat{\mathbf{q}})\frac{1}{4\pi}\int d\widehat{\mathbf{Q}} i^{\ell-1}Y^*_{\ell m}(\widehat{\mathbf{Q}})C_{\mathbf{Q}} \\ &\times \frac{2V}{\pi}\sum_{\ell' m'}\int dQ'Q'^2\mathrm{i}^{\ell'}4\pi\frac{\pi}{2qQ'}\delta(q-Q')(-Q')Y^*_{\ell' m'}(\widehat{\mathbf{q}})\frac{1}{4\pi}\int d\widehat{\mathbf{Q}}'(-\mathrm{i})^{\ell'-1}Y_{\ell' m'}(\widehat{\mathbf{Q}}')C^*_{\mathbf{Q}'} \\ &\times \delta(\omega-\Omega_{Q'})\delta_{QQ'}\ . \end{aligned} \tag{6.59}$$

Now using the identities $\sum_{\ell m}Y_{\ell m}(\hat{\mathbf{r}})Y^*_{\ell m}(\hat{\mathbf{r}}') = \delta(\hat{\mathbf{r}}-\hat{\mathbf{r}}')$, $\delta(\mathbf{r}-\mathbf{r}') = \frac{1}{r^2}\delta(r-r')\delta(\hat{\mathbf{r}}-\hat{\mathbf{r}}')$,

Eq. (6.59) reduces to

$$\begin{aligned} I(\mathbf{q},\omega) &\propto \frac{2V}{\pi}\int d^3Q\frac{\pi}{2}q\delta(\mathbf{q}-\mathbf{Q})C_{\mathbf{Q}}\frac{2V}{\pi}\int d^3Q'\frac{\pi}{2}q\delta(\mathbf{q}-\mathbf{Q}')C^*_{\mathbf{Q}'}\delta(\omega-\Omega_{Q'})\delta_{QQ'} \\ &= \left(\frac{2V}{\pi}\right)^2\left(\frac{\pi}{2}\right)^2 q^2|C_{\mathbf{q}}|^2\delta(\omega-\Omega_q)\delta_{qq} \\ &= V^2q^2|C_{\mathbf{q}}|^2\delta(\omega-\Omega_q) \\ &= \frac{2k_BTV}{\rho c^2}\delta(\omega-\Omega_q)\ . \end{aligned} \tag{6.60}$$

which is identical to (6.57).

To summarize, the intensity of the scattered radiation for an isotropic fluid medium will be, from (6.41), incorporating (6.57), (6.60)

$$I(\mathbf{q},\omega) = \frac{|E_0|^2k_f^4\epsilon_r^2p^2k_BTV}{8\pi^2R^2\rho c^2}\delta(\omega-cq)\ . \tag{6.61}$$

We note that the BLS spectrum will exhibit a characteristic peak (delta function) at frequency equal to $\omega_f = \omega_i + cq$, which means that a phonon was absorbed (anti-Stokes), while a respective peak will appear also at frequency $\omega_f = \omega_i - cq$ (Stokes). The intensity of the peak will be proportional to the temperature and the scattering volume.

6.4 A solid sphere in vacuum

As a particular case, let us now study a solid sphere of radius S in vacuum [101]. The displacement field $\mathbf{u}(\mathbf{r})$ inside the sphere is given by Eq. (3.4) and the appropriate boundary conditions now are $\tau_r|_{r=S} = \tau_\theta|_{r=S} = \tau_\phi|_{r=S} = 0$, because the surface traction vanishes in vacuum. The boundary conditions for the angular components of $\boldsymbol{\tau}$ are the same as in the case of a solid sphere in a fluid host. Therefore Eqs. (3.11), (3.12) still hold. The boundary condition concerning the radial part, $\tau_r|_{r=S} = 0$, leads to

$$a_{N\ell m}\sqrt{\ell(\ell+1)}\frac{x_tj'_\ell(x_t)-j_\ell(x_t)}{x_t} - a_{L\ell m}\frac{\left[\ell(\ell+1)-x_t^2/2\right]j_\ell(x_l)-2x_lj'_\ell(x_l)}{x_l} = 0\ , \tag{6.62}$$

From Eqs. (3.11) and (6.62) we obtain

$$\ell(\ell+1)\frac{x_tj'_\ell(x_t)-j_\ell(x_t)}{x_tj'_\ell(x_t)-[\ell(\ell+1)-1-x_t^2/2]j_\ell(x_t)} = \frac{\left[\ell(\ell+1)-x_t^2/2\right]j_\ell(x_l)-2x_lj'_\ell(x_l)}{x_lj'_\ell(x_l)-j_\ell(x_l)}\ . \tag{6.63}$$

Eq. (6.63), for a given ℓ, provides the discrete set of eigenfrequencies of the spheroidal modes, $\Omega_{n\ell}$, $n = 1, 2, 3, \ldots$, which appear in addition to the torsional eigenmodes given

by Eq. (3.11). As we shall see below, the torsional modes do not contribute to the BLS intensity, therefore we will have to deal only with the spheroidal eigenmodes. We recall that $Q_\nu = \Omega_{n\ell}/c_\nu$, and $x_\nu = Q_\nu S \quad \nu = l, t$, omitting, for simplicity, the indices $n\ell$ in the wavenumbers Q_ν (and x_ν) associated with a given eigenmode. The subscript p in Eq. (6.37) is a collective index which denotes the eigenmodes, and in the present case $p = n\ell m$.

Two quantities are necessary in order to calculate the BLS intensity, $\delta\epsilon_p(\mathbf{q})$ and $|a_{Lp}|^2$. From on Eq. (6.38), we obtain [5]

$$\begin{aligned}
\delta\epsilon_p(\mathbf{q}) &\propto \int d^3r e^{-\mathrm{i}\mathbf{q}\cdot\mathbf{r}} \boldsymbol{\nabla}\cdot[\mathbf{u}_p(\mathbf{r})\Theta(S-r)] \\
&= \int d^3r e^{-\mathrm{i}\mathbf{q}\cdot\mathbf{r}} [\boldsymbol{\nabla}\cdot\mathbf{u}_p(\mathbf{r})\Theta(S-r) - \mathbf{u}_p(\mathbf{r})\cdot\hat{\mathbf{r}}\delta(S-r)] \Rightarrow \\
\delta\epsilon_p(\mathbf{q}) &\propto 4\pi(-\mathrm{i})^\ell Y_{\ell m}(\hat{\mathbf{q}}) a_{Ln\ell m} \mathcal{W}_{n\ell}(S, q, Q_l, Q_t)
\end{aligned} \tag{6.64}$$

where $\mathbf{u}_p(\mathbf{r})$ is the displacement field [see Eq. (3.4)] associated with the given eigenmode and the function $\mathcal{W}_{n\ell}(S, q, Q_l, Q_t)$ is defined as

$$\mathcal{W}_{n\ell}(S, q, Q_l, Q_t) = \frac{S^2}{q^2 - Q_l^2}[q^2 j_\ell(qS) j'_\ell(x_l) - qQ_l j'_\ell(qS) j_\ell(x_l)] + C\sqrt{\ell(\ell+1)}S^2 \frac{j_\ell(qS) j_\ell(x_t)}{x_t} \tag{6.65}$$

and C is calculated by rewriting Eq. (3.11) as $a_{N\ell m} = -a_{L\ell m}C$. It can be readily seen that the torsional (M) modes are not active in this case.

To calculate the phonon population, or else the elastic field amplitude $|a_{Lp}|^2$, we follow the same steps as in the case of the homogeneous fluid, by distributing equally thermal energy $k_B T$ to each normal oscillation mode. Thus, for a body of temperature T in vacuum, the stored time-average thermal energy of a normal oscillation mode (i.e., an eigenmode $p = n\ell m$) is, according to Bose-Einstein distribution,

$$\frac{1}{2}\rho\Omega_{n\ell}^2 \int d^3r |\mathbf{u}_p(\mathbf{r})|^2 = \left[n(\Omega_{n\ell}) + \frac{1}{2}\right]\hbar\Omega_{n\ell} \tag{6.66}$$

where $n(\Omega_{n\ell}) = 1/[\exp(\hbar\Omega_{n\ell}/k_B T) - 1]$. For spheres with dimensions in the range of μm, like those we will study here, the eigenfrequencies lie in the GHz range so $\hbar\Omega_{n\ell} \sim 10^{-6}$ eV. At room temperature $k_B T \sim 0.02585$ eV. So, $\hbar\Omega_{n\ell}/k_B T \ll 1 \Rightarrow n(\Omega_{n\ell}) \simeq k_B T/\hbar\Omega_{n\ell}$ and Eq. (6.66) becomes

$$\int d^3r |\mathbf{u}_p(\mathbf{r})|^2 = \frac{2k_B T}{\rho\Omega_{n\ell}^2} \tag{6.67}$$

[5] We use the Heaviside step function Θ, because in this case the elastic field is confined inside the sphere.

With the help of Appendix C and Eqs. (B.8), (B.35), we calculate

$$\begin{aligned}\int d^3r|\mathbf{u}_p(\mathbf{r})|^2 &= \int d^3r\left[\mathcal{B}^{(0)}_{\ell m}Y_{\ell m}(\hat{\mathbf{r}})\hat{\mathbf{r}} - \mathcal{B}^{(2)}_{\ell m}\mathbf{X}_{\ell m}(\hat{\mathbf{r}})\times\hat{\mathbf{r}}\right]\cdot\left[\mathcal{B}^{(0)*}_{\ell' m'}Y^*_{\ell' m'}(\hat{\mathbf{r}})\hat{\mathbf{r}} - \mathcal{B}^{(2)*}_{\ell' m'}\mathbf{X}^*_{\ell' m'}(\hat{\mathbf{r}})\times\hat{\mathbf{r}}\right]\\ &= \int drr^2\int d\hat{\mathbf{r}}\{\mathcal{B}^{(0)}_{\ell m}\mathcal{B}^{(0)*}_{\ell' m'}Y_{\ell m}(\hat{\mathbf{r}})Y^*_{\ell' m'}(\hat{\mathbf{r}}) + \mathcal{B}^{(2)}_{\ell m}\mathcal{B}^{(2)*}_{\ell' m'}\mathbf{X}_{\ell m}(\hat{\mathbf{r}})\cdot\mathbf{X}^*_{\ell' m'}(\hat{\mathbf{r}})\}\\ &= \int_0^S drr^2\{|\mathcal{B}^{(0)}_{\ell m}|^2 + |\mathcal{B}^{(2)}_{\ell m}|^2\}\\ &= |a_{L\ell m}|^2\Gamma_{n\ell}\,, \end{aligned}\tag{6.68}$$

where $\Gamma_{n\ell}$ can be evaluated analytically [see Appendix A]

$$\begin{aligned}\Gamma_{n\ell}/S^3 = \bar{\Gamma}_{n\ell} = &\frac{j_\ell(x_l)j'_\ell(x_l)}{x_l} + \frac{1}{2}[j^2_\ell(x_l) - j_{\ell-1}(x_l)j_{\ell+1}(x_l)]\\ &+ C^2\left\{\frac{j^2_\ell(x_t)}{x_t^2} + \frac{j_\ell(x_t)j'_\ell(x_t)}{x_t} + \frac{1}{2}[j^2_\ell(x_t) - j_{\ell-1}(x_t)j_{\ell+1}(x_t)]\right\}\\ &+ 2C\sqrt{\ell(\ell+1)}\left[\frac{j_\ell(x_l)j_\ell(x_t)}{x_l x_t}\right]\,.\end{aligned}\tag{6.69}$$

Combining Eq. (6.67) and Eq. (6.68) we obtain

$$|a_{Ln\ell m}|^2 = \frac{2k_BT}{\rho\Omega^2_{n\ell}}\frac{1}{\Gamma_{n\ell}}\tag{6.70}$$

For the BLS spectral density we start again from the general formula (6.55) and using Eq. (6.64) we have for the case of a solid sphere in vacuum

$$\begin{aligned}I(\mathbf{q},\omega) &\propto \sum_{n\ell m}4\pi(-\mathrm{i})^\ell Y_{\ell m}(\hat{\mathbf{q}})a_{L\ell m}\mathcal{W}_{n\ell}(S,q,Q_l,Q_t)\\ &\times \sum_{n'\ell' m'}4\pi\mathrm{i}^{\ell'}Y^*_{\ell' m'}(\hat{\mathbf{q}})a^*_{L\ell' m'}\mathcal{W}_{n'\ell'}(S,q,Q_l,Q_t)\delta(\omega-\Omega_{n'\ell'})\delta_{nn'}\delta_{\ell\ell'}\\ I(\mathbf{q},\omega) &\propto \sum_{n\ell m}(4\pi)^2\mathcal{W}^2_{n\ell}(S,q,Q_l,Q_t)\delta(\omega-\Omega_{n\ell})\sum_{m'}Y_{\ell m}(\hat{\mathbf{q}})Y^*_{\ell m'}(\hat{\mathbf{q}})a_{L\ell m}a^*_{L\ell m'}\end{aligned}\tag{6.71}$$

In order to carry out the sum over m', two different possibilities exist. Both of them are based on the fact that the spherical symmetry of the problem will impose isotropy of space. Precisely, we can either multiply Eq. (6.71) by the factor $\frac{1}{4\pi}\int d\hat{\mathbf{q}}$ or, by choosing the direction of the wavenumber $\mathbf{q}$ along the z axis, $\mathbf{q} = q\hat{\mathbf{z}}$, in the same equation. We result in the following two equations, respectively,

$$I(\mathbf{q},\omega)\propto 4\pi\sum_{n\ell m}|a_{L\ell m}|^2\mathcal{W}^2_{n\ell}(S,q,Q_l,Q_t)\delta(\omega-\Omega_{n\ell})\tag{6.72}$$

where we used the identity $\int d\hat{\mathbf{q}} Y_{\ell m}(\hat{\mathbf{q}}) Y^*_{\ell m'}(\hat{\mathbf{q}}) = \delta_{mm'}$, and

$$I(\mathbf{q},\omega) \propto 4\pi \sum_{n\ell} (2\ell+1) |a_{L\ell 0}|^2 \mathcal{W}^2_{n\ell}(S,q,Q_l,Q_t) \delta(\omega - \Omega_{n\ell}) \tag{6.73}$$

where we used Eq. (B.7). The two expressions for the BLS intensity [Eqs. (6.72), (6.73)] coincide, because the magnitude of the coefficient $a_{L\ell m}$ is independent of the value of m, $|a_{L\ell m}|^2 = |a_{L\ell 0}|^2$, and so the sum over m on a quantity independent of m just produces a factor of $(2\ell+1)$, $\sum_m |a_{L\ell m}|^2 = (2\ell+1)|a_{L\ell 0}|^2$.

The Brillouin intensity of the fundamental ($n = 1$) vibrational eigenmodes of a free vibrating polystyrene elastic sphere as a function of the product of scattering wavevector q and radius S are shown in Fig. 6.2. The missing $(1,1)$ mode is the zero frequency translational mode of a free particle. Still *et al.* [98] calculated the BLS intensity for a solid sphere in vacuum numerically from Eq. (6.41), and arrived at the same result. Not only our results matched but we performed the calculations much faster and with greater accuracy, since the errors due to numerical integration are eliminated.

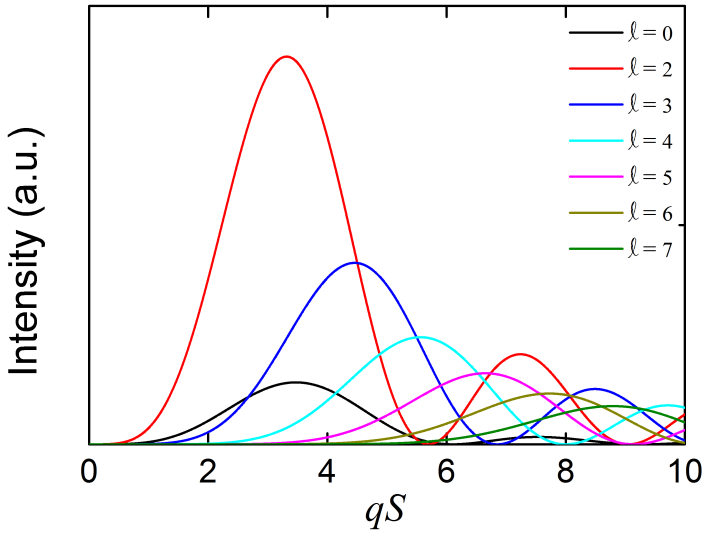

Figure 6.2: Brillouin intensity in arbitrary units for a free polystyrene sphere as a function of product of the wavevector q and the radius S. We depict the intensities for $n = 1$ and from $\ell = 0$ to 7, except from $\ell = 1$.

In an actual experimental setup it is not possible to measure the Brillouin intensity from a single isolated particle. Instead, phononic crystals are constructed from colloidal suspensions of spherical nanoparticles, e.g. polymer, which are deposited on a glass substrate and self-organize into crystal structures, usually followed by infiltration of appropriate fluid with refractive index almost equal to that of the polymer, in order to have

optical homogeneity as we already mentioned in § 6.2. As shown experimentally by Still *et al.* [98], a possible q dependence for the Brillouin intensity is lost because all scattering angles between $\theta = 0^\circ$ ($q = 0$) and 180° ($q_{max} = 4\pi n_r/\lambda$ with refractive index n_r) contribute to the spectra. Therefore, the theoretical BLS intensity at a given eigenfrequency must be obtained by integration of Eq. (6.73) over all possible qS values. The black vertical lines in Fig. 6.3 show the relative intensity values at the different eigenfrequencies (n, ℓ), resulting from the integration. We note that the relative intensities are in very good agreement with the experiment, despite the simplifications we considered to solve the theoretical problem. Because air exists between the spheres in the sample, they cannot interact strongly so the spectrum is greatly shaped by the eigenstates of the isolated sphere. However, the small interaction between the spheres causes the conversion from the discrete spectrum to continuous. A useful way to produce the continuous spectrum beginning from the isolated sphere is to broaden it, using a Gauss-Lorentz function given by the following expression [44, 102]

$$I(\omega) = \int dx A(x) \frac{\Gamma(x)}{[\omega - \Omega_p(x)]^2 - \Gamma^2(x)} \frac{e^{-\frac{(x-d)^2}{2\sigma^2}}}{\sqrt{2\pi}\sigma} \tag{6.74}$$

where x is the diameter of the particle with $\sigma = 0.03d$ [98] being its standard deviation and d its mean value, the experimental linewidth $\Gamma(x) = 0.28$ GHz [98], $\Omega_p(x) = 2\pi f_p d/x$ with f_p given in GHz, and $A(x)$ is a value proportional to the intensity of the eigenfrequency of the isolated particle which we want to broaden. Finally, the total broadened intensity will be the $\sum_p I(\omega)$ over all the eigenfrequencies, which we represent by the green line depicted in Fig. 6.3. Our results compare well with the experimental data, as well as with the fully-numerical results of Still *et al.* [98].

An important remark needs to be made here: in order to fit the experimental data we did not use the real values for the velocities of silica particles, but values that were slightly smaller (see caption of Fig. 6.3). This is an indication that, at this scale, the silica spheres must be porous and can be treated as effectively homogeneous.

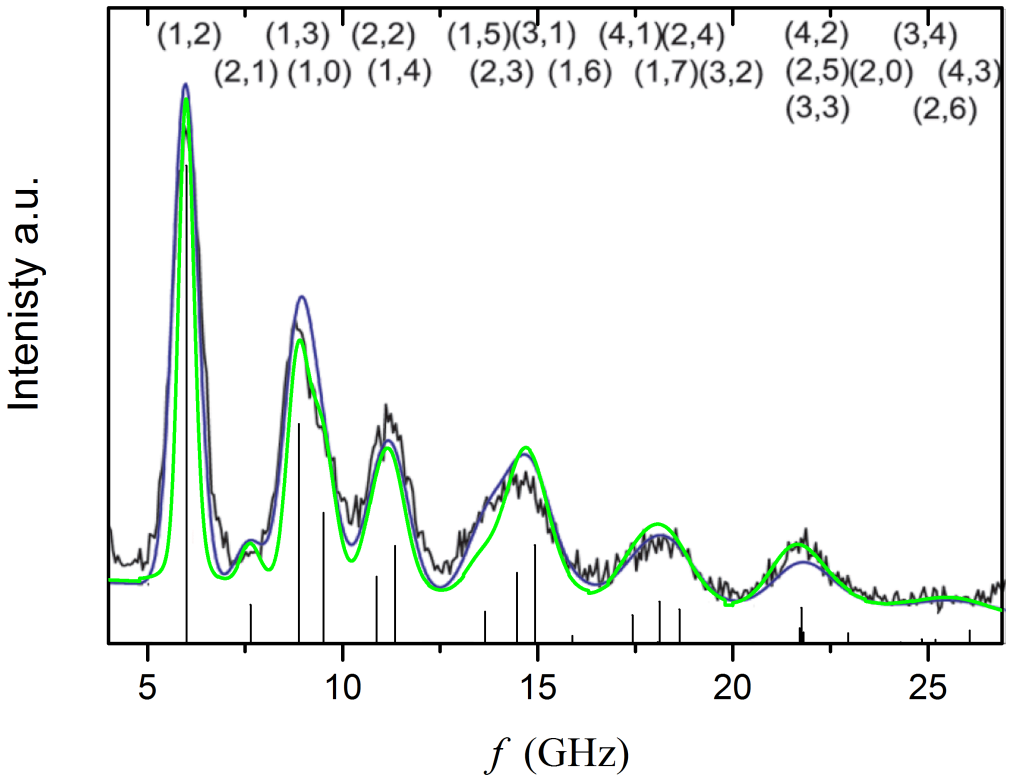

Figure 6.3: Brillouin intensity, in arbitrary units, from spherical silica particles with $c_l = 4226$ m/s and $c_t = 2530$ m/s, as a function of the frequency of the incident light. The black curve displays the experimental data [98], while the black vertical lines show the relative intensity values from the different eigenfrequencies (n, ℓ) that we calculated by integrating Eq. (6.73) over all possible qS values. The blue curve represents the broadening of the discrete spectrum performed by Still *et al.* [98], while the green curve is the result of our calculation.

Summary and perspectives

In summary, we generalized the LMS method to phononic crystals of poroelastic spheres immersed in a fluid medium, by combining Biot's theory with (multiple) scattering techniques. Specific applications of the method are presented for close-packed fcc crystals of submerged water-saturated porous silica and polymer spheres, encompassing the viscous and inertial coupling regimes. These structures can be viewed, also, as a particular class of double-porosity liquid-saturated granular materials. Calculated transmission and absorption spectra of finite slabs of these materials are analyzed by reference to the acoustic modes of the constituent spheres as well as to the dispersion diagrams of corresponding infinite crystals, providing a consistent interpretation of the observed features. For the elastically hard (silica) spheres with intermediate pore sizes, it is shown that, with increasing porosity, strong absorption leads to negligible transmission over an extended frequency range, which might be useful for broadband acoustic shielding applications. On the other hand, in the case of the elastically soft (polymer) spheres, our results reveal the existence of resonant modes with very long lifetime, localized in the spheres, in the inertial-coupling regime, i.e., when the radius of the spheres' pores is much larger than the viscous length. These modes, which can be easily tuned in frequency by adjusting the intrinsic porosity of the spheres, induce narrow dispersionless absorption bands as well as directional gaps in the transmission spectrum of finite slabs of the double-porosity material. This work paves the way towards a new class of phononic structures that exhibit unprecedented properties driven by the slow longitudinal waves, which are unique to poroelastic materials, and multiple-scattering effects. We note that these structures cannot be described by treating the poroelastic material as an effective homogeneous medium, and rigorous methods based on Biot's theory, such as that developed in the present thesis, are required.

Porosity naturally occurs in micro- and nanoparticles and the acoustic response of colloidal assemblies of such particles, in the hypersonic (GHz) regime, can be probed by BLS experiments. This is a powerful non-destructive characterization technique, which utilizes inelastic light scattering due to phonon-induced spatiotemporal variations of the refractive index of a material in order to monitor its frequency response. In this thesis, we developed a rigorous full elasto-optic theoretical formulation of BLS by single spherical particles in vacuum, based on Green's function techniques, and derived analytical expressions for the

BLS intensities, thus improving the computational efficiency and accuracy of previous calculations. Our formalism can be extended to the case of a solid particle embedded in an index-matching liquid which, though more difficult to treat, is of interest because the acoustic field is not exclusively confined inside the particle, thus leading to a continuous spectrum and not to a discrete one as for the particle in vacuum. The formalism provides, also, the theoretical basis for a rigorous interpretation of BLS experiments on periodic structures (hypersonic phononic crystals) beyond indirect explanations, e.g., in terms of the eigenmodes, the scattering cross section and the density of states of the individual particles or the frequency band structure of the colloidal crystal, solely in the framework of an elastodynamic description.

Appendix A

The Helmholtz equation for scalar fields, $\nabla^2 F(\mathbf{r}) + q^2 F(\mathbf{r}) = 0$, has solutions of the form $F(\mathbf{r}) = \sum_{\ell m} f_\ell(qr) Y_{\ell m}(\hat{\mathbf{r}})$, where $Y_{\ell m}(\hat{\mathbf{r}})$ are the spherical harmonics, $\hat{\mathbf{r}}$ denoting the dependence on the angles θ, ϕ of the vector $\mathbf{r}$ in the spherical coordinates and $f_\ell(qr)$ is the radial part of the solution of Helmholtz equation

$$\left[\frac{1}{r^2}\frac{\partial}{\partial r}\left(r^2\frac{\partial}{\partial r}\right) + q^2 - \frac{\ell(\ell+1)}{r^2}\right] f_\ell(qr) = 0\ , \tag{A.1}$$

or equivalently

$$f_\ell''(x) + \frac{2}{x} f_\ell'(x) + \left[1 - \frac{\ell(\ell+1)}{x^2}\right] f_\ell(x) = 0,\ x = qr, \tag{A.2}$$

if ∇^2 is expressed in spherical coordinates. Eq. (A.2) has, for a specific value of ℓ, two linearly independent solutions. Known forms of those solutions are the spherical Bessel, Neumann or Hankel of the 1^{st} or 2^{nd} kind functions, that are given by the following expressions

$$j_\ell(x) = \sqrt{\frac{\pi}{2x}} J_{\ell+1/2}(x) = (2x)^\ell \sum_{s=0}^{\infty} \frac{(-1)^s (s+\ell)!}{s!(2s+2\ell+1)!} x^{2s} \tag{A.3}$$

$$n_\ell(x) = \sqrt{\frac{\pi}{2x}} N_{\ell+1/2}(x) = 2(-2x)^{-\ell-1} \sum_{s=0}^{\infty} \frac{(-1)^s (s-\ell)!}{s!(2s-2\ell)!} x^{2s} \tag{A.4}$$

$$h_\ell^+(x) = j_\ell(x) + \mathrm{i} n_\ell(x) \tag{A.5}$$

$$h_\ell^-(x) = j_\ell(x) - \mathrm{i} n_\ell(x)\ . \tag{A.6}$$

We note that only the spherical Bessel function is regular at $x = 0$. In the following we list some useful recurrence relations that spherical functions obey

$$xf'_\ell(x) = \ell f_\ell(x) - xf_{\ell+1}(x) \tag{A.7}$$
$$(2\ell+1)f_\ell(x) = xf_{\ell-1}(x) + xf_{\ell+1}(x) \tag{A.8}$$
$$xf_{\ell-1}(x) = xf'_\ell(x) + (\ell+1)f_\ell(x) \tag{A.9}$$
$$(2\ell+1)f'_\ell(x) = \ell f_{\ell-1}(x) - (\ell+1)f_{\ell+1}(x)\ . \tag{A.10}$$

Their asymptotic behavior ($x \gg 1$) is

$$j_\ell(x \gg 1) \sim \frac{1}{x}\sin\left(x - \frac{\ell\pi}{2}\right) \tag{A.11}$$
$$n_\ell(x \gg 1) \sim -\frac{1}{x}\cos\left(x - \frac{\ell\pi}{2}\right) \tag{A.12}$$
$$h^+_\ell(x \gg 1) \sim (-\mathrm{i})^{\ell+1}\frac{e^{\mathrm{i}x}}{x} \tag{A.13}$$
$$h^-_\ell(x \gg 1) \sim \mathrm{i}^{\ell+1}\frac{e^{-\mathrm{i}x}}{x}\ , \tag{A.14}$$

while for small arguments ($x \ll 1$) the next apply

$$j_\ell(x \ll 1) \sim \frac{x^\ell}{(2\ell+1)!!} \tag{A.15}$$
$$n_\ell(x \ll 1) \sim -\frac{(2\ell-1)!!}{x^{\ell+1}}\ . \tag{A.16}$$

With the help of (A.2) and (A.7) it can be shown that

$$\int dr r^2 f_\ell(qr)g_\ell(q'r) = \frac{r^2}{q'^2 - q^2}[qf'_\ell(qr)g_\ell(q'r) - q'g'_\ell(q'r)f_\ell(qr)]\ , \tag{A.17}$$

and

$$\int dr r^2[f'_\ell(qr)g'_\ell(q'r) + \ell(\ell+1)\frac{f_\ell(qr)}{qr}\frac{g_\ell(q'r)}{q'r}] = \tag{A.18}$$
$$= \frac{r^2}{q'}f'_\ell(qr)g_\ell(q'r) + \frac{q}{q'}\int dr r^2 f_\ell(qr)g_\ell(q'r)] \tag{A.19}$$
$$= \frac{r^2}{q'^2 - q^2}[q'f'_\ell(qr)g_\ell(q'r) - qg'_\ell(q'r)f_\ell(qr)]\ , \tag{A.20}$$

where f_ℓ, g_ℓ can be any linear combination of the solutions of Bessel's differential equation (A.2). In the special case where $f_\ell(qr) = g_\ell(qr) = j_\ell(qr)$, Eq. (A.17) for $q' \to q$ yields

$$\int dr r^2 j^2_\ell(qr) = \frac{r^3}{2}[j^2_\ell(qr) - j_{\ell-1}(qr)j_{\ell+1}(qr)]\ , \tag{A.21}$$

while integration in Eqs. (A.17) and (A.21) over the entire radial space leads to

$$\int_0^\infty dr r^2 [j'_\ell(qr) j'_\ell(q'r) + \ell(\ell+1)\frac{j_\ell(qr)}{qr}\frac{j_\ell(q'r)}{q'r}] = \int_0^\infty dr r^2 j_\ell(qr) j_\ell(q'r) = \frac{\pi}{2q^2}\delta(q-q') \ . \tag{A.22}$$

Appendix B

The spherical harmonics $Y_{\ell m}(\hat{\mathbf{r}})$ are the angular part of the solution of the Helmholtz equation and they satisfy the following differential equation

$$\begin{aligned} \nabla^2 Y_{\ell m}(\hat{\mathbf{r}}) &= \left[\frac{1}{r^2}\frac{\partial}{\partial r}\left(r^2\frac{\partial}{\partial r}\right) - \frac{\mathbf{L}^2}{r^2}\right] Y_{\ell m}(\hat{\mathbf{r}}) \\ &= -\frac{\mathbf{L}^2}{r^2} Y_{\ell m}(\hat{\mathbf{r}}) = -\frac{\ell(\ell+1)}{r^2} Y_{\ell m}(\hat{\mathbf{r}}) \ , \end{aligned} \tag{B.1}$$

where $\mathbf{L}$ is the angular momentum operator and the argument $\hat{\mathbf{r}}$ denotes the dependence on the angles θ, ϕ of the vector $\mathbf{r}$ in the spherical coordinates. The spherical harmonics $Y_{\ell m}(\hat{\mathbf{r}})$ are given from the expression

$$Y_{\ell m}(\hat{\mathbf{r}}) = (-1)^m \sqrt{\frac{2\ell+1}{4\pi}\frac{(\ell-m)!}{(\ell+m)!}} P_\ell^m(\cos\theta) e^{\mathrm{i}m\phi} \ , \tag{B.2}$$

with $\ell = 0, 1, 2, \cdots$, $m = -\ell, -\ell+1, \cdots, \ell-1, \ell$ and $P_\ell^m(\cos\theta)$ are the associated Legendre polynomials

$$P_\ell^m(x) = \frac{1}{2^\ell \ell!}(1-x^2)^{m/2}\frac{d^{\ell+m}}{dx^{\ell+m}}(x^2-1)^\ell \ , \quad x = \cos\theta \ , \text{for } m > 0, \tag{B.3}$$

while for $m < 0$ they are given from

$$P_\ell^{-m}(x) = (-1)^m \frac{(\ell-m)!}{(\ell+m)!} P_\ell^m(x) \ . \tag{B.4}$$

The above relations result in

$$Y_{\ell m}^*(\hat{\mathbf{r}}) = (-1)^m Y_{\ell -m}(\hat{\mathbf{r}}) \ , \tag{B.5}$$

and

$$Y_{\ell m}(-\hat{\mathbf{r}}) = (-1)^\ell Y_{\ell m}(\hat{\mathbf{r}}) \tag{B.6}$$

$$Y_{\ell m}(\theta = 0, \phi) = \sqrt{\frac{2\ell+1}{4\pi}}\delta_{m0} \ . \tag{B.7}$$

$Y_{\ell m}(\hat{\mathbf{r}})$ satisfy a series of important relations, like the orthonormality and completeness relations

$$\int d\hat{\mathbf{r}}\; Y_{\ell m}(\hat{\mathbf{r}}) Y^*_{\ell' m'}(\hat{\mathbf{r}}) = \delta_{\ell\ell'}\delta_{mm'} \tag{B.8}$$

$$\sum_{\ell m} Y_{\ell m}(\hat{\mathbf{r}}) Y^*_{\ell m}(\hat{\mathbf{r}}') = \delta(\hat{\mathbf{r}} - \hat{\mathbf{r}}')\;, \tag{B.9}$$

or the following relations that connect spherical harmonics of different order

$$\cos\theta Y_{\ell m}(\hat{\mathbf{r}}) = \zeta^m_{\ell+1} Y_{\ell+1 m}(\hat{\mathbf{r}}) + \zeta^m_{\ell} Y_{\ell-1 m}(\hat{\mathbf{r}}) \tag{B.10}$$

$$e^{\mathrm{i}\phi}\sin\theta Y_{\ell m}(\hat{\mathbf{r}}) = 2\left(\gamma^{-m}_{\ell} Y_{\ell-1 m+1}(\hat{\mathbf{r}}) - \gamma^{m+1}_{\ell+1} Y_{\ell+1 m+1}(\hat{\mathbf{r}})\right) \tag{B.11}$$

$$e^{-\mathrm{i}\phi}\sin\theta Y_{\ell m}(\hat{\mathbf{r}}) = 2\left(\gamma^{-m+1}_{\ell+1} Y_{\ell+1 m-1}(\hat{\mathbf{r}}) - \gamma^{m}_{\ell} Y_{\ell-1 m-1}(\hat{\mathbf{r}})\right) \tag{B.12}$$

$$m\cot\theta Y_{\ell m}(\hat{\mathbf{r}}) = -\left[\alpha^m_{\ell} e^{-\mathrm{i}\phi} Y_{\ell m+1}(\hat{\mathbf{r}}) + \alpha^{-m}_{\ell} e^{\mathrm{i}\phi} Y_{\ell m-1}(\hat{\mathbf{r}})\right]\;, \tag{B.13}$$

and even the following

$$\frac{\partial Y_{\ell m}(\hat{\mathbf{r}})}{\partial\theta} = \alpha^m_{\ell} e^{-\mathrm{i}\phi} Y_{\ell m+1}(\hat{\mathbf{r}}) - \alpha^{-m}_{\ell} e^{\mathrm{i}\phi} Y_{\ell m-1}(\hat{\mathbf{r}}) \tag{B.14}$$

$$= \mathrm{i}\psi_{\ell} X_{\ell m,\phi}(\hat{\mathbf{r}}) \tag{B.15}$$

$$\frac{\partial Y_{\ell m}(\hat{\mathbf{r}})}{\partial\phi} = \mathrm{i}m Y_{\ell m}(\hat{\mathbf{r}}) \tag{B.16}$$

$$= -\mathrm{i}\psi_{\ell}\sin\theta X_{\ell m,\theta}(\hat{\mathbf{r}})\;. \tag{B.17}$$

Finally, it applies

$$\begin{aligned}\nabla\left[f_{\ell}(qr) Y_{\ell m}(\hat{\mathbf{r}})\right] &= f_{\ell}(qr)\nabla Y_{\ell m}(\hat{\mathbf{r}}) + q f'_{\ell}(qr) Y_{\ell m}(\hat{\mathbf{r}})\hat{\mathbf{r}} \\ &= \mathrm{i}\psi_{\ell}\frac{f_{\ell}(qr)}{r}\left(X_{\ell m,\phi}(\hat{\mathbf{r}})\hat{\boldsymbol{\theta}} - X_{\ell m,\theta}(\hat{\mathbf{r}})\hat{\boldsymbol{\phi}}\right) \\ &+ q f'_{\ell}(qr) Y_{\ell m}(\hat{\mathbf{r}})\hat{\mathbf{r}}\;.\end{aligned} \tag{B.18}$$

In the above expressions ψ_{ℓ}, α^m_{ℓ}, γ^m_{ℓ}, ζ^m_{ℓ} are given from

$$\psi_{\ell} = \sqrt{\ell(\ell+1)} \tag{B.19}$$

$$\alpha^m_{\ell} = \frac{1}{2}[(\ell-m)(\ell+m+1)]^{1/2} \tag{B.20}$$

$$\gamma^m_{\ell} = \frac{1}{2}\left[(\ell+m)(\ell+m-1)\right]^{1/2} / \left[(2\ell-1)(2\ell+1)\right]^{1/2} \tag{B.21}$$

$$\zeta^m_{\ell} = [(\ell+m)(\ell-m)]^{1/2}/[(2\ell-1)(2\ell+1)]^{1/2}\;, \tag{B.22}$$

and $X_{\ell m,\theta}(\hat{\mathbf{r}})$, $X_{\ell m,\phi}(\hat{\mathbf{r}})$ are the components of the vector spherical harmonic functions $\mathbf{X}_{\ell m}(\hat{\mathbf{r}})$, that are defined as

$$\psi_\ell \mathbf{X}_{\ell m}(\hat{\mathbf{r}}) = \mathbf{L} Y_{\ell m}(\hat{\mathbf{r}}) \equiv -\mathrm{i}\mathbf{r} \times \nabla Y_{\ell m}(\hat{\mathbf{r}}) \; . \tag{B.23}$$

We note that here we adopt the usual notation r, θ, ϕ for the unitary vectors and the corresponding vector components in spherical coordinates, instead of the indices $1, 2, 3$, that we usually follow. By definition $\mathbf{X}_{00}(\hat{\mathbf{r}}) = \mathbf{0}$, while for $\ell \geq 1$ we have

$$\begin{aligned}
\psi_\ell \mathbf{X}_{\ell m}(\hat{\mathbf{r}}) &= \left[\alpha_\ell^{-m} \cos\theta \; e^{\mathrm{i}\phi} \; Y_{\ell m-1}(\hat{\mathbf{r}}) - m \sin\theta \; Y_{\ell m}(\hat{\mathbf{r}}) \right. \\
&+ \left. \alpha_\ell^{m} \cos\theta \; e^{-\mathrm{i}\phi} \; Y_{\ell m+1}(\hat{\mathbf{r}}) \right] \hat{\boldsymbol{\theta}} \\
&+ \mathrm{i} \left[\alpha_\ell^{-m} \; e^{\mathrm{i}\phi} \; Y_{\ell m-1}(\hat{\mathbf{r}}) - \alpha_\ell^{m} \; e^{-\mathrm{i}\phi} \; Y_{\ell m+1}(\hat{\mathbf{r}}) \right] \hat{\boldsymbol{\phi}} \qquad \text{(B.24)} \\
&= \alpha_\ell^{-m} \; Y_{\ell m-1}(\hat{\mathbf{r}}) \; (\hat{\mathbf{e}}_x + \mathrm{i}\hat{\mathbf{e}}_y) + m \; Y_{\ell m}(\hat{\mathbf{r}}) \; \hat{\mathbf{e}}_z \\
&+ \alpha_\ell^{m} \; Y_{\ell m+1}(\hat{\mathbf{r}}) \; (\hat{\mathbf{e}}_x - \mathrm{i}\hat{\mathbf{e}}_y) \; . \qquad \text{(B.25)}
\end{aligned}$$

From $\mathbf{L}^2 Y_{\ell m} = \ell(\ell+1) Y_{\ell m}$ and $\mathbf{L}^2 \mathbf{L} = \mathbf{L}\mathbf{L}^2$ it will apply that $\mathbf{L}^2 \mathbf{X}_{\ell m}(\hat{\mathbf{r}}) = \ell(\ell+1)\mathbf{X}_{\ell m}(\hat{\mathbf{r}})$. From (B.23) we derive

$$\mathbf{X}^*_{\ell m}(\hat{\mathbf{r}}) = (-1)^{m+1} \mathbf{X}_{\ell -m}(\hat{\mathbf{r}}) \; , \tag{B.26}$$

and also

$$\mathbf{X}_{\ell m}(\hat{\mathbf{r}}) \times \hat{\mathbf{r}} = X_{\ell m,\phi}(\hat{\mathbf{r}}) \hat{\boldsymbol{\theta}} - X_{\ell m,\theta}(\hat{\mathbf{r}}) \hat{\boldsymbol{\phi}} = \frac{-\mathrm{i} r \nabla Y_{\ell m}}{\psi_\ell} \tag{B.27}$$

and

$$\hat{\mathbf{r}} \times (\mathbf{X}_{\ell m}(\hat{\mathbf{r}}) \times \hat{\mathbf{r}}) = \mathbf{X}_{\ell m}(\hat{\mathbf{r}}) \; . \tag{B.28}$$

The following relations describe the action of the operators $\nabla\times$ and $\nabla\cdot$ on $\mathbf{X}_{\ell m}(\hat{\mathbf{r}})$

$$\begin{aligned}
\nabla \times \mathbf{X}_{\ell m}(\hat{\mathbf{r}}) &= \frac{1}{r} \left[\mathrm{i}\psi_\ell Y_{\ell m}(\hat{\mathbf{r}}) \hat{\mathbf{r}} - X_{\ell m,\phi}(\hat{\mathbf{r}}) \hat{\boldsymbol{\theta}} + X_{\ell m,\theta}(\hat{\mathbf{r}}) \hat{\boldsymbol{\phi}} \right] \\
&= \frac{1}{r} \left[\mathrm{i}\psi_\ell Y_{\ell m}(\hat{\mathbf{r}}) \hat{\mathbf{r}} - \mathbf{X}_{\ell m}(\hat{\mathbf{r}}) \times \hat{\mathbf{r}} \right] \\
&= \frac{\mathrm{i}}{\psi_\ell} \left[\frac{\psi_\ell^2}{r} Y_{\ell m}(\hat{\mathbf{r}}) \hat{\mathbf{r}} + \nabla Y_{\ell m}(\hat{\mathbf{r}}) \right] \qquad \text{(B.29)}
\end{aligned}$$

and

$$\nabla \cdot \mathbf{X}_{\ell m}(\hat{\mathbf{r}}) = 0, \tag{B.30}$$

while with their help we obtain

$$\begin{aligned}
\nabla \times f_\ell(x) \mathbf{X}_{\ell m}(\hat{\mathbf{r}}) &= q \left\{ \mathrm{i}\psi_\ell \frac{f_\ell(x)}{x} Y_{\ell m}(\hat{\mathbf{r}}) \hat{\mathbf{r}} - \left[f'_\ell(x) + \frac{f_\ell(x)}{x} \right] \mathbf{X}_{\ell m}(\hat{\mathbf{r}}) \times \hat{\mathbf{r}} \right\} \qquad \text{(B.31)} \\
\nabla \cdot [f_\ell(x) \mathbf{X}_{\ell m}(\hat{\mathbf{r}})] &= 0 \qquad \text{(B.32)} \\
\nabla^2 [f_\ell(x) \mathbf{X}_{\ell m}(\hat{\mathbf{r}})] &= -\nabla \times [\nabla \times f_\ell(x) \mathbf{X}_{\ell m}(\hat{\mathbf{r}})] = -q^2 f_\ell(x) \mathbf{X}_{\ell m}(\hat{\mathbf{r}}) \qquad \text{(B.33)}
\end{aligned}$$

with $x = qr$. For the last one we used the relation

$$\begin{aligned} \nabla \{\nabla \cdot [f_\ell(x)\mathbf{X}_{\ell m}(\hat{\mathbf{r}})]\} &= \nabla [\nabla f_\ell(x) \cdot \mathbf{X}_{\ell m}(\hat{\mathbf{r}}) + f_\ell(x) \nabla \cdot \mathbf{X}_{\ell m}(\hat{\mathbf{r}})] \\ &= \nabla [\nabla f_\ell(x) \cdot \mathbf{X}_{\ell m}(\hat{\mathbf{r}})] = 0 \, . \end{aligned} \tag{B.34}$$

The vector spherical harmonics satisfy the following orthonormality relation

$$\int d\hat{\mathbf{r}} a \; \mathbf{X}_{\ell m}(\hat{\mathbf{r}}) \cdot \mathbf{X}^*_{\ell' m'}(\hat{\mathbf{r}}) = \delta_{\ell\ell'}\delta_{mm'} \tag{B.35}$$

$$\int d\hat{\mathbf{r}} \; \mathbf{X}_{\ell m}(\hat{\mathbf{r}}) \cdot [\hat{\mathbf{r}} \times \mathbf{X}^*_{\ell' m'}(\hat{\mathbf{r}})] = 0 \, , \tag{B.36}$$

resulting in

$$\begin{aligned} & \sum_{\ell m} \left\{ \mathcal{A}^{(1)}_{\ell m}(r) \mathbf{X}_{\ell m}(\hat{\mathbf{r}}) + \mathcal{A}^{(2)}_{\ell m}(r) \, [\hat{\mathbf{r}} \times \mathbf{X}_{\ell m}(\hat{\mathbf{r}})] \right\} = 0 \\ \Rightarrow \quad & \mathcal{A}^{(1)}_{\ell m}(r) = 0 = \mathcal{A}^{(2)}_{\ell m}(r) \, . \end{aligned} \tag{B.37}$$

At last, it can be shown that

$$\int d\hat{\mathbf{r}} \; \mathbf{X}_{\ell m}(\hat{\mathbf{r}}) \cdot \nabla \times [f(r) \mathbf{X}^*_{\ell' m'}(\hat{\mathbf{r}})] = 0 \, , \tag{B.38}$$

and, with the help of (B.8), (B.25), that

$$\begin{aligned} \int d\hat{\mathbf{r}} \; Y_{\ell m}(\hat{\mathbf{r}}) \mathbf{X}^*_{\ell' m'}(\hat{\mathbf{r}}) &= \frac{\delta_{\ell\ell'}}{\psi_\ell} \Big[\delta_{m+1m'} \alpha^{-m'}_{\ell'} (\hat{\mathbf{e}}_x - \mathrm{i}\hat{\mathbf{e}}_y) \\ &+ \delta_{mm'} m \hat{\mathbf{e}}_z + \delta_{m-1m'} \alpha^{m'}_{\ell'} (\hat{\mathbf{e}}_x + \mathrm{i}\hat{\mathbf{e}}_y) \Big] \, , \end{aligned} \tag{B.39}$$

$$\begin{aligned} \int d\hat{\mathbf{r}} \; Y_{\ell m}(\hat{\mathbf{r}}) Y^*_{\ell' m'}(\hat{\mathbf{r}}) \, \hat{\mathbf{r}} &= \delta_{m+1m'} \left(-\gamma^{m+1}_{\ell+1} \delta_{\ell+1\ell'} + \gamma^{-m}_{\ell} \delta_{\ell-1\ell'} \right) (\hat{\mathbf{e}}_x - \mathrm{i}\hat{\mathbf{e}}_y) \\ &+ \delta_{m-1m'} \left(\gamma^{-m+1}_{\ell+1} \delta_{\ell+1\ell'} - \gamma^{m}_{\ell} \delta_{\ell-1\ell'} \right) (\hat{\mathbf{e}}_x + \mathrm{i}\hat{\mathbf{e}}_y) \\ &+ \delta_{mm'} \left(\zeta^{m}_{\ell+1} \delta_{\ell+1\ell'} + \zeta^{m}_{\ell} \delta_{\ell-1\ell'} \right) \hat{\mathbf{e}}_z \, , \end{aligned} \tag{B.40}$$

and

$$\begin{aligned} \int d\hat{\mathbf{r}} \; Y_{\ell m}(\hat{\mathbf{r}}) \mathbf{X}^*{}_{\ell' m'}(\hat{\mathbf{r}}) \times \hat{\mathbf{r}} &= \frac{\mathrm{i}\delta_{m'm+1}}{\psi_{\ell'}} \Big[-(\ell'+1) \gamma^{m'}_{\ell'} \delta_{\ell'\ell+1} - \ell' \gamma^{-m'+1}_{\ell'+1} \delta_{\ell'\ell-1} \Big] (\hat{\mathbf{e}}_x - \mathrm{i}\hat{\mathbf{e}}_y) \\ &+ \frac{\mathrm{i}\delta_{m'm-1}}{\psi_{\ell'}} \Big[(\ell'+1) \gamma^{-m'}_{\ell'} \delta_{\ell'\ell+1} + \ell' \gamma^{m'+1}_{\ell'+1} \delta_{\ell'\ell-1} \Big] (\hat{\mathbf{e}}_x + \mathrm{i}\hat{\mathbf{e}}_y) \\ &+ \frac{\mathrm{i}\delta_{m'm}}{\psi_{\ell'}} \Big[(\ell'+1) \zeta^{m'}_{\ell'} \delta_{\ell'\ell+1} - \ell' \zeta^{m'}_{\ell'+1} \delta_{\ell'\ell-1} \Big] \hat{\mathbf{e}}_z \, . \end{aligned} \tag{B.41}$$

By defining the quantities

$$\chi_\ell = \sqrt{\frac{(\ell-1)(\ell+1)}{\ell^2}} \tag{B.42}$$

$$\xi_\ell^m = \frac{1}{2(\ell+1)}\sqrt{\frac{\ell(\ell+2)(\ell+m+1)(\ell+m+2)}{(2\ell+1)(2\ell+3)}}\,, \tag{B.43}$$

we evaluate the following integrals

$$\int d\hat{\mathbf{r}}\cos\theta \mathbf{X}_{\ell m}(\hat{\mathbf{r}})\cdot\mathbf{X}^*{}_{\ell' m'}(\hat{\mathbf{r}}) = \left[\chi_\ell\zeta_\ell^m\delta_{\ell'\ell-1} + \chi_{\ell+1}\zeta_{\ell+1}^m\delta_{\ell'\ell+1}\right]\delta_{m'm} \tag{B.44}$$

$$\int d\hat{\mathbf{r}}\cos\theta \mathbf{X}_{\ell m}(\hat{\mathbf{r}})\cdot[\hat{\mathbf{r}}\times\mathbf{X}^*{}_{\ell' m'}(\hat{\mathbf{r}})] = \frac{\mathrm{i}m}{\psi_\ell^2}\delta_{\ell'\ell}\delta_{m'm} \tag{B.45}$$

$$\int d\hat{\mathbf{r}}\sin\theta\sin\phi \mathbf{X}_{\ell m}(\hat{\mathbf{r}})\cdot\mathbf{X}^*{}_{\ell' m'}(\hat{\mathbf{r}}) = \mathrm{i}\left[\xi_\ell^m\delta_{\ell'\ell+1} - \xi_{\ell-1}^{-m-1}\delta_{\ell'\ell-1}\right]\delta_{m'm+1} \tag{B.46}$$

$$+ \mathrm{i}\left[\xi_\ell^{-m}\delta_{\ell'\ell+1} - \xi_{\ell-1}^{m-1}\delta_{\ell'\ell-1}\right]\delta_{m'm-1} \tag{B.47}$$

$$\int d\hat{\mathbf{r}}\sin\theta\sin\phi \mathbf{X}_{\ell m}(\hat{\mathbf{r}})\cdot[\hat{\mathbf{r}}\times\mathbf{X}^*{}_{\ell' m'}(\hat{\mathbf{r}})] = \frac{\delta_{\ell'\ell}}{\psi_\ell^2}\left[\alpha_\ell^m\delta_{m'm+1} - \alpha_\ell^{-m}\delta_{m'm-1}\right] \tag{B.48}$$

$$\int d\hat{\mathbf{r}}\sin\theta\cos\phi \mathbf{X}_{\ell m}(\hat{\mathbf{r}})\cdot\mathbf{X}^*{}_{\ell' m'}(\hat{\mathbf{r}}) = \left[-\xi_\ell^m\delta_{\ell'\ell+1} + \xi_{\ell-1}^{-m-1}\delta_{\ell'\ell-1}\right]\delta_{m'm+1} \tag{B.49}$$

$$+ \left[\xi_\ell^{-m}\delta_{\ell'\ell+1} - \xi_{\ell-1}^{m-1}\delta_{\ell'\ell-1}\right]\delta_{m'm-1} \tag{B.50}$$

$$\int d\hat{\mathbf{r}}\sin\theta\cos\phi \mathbf{X}_{\ell m}(\hat{\mathbf{r}})\cdot[\hat{\mathbf{r}}\times\mathbf{X}^*{}_{\ell' m'}(\hat{\mathbf{r}})] = \frac{\mathrm{i}\delta_{\ell'\ell}}{\psi_\ell^2}\left[\alpha_\ell^m\delta_{m'm+1} + \alpha_\ell^{-m}\delta_{m'm-1}\right]\,. \tag{B.51}$$

It is useful to note here that in the more general case three vector spherical harmonics can be defined [104]

$$\mathbf{X}_{\ell m}^{(1)}(\hat{\mathbf{r}}) \equiv Y_{\ell m}(\hat{\mathbf{r}})\hat{\mathbf{r}}\,, \tag{B.52}$$

$$\mathbf{X}_{\ell m}^{(2)}(\hat{\mathbf{r}}) \equiv -\frac{\mathrm{i}}{\psi_\ell}\mathbf{r}\times\boldsymbol{\nabla}Y_{\ell m}(\hat{\mathbf{r}})\,, \tag{B.53}$$

$$\mathbf{X}_{\ell m}^{(3)}(\hat{\mathbf{r}}) \equiv \frac{r}{\psi_\ell}\boldsymbol{\nabla}Y_{\ell m}(\hat{\mathbf{r}})\,, \tag{B.54}$$

forming a complete set and orthonormal basis in the sense

$$\sum_{\ell m\sigma}\mathbf{X}_{\ell m}^{(\sigma)}(\hat{\mathbf{r}})\mathbf{X}_{\ell m}^{(\sigma)*}(\hat{\mathbf{r}}') = \mathbb{1}\delta(\hat{\mathbf{r}}-\hat{\mathbf{r}}')\,, \tag{B.55}$$

$$\int d\hat{\mathbf{r}}\ \mathbf{X}_{\ell m}^{(\sigma)}(\hat{\mathbf{r}})\cdot\mathbf{X}_{\ell' m'}^{(\sigma')*}(\hat{\mathbf{r}}) = \delta_{\ell\ell'}\delta_{mm'}\delta_{\sigma\sigma'}\,, \tag{B.56}$$

where the first is written in dyadic notation and σ is meant to assume the values $1, 2, 3$. Then it is easy to express the vector spherical waves (2.56), (2.57) and (2.58) in the vector spherical harmonic basis, using also (B.18), (B.31),

$$\mathbf{J}_{L\ell m}(\mathbf{r}) = j'_\ell(q_l r)\mathbf{X}^{(1)}_{\ell m}(\hat{\mathbf{r}}) + \frac{j_\ell(q_l r)}{q_l r}\psi_\ell \mathbf{X}^{(3)}_{\ell m}(\hat{\mathbf{r}}) \ , \tag{B.57}$$

$$\mathbf{J}_{N\ell m}(\mathbf{r}) = -\frac{j_\ell(q_t r)}{q_t r}\psi_\ell \mathbf{X}^{(1)}_{\ell m}(\hat{\mathbf{r}}) - \left[j'_\ell(q_t r) + \frac{j_\ell(q_t r)}{q_t r}\right]\mathbf{X}^{(3)}_{\ell m}(\hat{\mathbf{r}}) \ , \tag{B.58}$$

$$\mathbf{J}_{M\ell m}(\mathbf{r}) = j_\ell(q_t r)\mathbf{X}^{(2)}_{\ell m}(\hat{\mathbf{r}}) \ . \tag{B.59}$$

We note that everytime the superscript is omitted, we tacitly assume that $\mathbf{X}_{\ell m}(\hat{\mathbf{r}}) \equiv \mathbf{X}^{(2)}_{\ell m}(\hat{\mathbf{r}})$.

Appendix C

Writing, in the general case, the elastic field $\mathbf{u}(\mathbf{r})$ as a linear combination of (2.56), (2.57) and (2.58), with appropriate coefficients $a_{P\ell m}$, $P = L, M, N$, we can express $\mathbf{u}(\mathbf{r})$ in spherical coordinates

$$\begin{aligned} u_r &= \sum_{\ell m} \mathcal{B}^{(0)}_{\ell m} Y_{\ell m}(\hat{\mathbf{r}}) \\ u_\theta &= \sum_{\ell m} \left[\mathcal{B}^{(1)}_{\ell m} X_{\ell m;\theta}(\hat{\mathbf{r}}) - \mathcal{B}^{(2)}_{\ell m} X_{\ell m;\phi}(\hat{\mathbf{r}}) \right] \\ u_\phi &= \sum_{\ell m} \left[\mathcal{B}^{(2)}_{\ell m} X_{\ell m;\theta}(\hat{\mathbf{r}}) + \mathcal{B}^{(1)}_{\ell m} X_{\ell m;\phi}(\hat{\mathbf{r}}) \right] . \end{aligned} \tag{C.1}$$

Accordingly, we can find, after a relatively easy algebraic manipulation, the corresponding relations for the surface traction $\boldsymbol{\tau}(\mathbf{r})$ in spherical coordinates [Eq. (1.46)] using the above general form (C.1) for the elastic field $\mathbf{u}(\mathbf{r})$

$$\begin{aligned} \tau_r &= \sum_{\ell m} \mathcal{B}^{(3)}_{\ell m} Y_{\ell m}(\hat{\mathbf{r}}) \\ \tau_\theta &= \sum_{\ell m} \left[\mathcal{B}^{(4)}_{\ell m} X_{\ell m;\theta}(\hat{\mathbf{r}}) - \mathcal{B}^{(5)}_{\ell m} X_{\ell m;\phi}(\hat{\mathbf{r}}) \right] \\ \tau_\phi &= \sum_{\ell m} \left[\mathcal{B}^{(5)}_{\ell m} X_{\ell m;\theta}(\hat{\mathbf{r}}) + \mathcal{B}^{(4)}_{\ell m} X_{\ell m;\phi}(\hat{\mathbf{r}}) \right] , \end{aligned} \tag{C.2}$$

where

$$
\begin{aligned}
\mathcal{B}^{(0)}_{\ell m} &= a_{L\ell m} f'_\ell(x_l) - a_{N\ell m}\psi_\ell \frac{f_\ell(x_t)}{x_t} \\
\mathcal{B}^{(1)}_{\ell m} &= a_{M\ell m} f_\ell(x_t) \\
\mathcal{B}^{(2)}_{\ell m} &= \mathrm{i}\left[-a_{L\ell m}\psi_\ell \frac{f_\ell(x_l)}{x_l} + a_{N\ell m}\frac{x_t f'_\ell(x_t) + f_\ell(x_t)}{x_t}\right] \\
\mathcal{B}^{(3)}_{\ell m} &= -a_{L\ell m}\rho q_l \left[c_l^2 f_\ell(x_l) + 2c_t^2 \frac{2x_l f'_\ell(x_l) - \psi_\ell^2 f_\ell(x_l)}{x_l^2}\right] \\
&\quad -a_{N\ell m} 2\rho c_t^2 q_t \psi_\ell \frac{x_t f'_\ell(x_t) - f_\ell(x_t)}{x_t^2} \\
\mathcal{B}^{(4)}_{\ell m} &= a_{M\ell m}\rho c_t^2 q_t \frac{x_t f'_\ell(x_t) - f_\ell(x_t)}{x_t} \\
\mathcal{B}^{(5)}_{\ell m} &= -2\mathrm{i}\rho c_t^2 \left\{ a_{L\ell m}\psi_\ell q_l \frac{x_l f'_\ell(x_l) - f_\ell(x_l)}{x_l^2} \right. \\
&\quad \left. + a_{N\ell m} q_t \frac{f_\ell(x_t)\left[1 + x_t^2/2 - \psi_\ell^2\right] + x_t f'_\ell(x_t)}{x_t^2} \right\}
\end{aligned}
\tag{C.3}
$$

and $x_\nu = q_\nu r$, $\nu = l, t$. The above expressions apply in the case of elastic media that allow the propagation of both longitudinal and transverse waves. Although, in the case of non-viscous fluids, where only longitudinal waves can propagate, the expressions (C.3) are replaced by

$$
\begin{aligned}
\mathcal{B}^{(0)}_{\ell m} &= a_{L\ell m} f'_\ell(x_l) \\
\mathcal{B}^{(1)}_{\ell m} &= 0 \\
\mathcal{B}^{(2)}_{\ell m} &= -\mathrm{i} a_{L\ell m}\psi_\ell \frac{f_\ell(x_l)}{x_l} \\
\mathcal{B}^{(3)}_{\ell m} &= -a_{L\ell m}\rho q_l c_l^2 f_\ell(x_l) \\
\mathcal{B}^{(4)}_{\ell m} &= 0 \\
\mathcal{B}^{(5)}_{\ell m} &= 0\,.
\end{aligned}
\tag{C.4}
$$

Appendix D

Double porosity models must reduce to single porosity models in the appropriate limit. It is, therefore, necessary to remind ourselves of the basic results for single porosity models in poroelasticity. The results presented in this appendix apply specifically to the single porosity models, or else, to the properties characteristic of the matrix material in double porosity.

For isotropic materials and hydrostatic pressure variations, the two independent variables in linear mechanics of porous media are the confining (external) pressure p_c and the fluid (pore) pressure p. The differential pressure $p_d \equiv p_c - p$ is often used to eliminate the confining pressure. The equations of the fundamental dilatations are then

$$-\frac{\delta V}{V} = \frac{\delta p_d}{K} + \frac{\delta p}{K_s} \quad \text{for the total volume } V, \tag{D.1}$$

$$-\frac{\delta V_\phi}{V_\phi} = \frac{\delta p_d}{K_p} + \frac{\delta p}{K_\phi} \quad \text{for the pore volume } V_\phi = \phi V, \text{ and} \tag{D.2}$$

$$-\frac{\delta V_f}{V_f} = \frac{\delta p}{K_f} \quad \text{for the fluid volume } V_f, \tag{D.3}$$

where K is the drained frame bulk modulus[1], K_s is the unjacketed bulk modulus for the composite frame, K_p is the jacketed pore modulus, K_ϕ is the unjacketed pore modulus and K_f the bulk modulus of the pore fluid.

We define the dependent variables $e \equiv \frac{\delta V}{V}$ and $\zeta \equiv \frac{\delta V_\phi - \delta V_f}{V}$, both of which are positive on expansion, and which are respectively the total volume dilatation and the increment of fluid content. Then, it follows directly

$$\begin{pmatrix} e \\ -\zeta \end{pmatrix} = \begin{pmatrix} 1/K & 1/K_s - 1/K \\ -\phi/K_p & \phi(1/K_p + 1/K_f - 1/K_\phi) \end{pmatrix} \begin{pmatrix} -p_c \\ -p \end{pmatrix} . \tag{D.4}$$

We can define now the Skempton's pore-pressure buildup coefficient B to be

$$B \equiv \left. \frac{\partial p}{\partial p_c} \right|_{\zeta=0} , \tag{D.5}$$

[1] $K \equiv K_b$, $\phi \equiv f$ the porosity

and is therefore given by

$$B = \frac{1}{1 + K_p(1/K_f - 1/K_\phi)} \ . \tag{D.6}$$

It follows immediately from this definition that the undrained modulus K_u is determined by

$$K_u \equiv -\frac{1}{V}\frac{\partial V}{\partial p_c}\Big|_{\zeta=0} = \frac{K}{1-\alpha B} \ . \tag{D.7}$$

where we introduced the Biot-Willis parameter $\alpha = 1 - \frac{K}{K_s}$. Finally we condense the general relations together with the reciprocity relations [103] into symmetric form as

$$\begin{pmatrix} e \\ -\zeta \end{pmatrix} = \begin{pmatrix} 1/K & -\alpha/K \\ -\alpha/K & \alpha/BK \end{pmatrix} \begin{pmatrix} -p_c \\ -p \end{pmatrix} \ . \tag{D.8}$$

A storage compressibility can be defined as

$$S \equiv \frac{\delta\zeta}{\delta p}\Big|_{\delta p_c=0} = \frac{\alpha}{BK} \ . \tag{D.9}$$

This storage compressibility is the change in increment of fluid content per unit change in the fluid pressure, defined for a condition of no change in external pressure. Finally note that $K_p = \phi K/\alpha$.

The total strain energy functional (including shear) for this problem may be written in the form

$$2E = \delta\tau_{ij}\delta\epsilon_{ij} + \delta p_f \delta\zeta \ , \tag{D.10}$$

where $\delta\epsilon_{ij}$ is the change in the average strain, with $\delta\epsilon_{ii} = e$ being the dilatation, $\delta\tau_{ij}$ being the change in the average stress tensor for the saturated porous medium with $\frac{1}{3}\delta\tau_{ii} = -\delta p_c$. [From [66], pp. 24614,5]

Appendix E

The double-porosity water-saturated polymer structure under study can be viewed as a special case of the model presented in Refs. [66, 67], whose terminology and notation we adopt here to facilitate comparison. Our unconsolidated fluid-saturated polymer spheres correspond to the porous matrix (called "phase 1" in Ref. [66]) and the interstitial void space filled by water corresponds to the water-filled fractures (called "phase 2" in Ref. [66]), occupying, respectively, fractional volumes $v^{(1)} \equiv v$ and $v^{(2)} \equiv 1 - v$. We shall derive the expression for the effective-medium velocity for such a crystal, in the case where viscous losses are neglected. The condition of perfect locking in the motion between the solid and the two fluid components, valid in the long-wavelength regime that interests us here, implies $\mathbf{u} = \mathbf{U}^{(k)}$ for the corresponding displacement fields of the solid and two fluids ($k = 1$ for the fluid in the matrix pores and $k = 2$ for the fluid in the fractures). Thus the total kinetic energy of the system is written as $T = \frac{1}{2}\rho_{\rm tot}\dot{\mathbf{u}} \cdot \dot{\mathbf{u}}$, where $\rho_{\rm tot} = v(1-f)\rho_s + [1-v(1-f)]\rho_f$ the total inertia of the system, and use of Lagrange's equation leads to the following expression for the stress tensor (a $\mathrm{e}^{-\mathrm{i}\Omega t}$ dependence is assumed)

$$\tau_{ij,j} = \partial_t \partial_{\dot{u}_i} T = -\Omega^2 \rho_{\rm tot} u_i \ . \tag{E.1}$$

On the other hand the weak-frame approximation ($K, \mu \to 0$), valid for unconsolidated grains, yields [see Eqs. (2.44), (2.45)]

$$\tau_{ij,j} = -p_{c,i}, \tag{E.2}$$

with p_c being the confining pressure applied to the boundaries of the whole structure. Combining Eqs. (E.1) and (E.2) and since, by definition, the dilatational strain $e = u_{i,i}$, and, $p_{c,ii} = -k^2 p_c$, with k being the wavenumber, we obtain the effective-medium velocity

$$\overline{c}^2 = \lim_{\Omega \to 0} \left(\frac{\Omega}{k} \right)^2 = -\frac{p_c}{e} \frac{1}{\rho_{\rm tot}}. \tag{E.3}$$

The initial condition $\mathbf{u} = \mathbf{U}^{(k)}$, or, equivalently, $\zeta^{(k)} = 0$, $k = 1, 2$, for the two fluid contents, arising from the long-wavelength regime, leads to a simplified form for the stress-strain phenomenological linear system, described by Eq. (2.43), which, in the general case

of the unconsolidated-grain limit, is written as

$$\begin{pmatrix} -p_c \\ -p^{(1)} \\ -p^{(2)} \end{pmatrix} = \begin{pmatrix} \widetilde{a}_{11} & \widetilde{a}_{12} & \widetilde{a}_{11} \\ \widetilde{a}_{12} & \widetilde{a}_{22} & \widetilde{a}_{12} \\ \widetilde{a}_{11} & \widetilde{a}_{12} & \widetilde{a}_{11} \end{pmatrix} \begin{pmatrix} e \\ -\zeta^{(1)} \\ -\zeta^{(2)} \end{pmatrix} . \tag{E.4}$$

In the above expression, $\widetilde{a}_{ij}$ are the inverse-matrix elements of the matrix defined in Eq. (2.43), and $p^{(k)}$ are the pressures in the fluids of each phase k. Indeed, Eq. (E.4) reduces to the form

$$\begin{pmatrix} -p_c \\ -p^{(1)} \\ -p^{(2)} \end{pmatrix} = \begin{pmatrix} \widetilde{a}_{11} \\ \widetilde{a}_{12} \\ \widetilde{a}_{11} \end{pmatrix} e \, , \tag{E.5}$$

from which $p_c = p^{(2)} = -\widetilde{a}_{11} e$ (being naturally expected, since, in the unconsolidated-grain limit, "phase 2" completely surrounds "phase 1") and $p^{(1)} = p_c \frac{\widetilde{a}_{12}}{\widetilde{a}_{11}}$. Explicit expressions for $\widetilde{a}_{11}$, $\widetilde{a}_{12}$ can be found to be [see Table **??**]

$$\widetilde{a}_{11} \equiv \mathcal{D}^{-1}(a_{22}a_{33} - a_{23}^2) = \frac{\widetilde{a}_{12}}{B^{(1)}} \, , \tag{E.6}$$

$$\begin{aligned} \widetilde{a}_{12} &\equiv \mathcal{D}^{-1}(a_{13}a_{23} - a_{12}a_{33}) = \\ &= B^{(1)} \left[\frac{1-v}{K_f} + \frac{v}{K_u^{(1)}} \right]^{-1} \, , \end{aligned} \tag{E.7}$$

with $\mathcal{D} = a_{11}a_{22}a_{33} + 2a_{12}a_{13}a_{23} - a_{11}a_{23}^2 - a_{22}a_{13}^2 - a_{33}a_{12}^2$,

$$\frac{1}{K_u^{(1)}} = \frac{1 - \alpha^{(1)} B^{(1)}}{K^{(1)}} \, , \tag{E.8}$$

the inverse *undrained* modulus for "phase 1", and, $\alpha^{(1)}$ and $B^{(1)}$, the corresponding Biot-Willis and Skempton coefficients, respectively. Combining the above expressions (E.5)-(E.8) we find $p^{(1)} = p_c B^{(1)}$ and

$$-\frac{p_c}{e} = \widetilde{a}_{11} = \left[\frac{1-v}{K_f} + \frac{v}{K_u^{(1)}} \right]^{-1} . \tag{E.9}$$

After substitution of Eq. (E.9) in (E.3) we finally obtain the effective-medium velocity at the long wavelength regime for the double-porosity medium in the unconsolidated-grain limit as

$$\bar{c}^2 = \lim_{\Omega \to 0} \left(\frac{\Omega}{k} \right)^2 = \frac{K_{\text{eff}}}{\rho_{\text{eff}}} \, , \tag{E.10}$$

where the effective elastic parameters are defined by

$$\frac{1}{K_{\text{eff}}} \equiv \frac{1-v}{K_f} + \frac{v}{K_u^{(1)}} , \tag{E.11}$$

$$\rho_{\text{eff}} \equiv \rho_{\text{tot}} . \tag{E.12}$$

The quantity K_{eff}^{-1} has a clear physical meaning, being an average-law contribution of the two phases: that of the host fluid (fractures) and that of the porous water-saturated undrained spheres (porous matrix). In the case of close-packed ($v = 0.74$) polystyrene spheres immersed in water we obtain: $\rho_{\text{eff}} = 1.0333\rho_f$, $K_{\text{eff}} = 1.397K_f$ and $\overline{c} = 1721$ m s^{-1}, the latter being in excellent agreement with the value deduced from our multiple-scattering calculations, $\overline{c} = 1717$ m s^{-1}.

Bibliography

[1] *Acoustic Metamaterials and Phononic Crystals*, edited by P. A. Deymier (Springer Series in Solid-State Sciences 173, Berlin, 2013).

[2] *Phononic Crystals: Fundamentals and Applications*, edited by A. Khelif and A. Adibi (Springer Science+Business Media, New York, 2016).

[3] J. P. Dowling, J. Acoust. Soc. Am. **91**, 2539 (1992).

[4] X. Zhang, Z. Liu, Y. Liu, and F. Wu, Phys. Lett. A **313**, 455 (2003).

[5] Y. Lai, X. Zhang, and Z. Q. Zhang, Appl. Phys. Lett. **79**, 3224 (2001).

[6] Y. Lai and Z. Q. Zhang, Appl. Phys. Lett. **83**, 3900 (2003).

[7] M. Sigalas and E. N. Economou, J. Sound Vib. **158**, 377 (1992).

[8] M. S. Kushwaha, P. Halevi, L. Dobrzynski, and B. Djafari-Rouhani, Phys. Rev. Lett. **71**, 2022 (1993).

[9] Z. Y. Liu, X. X. Zhang, Y. W. Mao, Y. Y. Zhu, Z. Y. Yang, C. T. Chan, and P. Sheng, Science **289**, 1735 (2000).

[10] B. Rostami-Dogolsara, M. K. Moravvej-Farshi, and F. Nazari, Phys. Rev. B **93**, 014304 (2016).

[11] A. Khelif, B. Djafari-Rouhani, J. O. Vasseur, P. A. Deymier, Ph. Lambin, and L. Dobrzynski, Phys. Rev. B **65**, 174308 (2002).

[12] J. H. Sun and T. T. Wu, Phys. Rev. B **71**, 174303 (2005).

[13] F. L. Hsiao, A. Khelif, H. Moubchir, A. Choujaa, C. C. Chen, and V. Laude, Phys. Rev. E **76**, 056601 (2007).

[14] S. Amoudache, R. Moiseyenko, Y. Pennec, B. Djafari-Rouhani, A. Khater, R. Lucklum, and R. Tigrine, J. Appl. Phys. **119**, 114502 (2016).

[15] S. Yang, J. H. Page, Z. Y. Liu, M. L. Cowan, C. T. Chan, and P. Sheng, Phys. Rev. Lett **93**, 024301 (2004).

[16] H. S. Lim, M. H. Kuok, S. C. Ng, and Z. K. Wang, Appl. Phys. Lett **84**, 4182 (2004).

[17] T. Still, R. Sainidou, M. Retsch, U. Jonas, P. Spahn, G. P. Hellmann, and G. Fytas, Nano Lett. **8**, 3194 (2008).

[18] T. Still, G. Gantzounis, D. Kiefer, G. Hellmann, R. Sainidou, G. Fytas, and N. Stefanou, Phys. Pev. Lett. **106**, 175505 (2011).

[19] *Porous Media Applications in Biological Systems and Biotechnology*, edited by K. Vafai (CRC Press, Taylor & Francis Group, Boca Raton, 2010).

[20] *Porous Materials: Processing and Applications*, P. S. Liu and G. F. Chen (Elsevier, Amsterdam, 2014).

[21] *Handbook of Porous Media*, edited by K. Vafai (CRC Press, Taylor & Francis Group, Boca Raton, 2015).

[22] W. Trabelsi, H. Franklin, A. Tinel, and S. Derible, Ultrasonics **54**, 1097 (2014).

[23] I. E. Psarobas, N. Stefanou, and A. Modinos, Phys. Rev. B **62**, 278 (2000).

[24] R. Sainidou, N. Stefanou, I.E. Psarobas, and A. Modinos, Comput. Phys. Commun. **166**, 197 (2005).

[25] M. A. Biot, J. Acoust. Soc. Am. **28**, 168 (1956).

[26] M. A. Biot, J. Acoust. Soc. Am. **28**, 179 (1956).

[27] M. A. Biot, J. Acoust. Soc. Am. **34**, 1254 (1962).

[28] M. A. Biot, J. Appl. Phys. **33**, 1482 (1962).

[29] *Hierarchically Structured Porous Materials*, edited by B. L. Su, C. Sanchez, and X. Y. Yang (Wiley-VCH Verlag GmbH & Co. KGaA, Weinheim, 2011).

[30] H. Sai, K. W. Tan, K. Hur, E. Asenath-Smith, R. Hovden, Y. Jiang, M. Riccio, D. A. Muller, V. Esler, L. A. Estroff, S. M. Gruner, and U. Wiesner, Science **341**, 530 (2013).

[31] M. Sušec, S. C. Ligon, J. Stampfl, R. Liska, and P. Krajnc, Macromol. Rapid Commun. **34**, 938 (2013).

[32] J. Wang, B. H. Lessard, M. Maric, and B. D. Favis, Polymer **55**, 3461 (2014).

[33] J. F. Gao, J. S. P. Wong, M. J. Hu, W. Li, and R. K. Y. Li, Nanoscale **6**, 1056 (2014).

[34] M. G. Seo, S. B. Kim, J. H. Oh, S. J. Kim, and M. A. Hillmyer, J. Am. Chem. Soc. **137**, 600 (2015).

[35] S. A. Saba, M. P. S. Mousavi, P. Bühlmann, and M. A. Hillmyer, J. Am. Chem. Soc. **137**, 8896 (2015).

[36] C. Y. Park, Y. J. La, T. H. An, Y. Jeong, S. Y. Kang, S. H. Joo, H. J. Ahn, T. J. Shin, and K. T. Kim, Nat. Commun. **6**, 6392 (2015).

[37] C. Boutin and P. Royer, Geophys. J. Int. **203**, 1694 (2015).

[38] H. Franklin, F. Luppé, and J. M. Conoir, J. Acoust. Soc. Am. **135**, 2513 (2014).

[39] V. H. Nguyen, E. Rohan, and S. Naili, Int. J. Eng. Sci. **101**, 92 (2016).

[40] R. Venegas and O. Umnova, J. Acoust. Soc. Am. **130**, 2765 (2011).

[41] F. Chevillotte, C. Perrot, and E. Guillon, J. Acoust. Soc. Am. **134**, 4681 (2013).

[42] S. G. Kargl and R. Lim, J. Acoust. Soc. Am. **94**, 1527 (1993).

[43] D. L. Johnson and T. J. Plona, J. Acoust. Soc. Am. **72**, 556 (1982).

[44] W. Cheng, J. Wang, U. Jonas, W. Steffen, G. Fytas and R. S. Penciu and E. N. Economou, J. Chem. Phys. **123**, 121104 (2005).

[45] W. Cheng, J. Wang, U. Jonas, G. Fytas and N. Stefanou, Nat. Mater **5**, 830 (2006).

[46] E. Alonso-Redondo, M. Schmitt, Z. Urbach, C. M. Hui, R. Sainidou, P. Rempert, K. Matyjaszewski, M. R. Bockstaller and G. Fytas, Nat. Commun **6**, 8309 (2015).

[47] M. Montagna, Phys. Rev. B **77**, 045418 (2008).

[48] Y. Li, H. S. Lim, S. C. Ng, Z. K. Wang, M. H. Kuok, Chem. Phys. Lett. **461**, 111 (2008).

[49] *Mathematical Methods for Physicists*, G. B. Arfken and H. J. Weber (Academic Press, International edition, 1995).

[50] *Theory of Elasticity*, L. D. Landau and E. M. Lifshitz, 3rd ed. (Butterworth-Heinemann Ltd., Oxford, 1986).

[51] *Acoustic Fields and Waves in Solids, vol. I,* B. A. Auld (John Wiley & Sons Inc., New York, 1973).

[52] *Phononic Crystals: Layer Multiple Scattering Method and Applications*, R. Sainidou (PhD thesis, Athens, 2004).

[53] D. Brill and G. Gaunaurd, J. Acoust. Soc. Am. **81**, 1 (1987).

[54] M. A. Biot and D. G. Willis, J. Appl. Mech. **24**, 594 (1957).

[55] *Classical Mechanics*, H. Goldstein, C. P. Poole, J. L. Safko, 3rd ed. (Addison Wesley, 2002).

[56] R. D. Stoll and G. M. Bryan, J. Acoust. Soc. Am. **47**, 1440 (1970).

[57] J. G. Berryman, Appl. Phys. Lett. **37**, 382 (1980).

[58] J. G. Berryman, Appl. Phys. B **27**, 7789 (1983).

[59] P. N. Sen, C. Scala and M. H. Cohen, Geophysics **46**, 781 (1981).

[60] D. L. Johnson, T. J. Plona, C. Scala, F. Pasierb and H. Kojima, Phys. Rev. Lett. **49**, 1840 (1982).

[61] D. L. Johnson, Appl. Phys. Lett. **37**, 1065 (1980).

[62] D. L. Johnson, P. Sen, Phys. Rev. B **24**, 2486 (1981).

[63] *Handbook of Mathematical Functions*, edited by M. Abramowitz and I. A. Stegun (Dover, New York, 1965).

[64] D. L. Johnson, J. Koplik, and R. Dashen, J. Fluid Mech. **176**, 379 (1987).

[65] *A Textbook of Sound*, A. W. Wood (Macmillan, New York, 1941).

[66] J. G. Berryman and H. F. Wang, J. Geophys. Res. **100**, 24611 (1995);

[67] J. G. Berryman and H. F. Wang, Int. J. Rock Mech. Mining Sci. **37**, 63 (2000);

[68] *Mixture theories for rock properties,* in *Rock Physics & Phase Relations: A Handbook of Physical Constants (ed. T. J. Ahrens)*, J. G. Berryman (American Geophysical Union, Washington D. C., 1995).

[69] Z. Hashin, S. Shtrikman, J. Appl. Phys. **33**, 3125 (1962).

[70] A. W. Skempton, Geotechnique **4**, 143 (1954).

[71] *Transversely isotropic poroelasticity arising from thin isotropic layers,* in *Mathematics of multiscale materials (ed. K. M. Golden, G. R. Grimmett, R. D. James, G. W. Milton, P. N. Sen)*, J. G. Berryman (Springer-Verlag, New York, 1998).

[72] W. C. Chew, *Waves and Fields in Inhomogeneous Media* (Van Nostrant Reinhold, New York, 1990).

[73] H. Lamb, Proc. London Math. Soc. **s1-13**, 189 (1882).

[74] H. Deresiewicz and R. Skalak, Bull. Seismol. Soc. Am. **53**, 783 (1963).

[75] S. M. Hasheminejad and S. A. Badsar, Quart. J. Mech. Appl. Math. **57**, 95 (2004).

[76] S. M. Hasheminejad and S. A. Badsar, Jpn. J. Appl. Phys. **43**, 2612 (2004).

[77] *Quantum Mechanics: Concepts and Applications*, N. Zettili (Wiley, New York, 2009).

[78] J. G. Berryman, J. Acoust. Soc. Am. **68**, 1809 (1980).

[79] J. G. Berryman, J. Acoust. Soc. Am. **68**, 1820 (1980).

[80] A. Alevizaki, R. Sainidou, P. Rembert, B. Morvan and N. Stefanou, Phys. Rev. B **94**, 174306 (2016).

[81] A. Alevizaki, R. Sainidou, P. Rembert, B. Morvan and N. Stefanou, Phys. Rev. B **95**, 214306 (2017).

[82] R. Sainidou, N. Stefanou, and A. Modinos, Phys. Rev. B **69**, 064301 (2004).

[83] C. Tserkezis and N. Stefanou, Phys. Rev. B **81**, 115112 (2010).

[84] Z. Y. Li, K. M. Ho, Phys. Rev. B **68**, 155101 (2003).

[85] C. Tserkezis, N. Stefanou, G. Gantzounis, N. Papanikolaou, Phys. Rev. B **84**, 115455 (2011).

[86] F. J. Lawrence, L. C. Botten, K. B. Dossou, R. C. McPhedran, C. M. de Sterke, Phys. Rev. A **82**, 053840 (2010).

[87] J. J. Kirkland, J. Chromatogr. **125**, 231 (1976).

[88] Z. G. Shi and Y. Q. Feng, Micropor. Mesopor. Mat. **116**, 701 (2008).

[89] L. H. Chen, G. S. Zhu, D. L. Zhang, H. Zhao, M. Y. Guo, W. Shi, and S. L. Qiu, J. Mater. Chem. **19**, 2013 (2009).

[90] Z. G. Shi, Q. Z. Guo, Y. T. Liu, Y. X. Xiao, and L. Xu, Mater. Chem. Phys. **126**, 826 (2011).

[91] Y. S. Cho, S. Y. Choi, Y. K. Kim, and, G. R. Yi, J. Colloid. Interf. Sci. **386**, 88 (2012).

[92] J. He, C. L. Yang, X. H. Xiong, and, B. W. Jiang, J. Polym. Sci., Part A: Polym. Chem. **50**, 2889 (2012).

[93] C. Cheng, T. Z. Yang, Y. H. He, L. Yang, and, L. X. Wang, Mater. Lett. **109**, 257 (2013).

[94] S. Grama and D. Horák, Physiol. Res. **64** (Suppl.1), S11 (2015).

[95] H. J. Xia, G. P. Wan, F. Yang, J. S. Wang, and, Q. Bai, Mater. Lett. **180**, 19 (2016).

[96] *Group Theory and Electronic Energy Bands in Solids*, J. F. Cornwell, (North-Holland, Amsterdam, 1969).

[97] I. E. Psarobas, A. Modinos, R. Sainidou and N. Stefanou, Phys. Rev. B **65**, 064307 (2002).

[98] T. Still, M. Mattarelli, D. Kiefer, G. Fytas and M. Montagna, J. Phys. Chem. Lett. **16**, 2440–2444 (2010).

[99] *Dynamical Theory of Crystal Lattices*, M. Born and K. Huang (Oxford University Press, Oxford, 1954).

[100] *Dynamical Light Scattering: With Applications to Chemistry, Biology, and Physics*, B. J. Berne and R. Pecora (John Wiley and Sons, New York, 2000).

[101] *Theoretical Study of Brillouin Light Scattering from Spherical Particles*, A. Zdagkas (MSc thesis, Athens, 2015).

[102] M. Faatz, W. Cheng, G. Wegner, G. Fytas and R. S. Penciu and E. N. Economou, Langmuir **21**, 6666 (2005).

[103] R. J. S. Brown and J. Korringa, Geophysics. **40**, 608 (1975).

[104] *Scattering Theory of Waves and Particles, 2nd ed.*, R. G. Newton (Springer-Verlag, Berlin, 1982).